Tenth Quarterly Report
Phase II
October 1, 2011

Prepared by
Dean Darryll Pines
Principal Investigator and EERC Project Director

Prof. Balakumar Balachandran, Chair
EERC Project Deputy Director

Dr. Azar Nazeri
EERC Research Manager

THE UNIVERSITY OF MARYLAND AND THE PETROLEUM INSTITUTE OF ABU DHABI, UAE

EERC Key Contributors

University of Maryland – College Park, MD, USA

Shapour Azarm
Balakumar Balachandran
David Bigio
Hugh A. Bruck
Nikil Chopra
Avram Bar-Cohen
Serguei Dessiatoun
Ashwani K. Gupta
Satyandra K. Gupta
Yunho Hwang
P.K. Kannan
Mohammad Modarres
Michael Ohadi
Reinhard Radermacher
Amir Shooshtari

Petroleum Institute – Abu Dhabi, UAE

Youssef Abdel-Majid
Ahmed Al Shoaibi
Saleh Al Hashimi
Ebrahim Al-Hajri
Ali Almansoori
Mohamed Alshehhi
Sai Cheong Fok
Afshin Goharzadeh
Hamad Karki
Isoroku Kubo
Peter Rodgers
Abdennour Seibi

Table of Contents

Executive Summary

The following is a summary of the major project activities that have taken place over the completed quarter. For more detail, see the individual reports in the last section of this report.

Thrust 1: Energy Recovery and Conversion

Sulfur Recovery from Gas Stream using Flameless and Flame Combustion Reactor
A.K. Gupta, A. Al Shoaibi

- Examined the effect of carbon dioxide's presence in the acid gas stream on Claus process chemistry and byproducts.
- Studied the effect of nitrogen presence in acid gas on Claus process reactions.
- Wrote a draft technical paper for presentation at the Aerospace Sciences Meeting in January 2012.
- Wrote technical paper on the results presented in the previous quarterly report for submission to the Journal of Applied Energy.

Separate Sensible and Latent Cooling with Solar Energy
R. Radermacher, Y. Hwang, I. Kubo

- Finished the shakedown test.
- Charged optimization testing.
- Started the actual test.

Waste Heat Utilization in the Petroleum Industry
R. Radermacher, Y. Hwang, S. Al Hashimi, P. Rodgers

- Optimized six steam cycles with steam extraction for CO_2 regeneration.
- Investigated the power increase due to feed water preheating.
- Developed a robust optimization technique for solving problems with uncertainty.

Thrust 2: Energy-Efficient Transport Process Projects

Multidisciplinary Design and Characterization of Polymer Composite Seawater Heat Exchanger Module
P. Rodgers, A. Bar-Cohen, S.K. Gupta, D. Bigio, H.A. Bruck

- Tested several heat exchanger prototypes at the HX test rig at the University of Maryland.
- Developed and utilized thermomechanical finite element model to assess thermal and structural performance of a polymer composite heat exchanger module.
- Assessed the effects on geometric variation on the development of thermomechanical stresses in polymer composite heat exchangers.

- Constructed model for moldability-based feasibility boundary.
- Removed features for efficient assessment of mold-filling feasibility of finned-plate geometries.
- Developed a fiber orientation measurement methodology.
- Prepared specimens with micro and nanoscale ingredients to study mixing effects in a twin screw extruder to characterize the development of multi-scale structure and associated properties for these novel polymer composites for PHX applications.
- Frank Robinson successfully defended his M.S. thesis on "Thermomechanical Behavior of Polymer Composite Heat Exchangers."
- A paper entitled "Polymer Heat Exchangers – An Enabling Technology for Water and Energy Savings" was accepted at the 2011 International Mechanical Engineering Congress & Exposition in Denver, Colorado.
- A paper entitled "Modeling and Validation of Prototype Thermally Enhanced Polymer Heat Exchanger" was accepted at the 2011 International Mechanical Engineering Congress & Exposition in Denver, Colorado.
- A paper entitled "An Integrated Approach to Design of Enhanced Polymer Heat Exchangers" was accepted for publication at the Journal of Mechanical Design.
- Presented paper entitled "An Integrated Approach to Design of Enhanced Polymer Heat Exchangers" to DETC Conference to be held on August 29-31 2011 in Washington, DC.

Study on Microchannel-Based Absorber/Stripper and Electrostatic Precipitators for CO_2 Separation from Flue Gas

S. Dessiatoun, A. Shooshtari, M. Ohadi, A. Goharzadeh

- Performed additional in-depth study of the processes and analysis of experimental results, on both mathematical modeling and experimental study.
- Collected new sets of data on the effect of flow rate on the rate of absorption. The results successfully demonstrated that reduction of flow rate enhances the absorption rate.

Microreactors for Oil and Gas Processes Using Microchannel Technologies

S. Dessiatoun, A. Shooshtari, M. Ohadi, A. Goharzadeh, E. Al-Hairi

- Obtained useful kinetic data from batch-scale polymerization with the produced catalyst.
- Initiated experiments in the microchannel reactor.

Thrust 3: Energy System Management

Integration of Engineering and Business Decisions for Robust Optimization of Petrochemical Systems

S. Azarm, P.K. Kannan, A. Almansoori, S. Al Hashimi

- Developed a preliminary Matlab-based model to simulate crude distillation, catalytic reforming, hydro treating and other important operations. This model can be integrated later with the dashboard to allow the dashboard-based DSS framework to consider costs and revenues in the crude distillation process for profit calculation.
- Improved the HYSYS reactor-distillation model with heat integration:
  - Developed a heat exchanger network to recover the energy from reaction gases and used it for heating feed streams.

    - Revised the previous HYSYS model by applying “adjust operation” to ensure the reactor-distillation process was working within practical operating conditions.
- Completed a preliminary draft for the invited book chapter on “Multi-Objective Optimization: Techniques and Applications in Chemical Engineering.”

Dynamics and Control of Drill Strings

B. Balachandran, H. Karki, Y. Abdelmagid

- Further studied the three-degree-of-freedom model; obtained model predictions of the drill-string dynamics for the string and the contact condition between rotor and shell.
- Enhanced the experimental apparatus to enable study of horizontal drilling and obtained experimental data. Numerical results were in good agreement with experimental results. Results from both numerical and experimental studies indicate that, even when neglecting external forces, nonlinear effects exist in the vertical configuration and are likely due to the geometry of the drill string.

Studies on Mobile Sensor Platforms

B. Balachandran, N. Chopra, H. Karki, S.C. Fok

- Added a Kinect sensor to the mobile agent to extract three-dimensional information about the environment and parts of the environment not in the field of view of the mobile agent.
- Obtained simulation results using the particle filtering-based estimation algorithm fastSLAM and a data association technique.

Development of a Probabilistic Model for Degradation Effects of Corrosion-Fatigue Cracking in Oil and Gas Pipelines

M. Modarres, A. Seibi

- Continued theoretical effort in support of model development: rupture analysis with application to Al-7075 and X70 carbon steel.
- Performed creep experiments of Al-7075T6 in an MTS tensile machine.
- Performed experiments on X-70 carbon steel samples.

Introduction

Dean Darryll Pines Assumes Leadership of the EERC

The A.J. Clark School of Engineering's Dean, Darryll Pines, has assumed the role of principal investigator of the EERC. Dean Pines replaces former UMD Provost Nariman Farvardin, who is now the President of the Stevens Institute of Technology. Prior to becoming Dean of the Clark School, Dr. Pines served as Chair of the Department of Aerospace Engineering. Dr. Pines brings extensive academic, administrative and research experience to the EERC, and we look forward to working with him on the continued collaboration between our two institutions.

Sabbaticals of PI Faculty at UMD

Dr. Ebrahim Al Hajri (PI) spent his sabbatical at UMD, where he worked with Dr. Mike Ohadi, Dr. Amir Shooshtari, and Dr. Serguei Dessiatoun. Dr. Al Hajri used the opportunity to do experimental work on the collaborative projects the PI is conducting with UMD. He also used the opportunity to meet with the ADNOC Scholars at UMD and conduct meetings with other EERC faculty and the UMD Steering Committee.

UMD Wins Solar Decathlon 2011

The University of Maryland's entry in 2011 Solar Decathlon competition won first place, a high honor for the University. UMD's entry, an 800 square-foot house called "Watershed" for its innovative use of solar energy and water reuse and conservation features, was designed by students and faculty from multiple disciplines, such as engineering, architecture, and computer science, participated in the project. The team was led by Professor Keith Herold of the Fischell Department of Bioengineering and Professor Amy Gardner, from the School of Architecture. PI Provost Ismail Tag and Mr. Tareq Al Amoudi visited the house during their visit to UMD, more details of which can be found below.

Summer Internship Program 2011

In the fourth year of the EERC Summer Internship program, five PI students—four undergraduates and one graduate student—were sponsored by four UMD professors. Each student worked with a UMD professor and graduate student supervisors on active EERC research projects. Our summer interns gained valuable hands-on experience in the labs while working with professors and students from culturally diverse backgrounds. Students also spent their free time exploring cultural, historical and scientific hallmarks, such as the White House and monuments in Washington D.C. The students also visited Baltimore's Wheelabrator Technologies to see a waste-to-energy facility in action.

Following is a summary of the research projects and tasks during the six-week internship of the five students this summer.

Student: **Salim Al Kaabi, Electrical Engineering Student**
Professor: **Sarah Bergbreiter**
Project: **Microrobotics**

Salim worked in Dr. Sarah Bergbreiter's laboratory, where Dr. Bergbreiter is conducting research on a new class of networked centimeter and millimeter sized mobile robots. To develop this new class of robots, she is working on solving problems with microrobotic locomotion, low-power and efficient actuators, and novel fabrication techniques. She hopes to adapt the technologies used by these tiny robots for use in medicine, consumer electronics, and science.

Salim's task was to work on detecting robots using a gyroscope and accelerometer. He was tasked with providing a C++ code that would help in integration of the acceleration data. He also used MatLab, gathered and analyzed experimental data, investigated the noise problem using a Mini-Kit CC2530 ZNP, and worked on optical sensors.

Salim believes that the theory covered in his PI coursework helped him understand the issues in this research. He also found that the environment at UMD enhanced his learning because he was surrounded by hard-working students, whom he found to be friendly and kind. He believes the internship experience is important for undergraduate students considering graduate studies because it provides a taste of what graduate studies are like and the amount of work that is required.

Salim Al Kaabi on the left.

Student:	**Reda Mohamed El Sholkami, Chemical Engineering Student**
Professor:	**Dr. A.K. Gupta**
Mentor:	**Mr. H. Selim**
Project:	**Sulfur Recovery from Gas Stream using Flameless and Flame Combustion**

Reda Mohamed was sponsored by Prof. A.K. Gupta to work in the combustion laboratory for his summer internship. Dr. Gupta's research is concerned with combustion, and in particular, his EERC project is concerned with the thermal process of sulfur recovery from sour gas by conventional flame combustion as well as flameless combustion. Reda's task was to obtain fundamental knowledge on the Claus process. He learned about the effect of the compositions of CO_2 and N_2 on the optimum temperature in the Claus process and about a novel error propagation approach for reducing the H_2S/O_2 reaction mechanism.

Additionally, Reda was able to use CHEMKIN and FLUENT software for reactive simulations and to compare the obtained simulation results with the experimental results. He was also introduced to the experimental work of the project. This included learning how to work safely in the laboratory, mainly due to the hazardous gases involved in the experimental work of this research project, such as H_2S.

Reda liked the fact that the graduate students appreciated the effort and time he put into performing his work. He was also able to observe the way all the graduate students and Dr. Gupta helped his student prepare and rehearse for his Ph.D. exam. He enjoyed the research environment, specifically having the opportunity to focus on a particular problem and try to generate the best possible solutions.

Reda Mohamed on the left.

Students:	**Salim Saeed Al Qayedi and Fawad Muhammad Taqi, Mechanical Engineering Students**
Professor:	**Dr. B. Balachandran**
Mentors:	**Dr. Balachandran (Fawad) and Mr. Nick Vlajic (Salim)**
Project:	**Dynamics and Control of Drill Strings**

Both Salim Algavedi and Fawad worked with Dr. Balachandran in the Vibration Laboratory for their internships. This laboratory is a focal point for studies of nonlinear phenomena, system identification, signal analyses, acoustics control, damping, and vibration control, with particular emphasis on mechanical, aerospace, and marine systems. The interns were tasked with understanding concepts such as correlation trends, outlier points, regression analysis, digital data acquisition, spectral analysis, signal processing, Discrete Fourier Transform (DFT) and Fast Fourier Transform (FFT). They used MatLab to analyze data, and apply filtration techniques.

They also did some experiments on the drill string. Their task was to gather data from the torque sensor and apply FFT and filtration techniques to remove noise using a data acquisition card and LabView software. They also used Virtual Instrumentation Engineering Workbench software and Solidworks to perform Finite Element Analysis (FEM) of drill strings.

Selim and Fawad believe that their training in the LabView software will be useful for their senior design projects at PI next year. Fawad also found that the task of modeling and FEM in Solidworks clearly showed the relationship between industrial experience and the theory they have covered in their PI coursework. The modeling and analysis techniques they learned at PI were vital in creating this model. Learning this CAD software has added to the lifelong skills they will use as engineers.

Fawad and Salim were both impressed by the diligence and self-motivation of the graduate students, showing that the students are dedicated to their work and motivated by themselves to do it as opposed to being pressured into completing their jobs. Salim also admired the IT department's technique to help students use different online programs without the need to download them. This allows the students to complete their work anywhere without the need to install these programs.

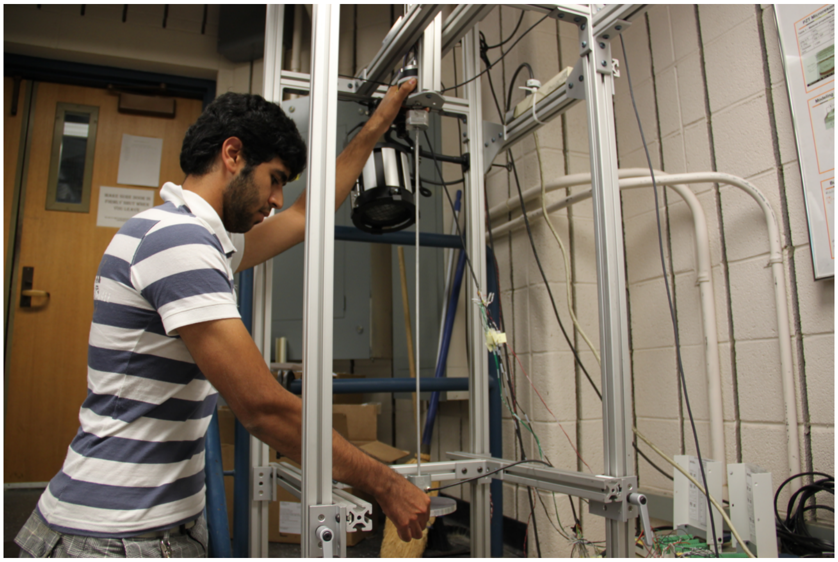

Salim working in the Vibration Lab.

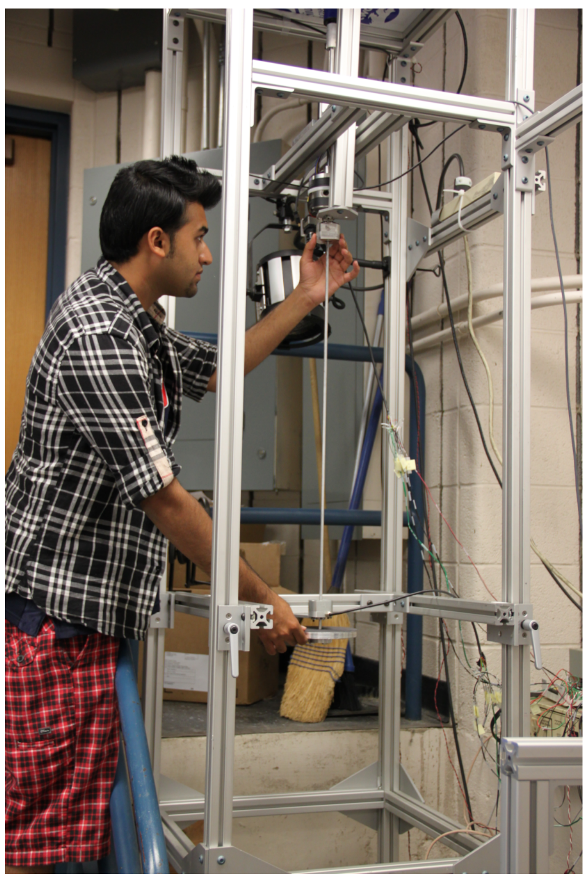

Fawad working in the Vibration Lab.

Student: **Adeel Butt, Graduate Chemical Engineering Student**
Professor: **Shapour Azarm**
Project: **Integration of Engineering and Business Decisions for Robust Optimization of Petrochemical Systems**

Adeel Butt, a PI graduate student in the Chemical Engineering Department, came to Maryland for a six-week internship. His research plan was focused on refinery simulation model development and optimization implementation. The overall objective of the project Adeel worked on is to develop a framework for integrating engineering and business decisions. In this quarter, their research efforts continued to extend the dashboard-based Decision Support System (DSS) by considering the crude oil processing units in the refinery.

Visiting the cultural and historical sites in Washington D. C.

From left, Fawad Taqi, Reda Mohamed, Salim Al Kaabi, Salim Al Qayedi, and Adeel Butt and the Wheelabrator operator visiting Wheelabrator Technologies in Baltimore.

PI Provost Dr. Ismail Tag and Mr. Tareq Al Amoudi Visit Washington D. C. and UMD, October 1 - October 3

PI Provost Dr. Ismail Tag and Mr. Tareq Al Amoudi, the Vice President of Administration, visited the United States on a tour of many states and PI Partner Universities. Dr. Tag and Mr. Al Amoudi arrived in Washington D. C. on Saturday October 1, and visited UMD on October 3.

On Sunday, they visited the Washington Mall to view UMD's entry in the 2011 Solar Decathlon. Dr. Tag later told EERC faculty that he had planned his trip to States around this event. Dr. Nazeri, and ADNOC Scholar Ali Al Alili from UMD accompanied Dr. Tag and Mr. Al Amoudi to this event, where they toured the majority of 19 houses in the competition. The University of Maryland's entry, an 800 square-foot house called "Watershed" for its innovative use of solar energy and water reuse and conservation features, took first place in this prestigious competition. Students and faculty from multiple disciplines, such as engineering, architecture, and computer science, participated in the project. The team was led by Professor Keith Herold of the Fischell Department of Bioengineering and Professor Amy Gardner, from the School of Architecture.

From left, Tareq Al Amoudi, Provost Tag, Dr. Nazeri, and Ali Al Alili in front of the Watershed.

The interior of the Watershed.

Provost Tag and Tareq Al Amoudi looking at a cross-section of the wall of the Watershed.

On Monday, Provost Tag and Mr. Al Almoudi attended several meetings with UMD faculty and administration and visited several labs. Provost Tag met with Dr. Mike Ohadi and visited the Virtual Reality lab, where he met with Dr. Amr Baz, while Mr. Al Amoudi met with some administration officials, including Margaret Brumfeld, Executive Director of Administrative Affairs for the Mechanical Engineering Department, and Janna Dolan, Director of Student Affairs.

Both visitors met with the current ADNOC Scholars, Ali Al Alili, Hesham Ismail, Hussain Al Hashimi, and Abdullah Al Tamimi. The ADNOC Scholars had the opportunity to show the visitors their labs and the projects they are currently working on. They also met with former UMD president, Dr. Dan Mote to discuss PI's strategic plan and with Dean Darryll Pines of the Clark School of Engineering, and the Principal Investigator of the EERC. Dr. Tag invited Dr. Pines to join the PI Advising Board, which Dean Pines accepted.


With the ADNOC Scholars: from left, Ali Al Alili, Hussain Al Hashimi, Provost Tag, Mr. Tareq Al Almoudi, and Abdullah Al Tamimi.

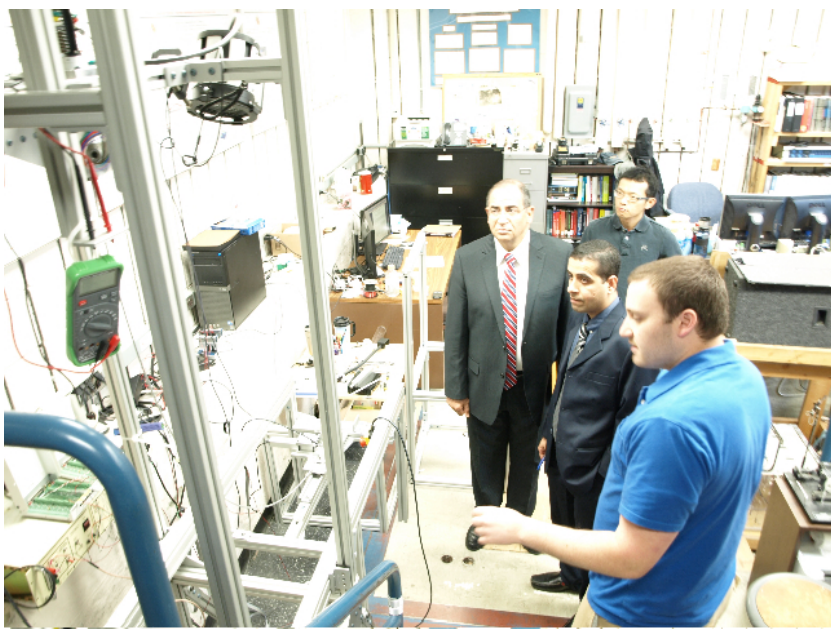
Visiting Professor Balachandran in the Vibrations Lab, where ADNOC Scholar Hesham Ismail works on his Ph.D. topic.

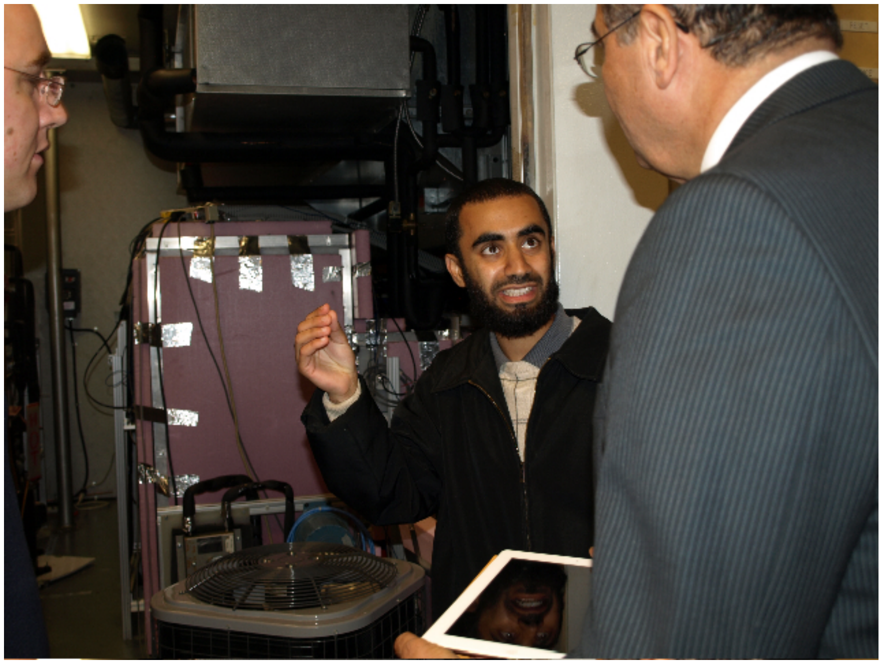

Ali Al Alili showing his laboratory to Provost Tag.

Individual Project Reports

Thrust 1
Energy Recovery and Conversion

Sulfur Recovery from Gas Stream using Flameless and Flame Combustion Reactor

UMD Investigators: **Ashwani K. Gupta**
GRA: **Hatem Selim**
PI Investigators: **Ahmed Al Shoaibi**
Start Date: **October 2006**

1. Objectives / Abstract

The main objective is to obtain fundamental information on thermal process of sulfur recovery from sour gas by conventional flame combustion as well as flameless combustion, using numerical and experimental studies. Our ultimate goal is to determine optimal operating conditions for enhanced sulfur conversion. Therefore, an experimental study of the flameless combustion processes of the Claus furnace is proposed so that the results can be used in the normal flame process for determining improved performance. In this study we will explore different operating conditions and perform in flame and exhaust gas analyses of both flame and flameless modes of reactor operation in order to seek our quest for better understanding of the process with the goal to attain enhanced sulfur capture efficiency.

Specific objectives are to provide:

- A comprehensive literature review of the existing flame combustion process for sulfur removal with special reference to sulfur chemistry
- Near isothermal reactor conditions and how such conditions assist in the enhanced sulfur recovery process
- CFD simulation of the flame and flameless combustion in the furnace.
- Determination of the chemical kinetics and the major reaction pathways to seek for high performance
- Design of a reactor for experimental verification of the numerical results
- Measurements and characterization of the combustion furnace under various conditions, including the conditions that utilize high temperature air combustion principles for flameless combustion
- Experiments with different sulfur content gas streams using the flame and flameless combustion furnace modes of operation.
- Installation of the appropriate diagnostics for quantification of stable and intermediate sulfur compounds in the process and exit stream
- Flow, thermal and chemical speciation characteristics of the reactor
- Product gas stream characteristics and evaluation of sulfur recovery and performance in the process

2. Deliverables

- Further investigation of the effect of CO_2 presence in acid gas stream on Claus process reactions
- Examination of the effect of nitrogen presence in acid gas stream on Claus process reactions
- A draft technical paper about the results presented in this quarterly report. The paper will be submitted and published at the forthcoming Aerospace Sciences Meeting (ASM), in January 2012
- A technical paper for journal publication. The paper is submitted to The Journal of Applied Energy

3. Executive Summary

During the reported quarter, progress continued with major focus on the experimental part of the project. Examination of the effect of carbon dioxide presence in the acid gas stream on Claus process chemistry and byproducts continued. Higher flow rates and higher concentrations of CO_2 have been used in order to further understand their role in the investigations. Oxygen was used as an oxidizer over air in order to delineate the effect of nitrogen on the reaction. Gas sampling was conducted along the centerline of the reactor using a sonic-throat rapid quenching micro sampling probe.

The effect of nitrogen presence in the acid gas on Claus process reactions has been studied as well. Different concentrations of N_2 were used to identify the effect of nitrogen on the process chemistry. Similarly, oxygen was used as an oxidizer over air in order to rule out the effect of nitrogen on the reaction. Gas sampling was conducted along the reactor centerline using the sonic-throat sampling probe.

We finished writing a draft technical paper on the results presented in this quarterly report, a paper will be submitted and published at the forthcoming Aerospace Sciences Meeting (ASM), to be held in January 2012.

We also finished writing the technical paper on the results presented in the previous quarterly report for journal publication, a paper will be written and submitted to The Journal of Applied Energy for possible publication.

4. Progress

4.1 Effect of CO_2 and N_2 Presence in Acid Gas stream on H_2S Combustion

Experiments were conducted to examine the combustion of H_2S/O_2 mixtures and examine the evolution of the end-products. Furthermore, the effect of the injection of CO_2 or N_2 along with H_2S in the reaction pool was examined. Hydrogen sulfide flow rate as well as oxygen flow rate was kept constant during all the experiments. However, carbon dioxide and nitrogen flow rates were changed in order to change their concentrations in the acid gas stream. Maximum concentration of carbon dioxide or nitrogen in the acid gas stream during the experiments was 30%, and then gradually decreased in increments of 10% with the simultaneous decrease of H_2S. Table 1 shows the flow rates of oxygen, hydrogen sulfide, carbon dioxide, and nitrogen for each case examined here.

Table 1. Flow rates of O_2, H_2S, CO_2 and N_2

	H_2S (cm^3/min)	CO_2/N_2 (cm^3/min)	O_2 (cm^3/min)
Acid Gas composition (100% H_2S, 0% CO_2/N_2)	105	0	52.5
Acid Gas composition (90% H_2S, 10% CO_2/N_2)	105	11.6	52.5
Acid Gas composition 80% H_2S, 20% CO_2/N_2)	105	26.25	52.5
Acid Gas composition (70% H_2S, 30% CO_2/N_2)	105	45	52.5

4.1.1 Reactor temperature distribution

Mean reactor temperature was measured using a K-type thermocouple. A traverse mechanism was used to move the thermocouple incrementally along the centerline of the reactor. Figure 1 shows the temperature distribution along the reactor centerline for H_2S/O_2 flame without and with the addition of carbon dioxide, while Figure 2 presents the reactor temperature along the centerline without and with the addition of nitrogen. Both cases represent 30% concentration of CO_2 and N_2 so that their maximum effect on the temperature can be observed. The addition of nitrogen and carbon dioxide caused the flame temperature to decrease immediately upon injection. However, the temperature drop was higher with the addition of nitrogen. This is attributed to the higher heat capacity of nitrogen. Moreover, nitrogen behaves as a reactant diluent. However, carbon dioxide acts an oxidizer in the reaction (discussed further here in the next section). This justifies the increase of the reactor temperature downstream in the case of CO_2 addition where the rate of H_2S oxidation is higher.

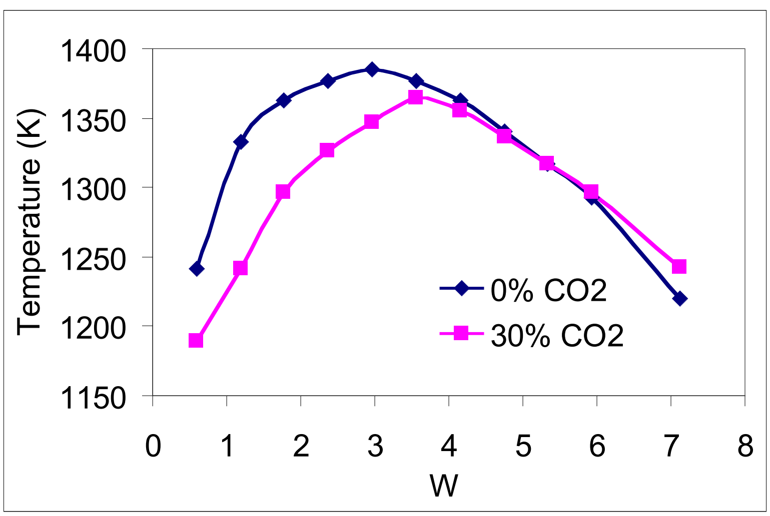

Figure 1. Effect of CO_2 addition on temperature distribution along reactor centerline.

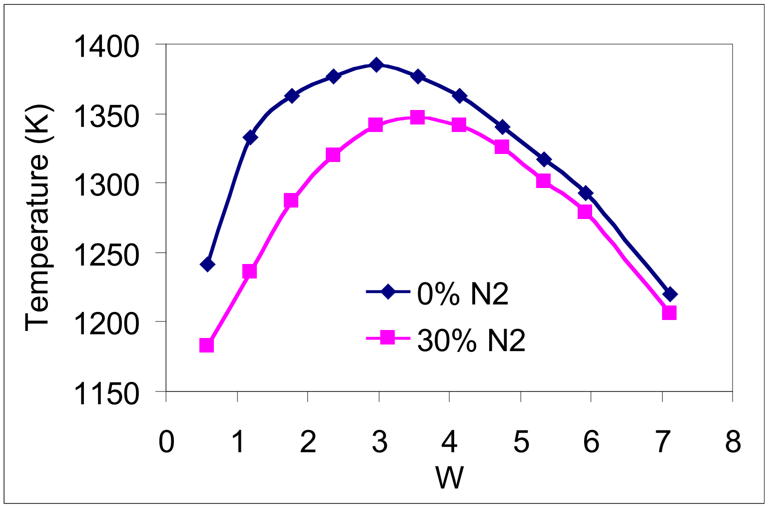

Figure 2. Effect of N_2 addition on temperature distribution along reactor centerline.

4.1.2 Combustion of CO_2-laden acid gas

The effect of carbon dioxide addition was examined at different concentrations in the acid gas stream. The baseline case was demonstrated first where the acid gas stream that reacted with oxygen was 100% H_2S. Carbon dioxide concentrations in the acid gas stream were varied between 0% and 30% with gradual increase in intervals of 10% increments. Figure 3 shows the behavior of both H_2S and SO_2 along the reactor centerline from the combustion of 100% H_2S acid gas stream with oxygen. Results reveal that hydrogen sulfide decays monotonically until it reaches to an asymptotic value. On the other hand, sulfur dioxide increase until it reaches a peak, and then decreases monotonically. The increase in SO_2 mole fraction is attributed to the reaction of H_2S with oxygen. On the other hand, the reduction of SO_2 is attributed to the reaction of SO_2 and H_2S to form sulfur. Sulfur conversion efficiency was evaluated (from the concentrations of H_2S and SO_2) and estimated to be 46%.

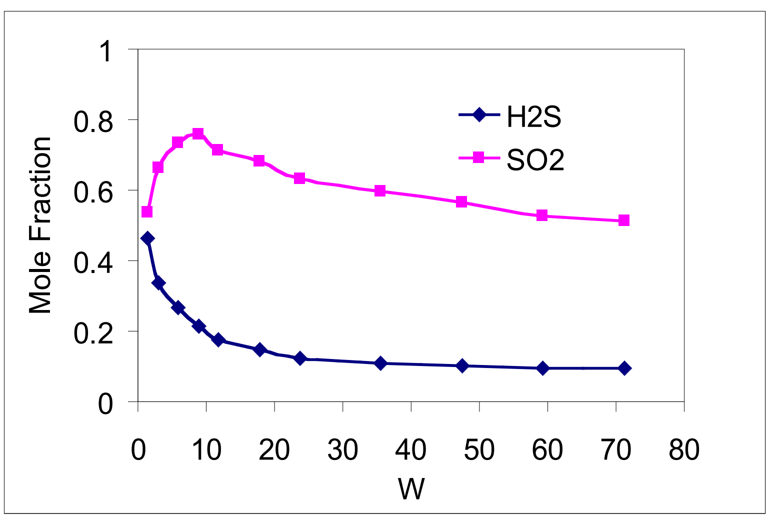

Figure 3. H_2S and SO_2 mole fraction along the reactor (100% H_2S acid gas).

Figure 4 shows H_2S and SO_2 mole fractions along the reactor centerline for acid gas composition of 90% H_2S and 10% CO_2. Hydrogen sulfide decays to a lower value compared to the 100% H_2S

acid gas case. Sulfur dioxide increases until it reaches a peak but does not decrease as much as it decreased in the previous case. This is attributed to the increase in the oxidation medium due to the presence of carbon dioxide. Carbon dioxide acts as an oxidizer provider, which attacks higher amounts of H_2S to form SO_2. In presence of oxygen, H_2S tends to react with oxygen to form SO_2 rather than reacting with SO_2 to form sulfur [1-3]. Figure 5 shows the mole fraction of carbon monoxide along the reactor centerline. Since the reactor temperature is not high enough for CO_2 dissociation, presence of carbon monoxide is likely due to the reaction of CO_2 with H (Reaction 1). Carbon monoxide decay to zero is attributed to its reaction of SO_2 (reaction 2). Sulfur conversion efficiency was calculated and found to be 31.5%.

$$H + CO_2 \rightarrow CO + OH \tag{1}$$

$$SO_2 + CO \rightarrow SO + CO_2 \tag{2}$$

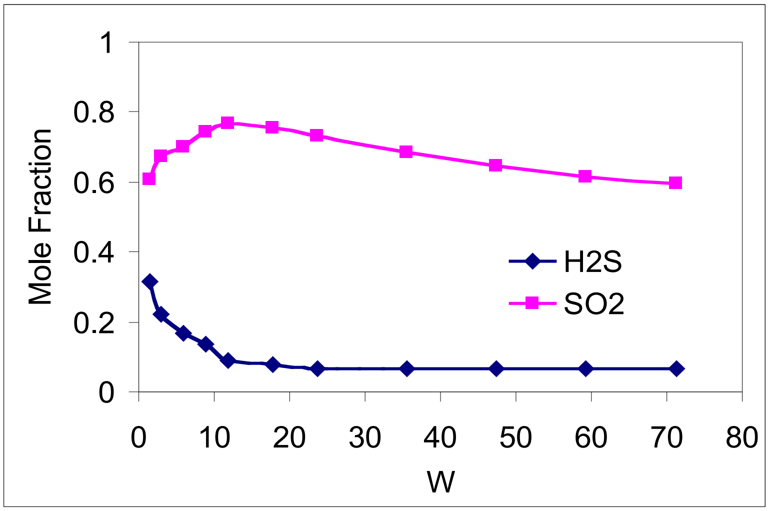

Figure 4. H_2S and SO_2 mole fraction along the reactor (90% H_2S, 10% CO_2 acid gas).

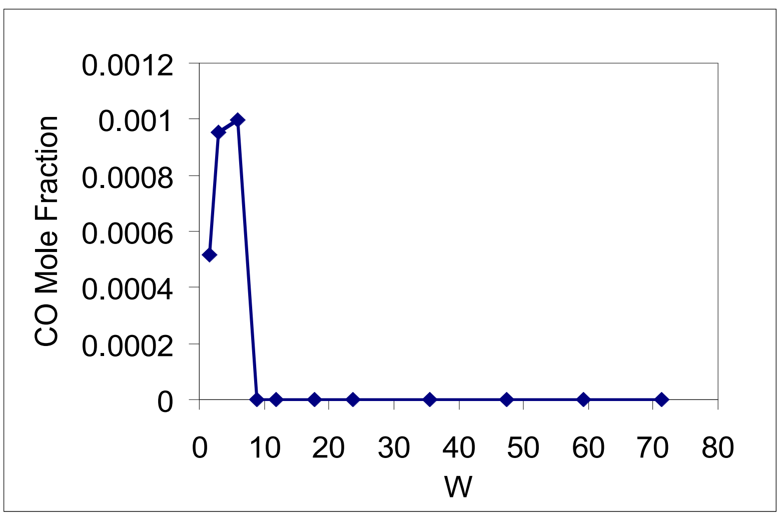

Figure 5. CO mole fraction along the reactor (90% H_2S, 10% CO_2 acid gas).

Figure 6 shows the mole fraction of H_2S and SO_2 along the reactor centerline from the combustion of 80% H_2S and 20% CO_2 acid gas stream mixture with oxygen. Hydrogen sulfide decreases until it reaches an asymptotic value. The asymptotic H_2S mole fraction is less than the previous cases. This validates the aforementioned hypothesis that CO_2 liberates oxygen, which reacts with H_2S to form SO_2. On the other hand, the reaction between H_2S and SO_2 dwindles according to the behavior of SO_2 mole fraction. Figure 7 shows the carbon monoxide mole fraction along the reactor centerline. Similar to the previous case, reactions 1 and 2 rule the behavior of CO along the reactor. Sulfur conversion efficiency was evaluated and estimated to be about 16.8%.

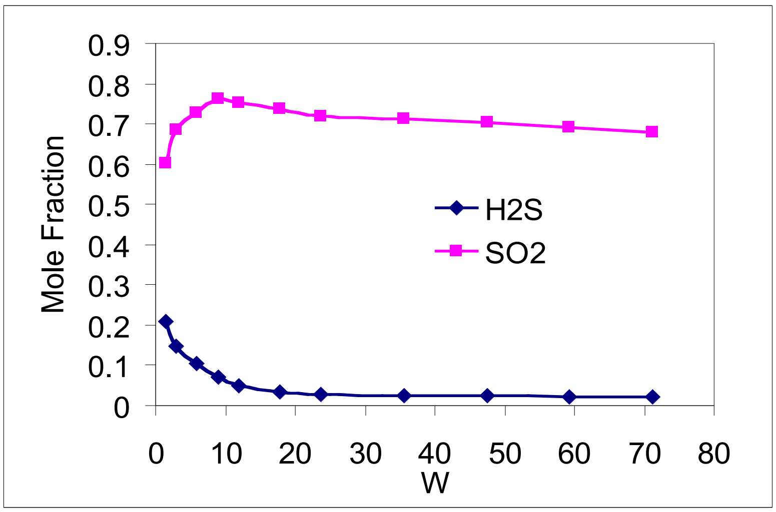

Figure 6. H_2S and SO_2 mole fraction along the reactor (80% H_2S, 20% CO_2 acid gas).

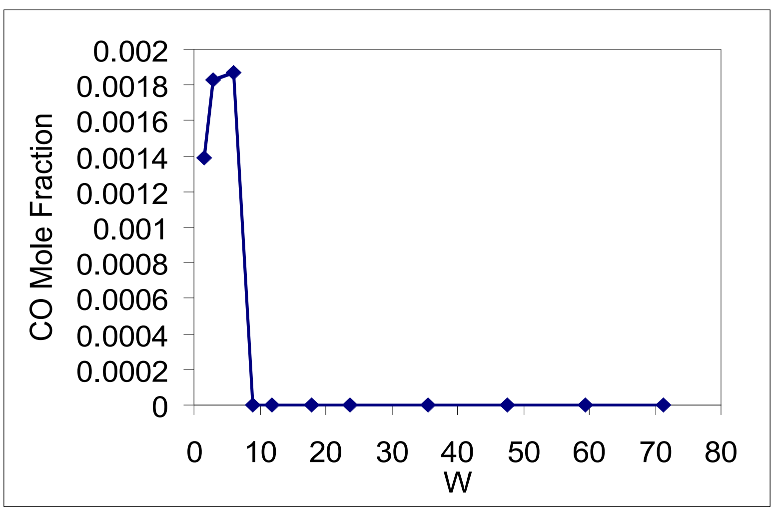

Figure 7. CO mole fraction along the reactor (80% H_2S, 20% CO_2 acid gas).

Figure 8 represents H_2S and SO_2 mole fractions for the combustion of acid gas composition of 70% H_2S and 30% CO_2. Similarly, H_2S decreases to an asymptotic value and SO_2 reaches a peak then decreases somewhat. Figure 9 shows CO mole fraction where higher amounts of CO were observed. Sulfur conversion efficiency was evaluated to be about 3.5%.

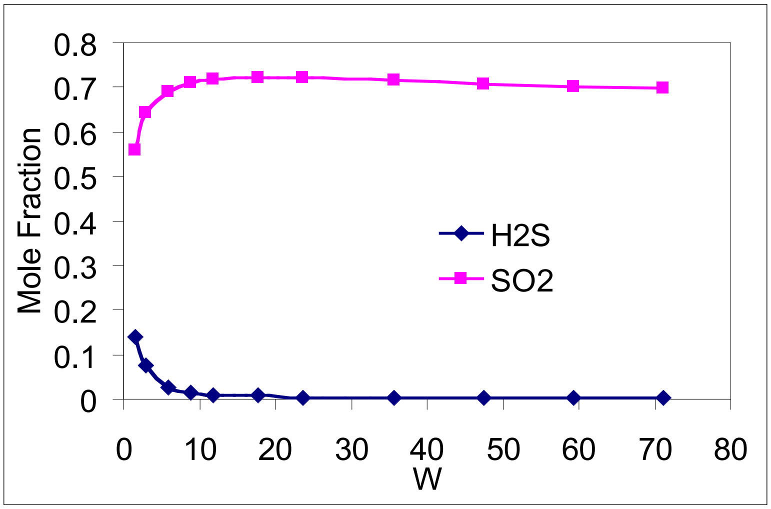

Figure 8. H_2S and SO_2 mole fraction along the reactor (70% H_2S, 30% CO_2 acid gas).

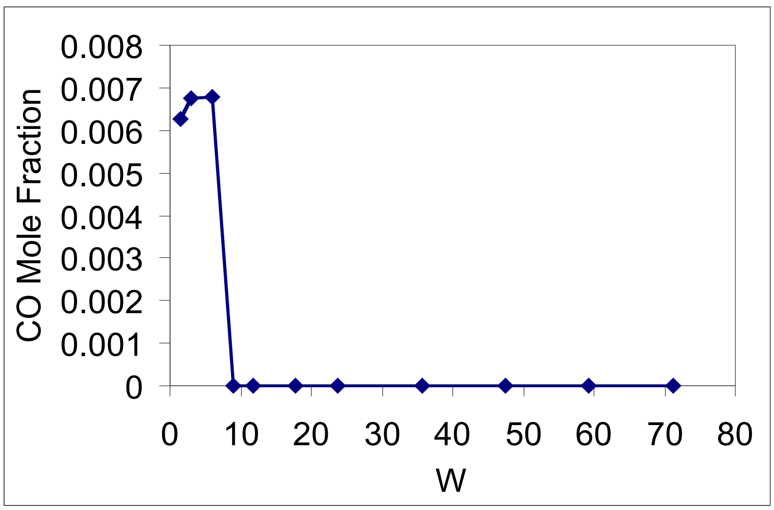

Figure 9. CO mole fraction along the reactor (70% H_2S, 30% CO_2 acid gas).

4.1.3 Combustion of N_2-laden acid gas

Acid gas streams with different nitrogen concentrations were examined in order to assess and identify the role of nitrogen on the chemical reaction. The same baseline case was used (100% H_2S acid gas stream). Figures 10, 11, and 12 show that the H_2S and SO_2 mole fractions of acid gas contained 10% N_2, 20% N_2, and 30% N_2, respectively. The results reveal that the behavior of SO_2 and H_2S does not change significantly with the increase of nitrogen in the acid gas. Nitrogen acts as a diluent of the mixture, which has minimal effect on the reaction of both H_2S and SO_2. These results support the previous findings by Selim and Gupta [4].

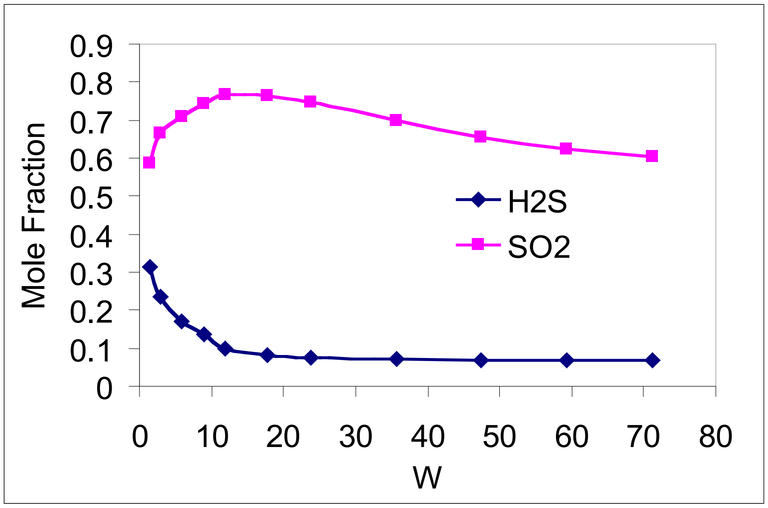

Figure 10. H_2S and SO_2 mole fraction along the reactor (90% H_2S, 10% N_2 acid gas).

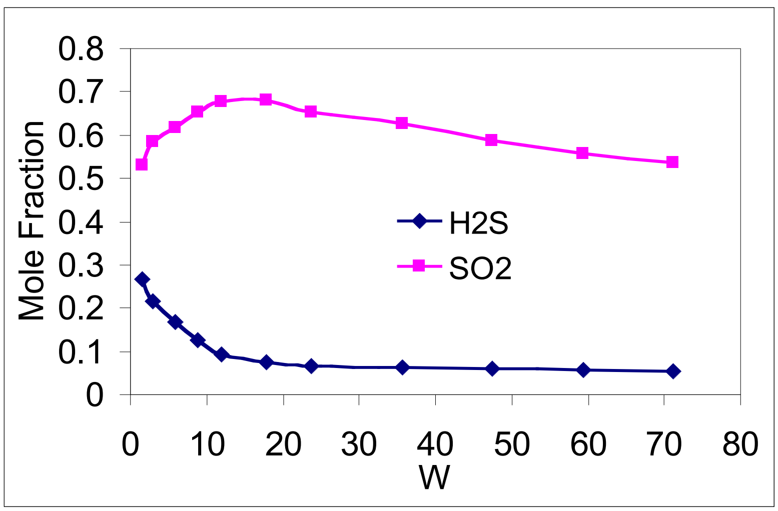

Figure 11. H_2S and SO_2 mole fraction along the reactor (80% H_2S, 20% N_2 acid gas).

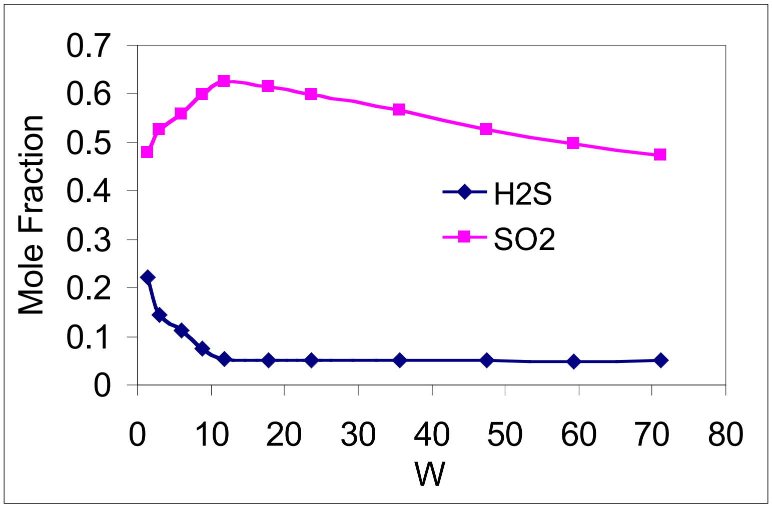

Figure 12. H_2S and SO_2 mole fraction along the reactor (70% H_2S, 30% N_2 acid gas).

4.2 Write technical papers

During the past quarter we submitted an abstract for consideration to the ASM 2012 conference held in January 2012. The abstract has been accepted. We are now preparing the full technical conference paper that will be submitted to the conference. The paper title is "Effect of CO_2 and N_2 Presence in Acid Gas stream on H_2S Combustion." In addition, we submitted a paper to The Journal of Applied Energy entitled "Fate of Sulfur with H_2S Injection in Methane/Air Flames." We are waiting to hear the reviewer's comments.

5. Summary

The study proposed and planned for the past quarter was successfully conducted in this quarter as per plans. Examination of the effect of nitrogen and carbon dioxide presence in H_2S acid gas stream was demonstrated. Concentration of nitrogen and carbon dioxide was varied by up to 30% in the acid gas in increments of 10%. The effect of each gas was examined individually. All the cases examined were compared with the baseline case of 100% H_2S acid gas stream. Temperature measurement showed that injection of CO_2 or N_2 decreases the flame temperature immediately upon injection. However, injection of CO_2 resulted in temperature increase downstream. Increase of carbon dioxide in the acid gas stream increased the SO_2 mole fraction in the product stream. In addition, the increase of CO_2 decreased the asymptotic value of H_2S after combustion. Furthermore, the presence of CO_2 decreased the amount of sulfur captured during the chemical reaction. This is attributed to the increase of the oxidizing medium in the reaction pool that is directly attributed to the presence of carbon dioxide in the mixture. The increase in oxygen dictated that the combustion of H_2S would form higher amounts of SO_2. Subsequently, the amount of sulfur captured and asymptotic value of H_2S decreased. On the other hand, the presence of nitrogen in the acid gas stream did not affect the chemical reaction significantly. Nitrogen acts as a diluent in the reactants, but did not affect the reaction chemically. Two technical papers were written for submission to a conference and a journal publication. The conference paper is to be submitted to the forthcoming Aerospace Sciences Meeting (ASM), to be held in January 2012. The paper title is "Effect of CO_2 and N_2 Presence in Acid Gas stream on H_2S Combustion." The second paper has been submitted to The Journal of Applied Energy with the paper title "Fate of Sulfur with H_2S Injection in Methane/Air Flames."

6. References

[1] Selim, H., Al Shoaibi, A., Gupta, A. K., "Effect of H_2S in methane/air flames on sulfur chemistry and products speciation," The Journal of Applied Energy, Vol. 88, Issue 8, August 2001, pp. 2593-2600.

[2] Selim, H., Gupta, A. K., and Sassi, M., "Implementation of Novel Error Propagation Based Reduction Approach in H2S/O2 Reaction Mechanism," 48th AIAA Aerospace Sciences Meeting (ASM), Orlando, FL, Jan. 4-7, 2009, AIAA-2010-1355.

[3] Selim, H., Gupta, A. K., and Sassi, M., "Reduced Mechanism for Hydrogen Sulfide Oxidation," 47th AIAA Aerospace Sciences Meeting (ASM), Orlando, FL, Jan. 5-8, 2009, AIAA-2009-1392.

[4] Selim, H., Gupta, A. K., and Sassi, M., "Acid Gas Composition Effects on the Reactor Temperature in Claus Reactor," 6th AIAA International Energy Conversion Engineering Conference (IECEC), Cleveland, OH, July 28-30, 2008, AIAA 2008-5797.

7. Difficulties Encountered/Overcome

None

8. Deliverables for the Next Quarter

- Preparation of the experimental setup for near-isothermal examination of Claus reactions
- Preliminary results of near-isothermal Claus process reactions

9. Publications

<u>**Conference Publications**</u>

1. Gupta, A. K. and Sassi, M. "Sulfur Recovery from Acid Gas Using the Claus Process and High Temperature Air Combustion Technology," American J. of Environmental Sciences, Vol. 4, No. 5, 2008, pp. 502-511.
2. Selim, H., Gupta, A. K. and Sassi, M. "Variation of Optimum Claus Reactor temperature with Acid Gas Composition," IECEC Conference, Cleveland, OH, July 28-30, 2008, Paper No. AIAA-2008-5797.
3. Selim, H., Gupta, A. K. and Sassi, M. "Reduced Mechanism for Hydrogen Sulfide Oxidation," 47th AIAA Aerospace Sciences Conference, Orlando, FL, January 5-8, 2009, Paper No. AIAA-2009-1392.
4. Selim, H. and Gupta, A. K. "Nonreactive Study for the Reactants Mixing in Claus Reactions," 7th Intl. Energy Conversion Engineering Conference (7th IECEC), Denver, CO, August 2-5, 2009, Paper No. AIAA-2009-4506.
5. Selim, H, Gupta, A. K. and Sassi, M. "Implementation of Novel Error Propagation Based Reduction Approach in H_2S/O_2 Reaction Mechanism," 48th AIAA Aerospace Sciences Conference, Orlando, FL, January 3-7, 2010, Paper AIAA-2010-1355.
6. Al Amoodi, N., Selim, H., Gupta, A. K., Sassi, M. and Al Shoaibi, A. "Numerical Simulations of the Thermal Stage in Claus Process: Equilibrium and Kinetic Investigation," 48th AIAA Aerospace Sciences Conference, Orlando, FL, January 3-7, 2010, AIAA-2010-1356.
7. Selim, H. Vijayan, V., Al Shoaibi, A., and Gupta, A. K., "Numerical and Experimental Studies on Mixing and Product Species Distribution in a Claus Reactor," 8th Intl. Energy Conversion Engineering Conference (8th IECEC), Nashville, TN, August 2-5, 2010, Paper No. AIAA-2010-7183.
8. Selim, H, Al Shoaibi, A., and Gupta, A. K., "Examination of Emission Spectra from Hydrogen Sulfide Flames," 49th AIAA Aerospace Sciences Conference, Orlando, FL, January 4-7, 2011, AIAA-2011-440.
9. Selim, H, Al Shoaibi, A., and Gupta, A. K., "Spatial Speciation of H_2S Combustion in Methane/Air Flame," To be submitted to 9th International Energy Conversion Engineering

Conference (9th IECEC), San Diego, CA, July 31-August 3, 2011.

10. Selim, H, Al Shoaibi, A., and Gupta, A. K., “Effect of CO_2 and N_2 Presence in Acid Gas stream on H_2S Combustion,” 50th AIAA Aerospace Sciences Conference, Nashville, TN, January 9-12, 2012.

Journal Publications

1. Selim H et al. Novel error propagation approach for reducing H_2S/O_2 reaction mechanism. Appl Energy (2011), doi:10.1016/j.apenergy. 2011.01.047.
2. Selim, H., Al Shoaibi, A., Gupta, A. K., “Effect of H_2S in methane/air flames on sulfur chemistry and products speciation,” The Journal of Applied Energy, Vol. 88, Issue 8, August 2001, pp. 2593-2600.
3. Selim, H., Al Shoaibi, A., Gupta, A. K., “Experimental examination of flame chemistry in hydrogen sulfide-based flames,” The Journal of Applied Energy, Vol. 88, Issue 8, August 2001, pp. 2601-2611.
4. Selim, H., Al Shoaibi, A., Gupta, A. K., “Fate of Sulfur with H_2S Injection in Methane/Air Flames,” Submitted to The Journal of Applied Energy.

Appendix

Justification and Background

Hydrogen sulfide is present in numerous gaseous waste streams from natural gas plants, oil refineries, and wastewater treatment plants, among other processes. These streams usually also contain carbon dioxide, water vapor, trace quantities of hydrocarbons, sulfur, and ammonia. Waste gases with ammonia are called sour gases, while those without ammonia are called acid gases. Sulfur must be recovered from these waste streams before flaring them. Sulfur recovery from sour or acid gas typically involves application of the well-known Claus process, using the reaction between hydrogen sulfide and sulfur dioxide (produced at the Claus process furnace from the combustion of H_2S with air and/or oxygen), yielding elemental sulfur and water vapor: $2H_2S(g) + SO_2(g) = (3/n)\ S_n(g) + 2H_2O(g)$ with $\Delta H_r = -108$ kJ/mol. Therefore, higher conversions for this exothermic, equilibrium-limited reaction call for low temperatures, which lead to low reaction rates that dictate the use of a catalyst. The catalytic conversion is usually carried out in a multistage, fixed-bed, adsorptive reactor process, which counteracts the severe equilibrium limitations at high conversions. This technology process can convert about 96% to 97% of the influent sulfur in H_2S to S. However, higher removal requires critical examination of the process and use of a near isothermal reactor, since the conversion is critically dependent upon the exothermic and endothermic conditions of the reactions.

Flameless combustion has been shown to provide uniform thermal field in the reactor so that the reactor temperature is near uniform. Reactor size can also be reduced and combustion-generated pollutants emissions can be reduced by up to 50%. Energy efficiency can be increased by up to 30%. The application of this technology appears to offer great advantages for the processes under consideration. The UAE, which pumps about 2.4 million bpd of crude oil, is also home to the world's fifth biggest gas reserves at about 200 trillion cubic feet. Abu Dhabi Gas Industries (GASCO), an operating company of the Abu Dhabi National Oil Company (ADNOC), is leading a drive to boost gas production in the UAE from five to seven billion cubic feet per day. This calls for sulfur recovery capacity of over 3,000 metric tons per day with the associated SOx and NOx emissions. Therefore, the adoption and further development of flameless combustion technology for sulfur recovery among other commercial and industrial heating processes is expected to be crucial and beneficial, both economically and environmentally.

The conventional sulfur recovery process is based upon the withdrawal of sulfur by in situ condensation within the reactor. The selective removal of water should, however, be a far more effective technique, as its effect on the equilibrium composition in the mass action equation is much greater. The in situ combination of the heterogeneously catalyzed Claus reaction and an adsorptive water separation seems especially promising, as both reaction and adsorption exhibit similar kinetics, and pressure can be adapted to the needs of the adsorptive separation. Such an adsorptive reactor will lead to almost complete conversion as long as the adsorption capacity is not exhausted. There are numerous possibilities for implementing these two functions, ranging from fixed-beds with homogeneous catalyst/adsorbent mixtures to spatially structured distributions or even fluidized beds. Most of the previous studies have concentrated on the Claus catalytic conversion reactors and the TGTU. However, some previous studies have identified the Claus furnace as one of the most important yet least understood parts of the modified Claus process. The furnace is where the combustion reaction and the initial sulfur conversion (through an endothermic gaseous reaction) take place. It is also where the SO_2 required by the downstream catalytic stages is produced and the contaminants (such as ammonia and BTX (benzene, toluene, xylene) are supposedly destroyed. The main two reactions in the Claus furnace are: $H_2S + 3/2\ O_2 = SO_2 + H_2O$, with $\Delta H_r = -518$ kJ/mol, and $2H_2S + SO_2 = 3/2\ S_2 + 2H_2O$, with $\Delta H_r = +47$ kJ/mol. This last endothermic reaction is responsible for up to 67% conversion of the sulfur at about 1200 °C. Moreover, many side reactions take place in the furnace; these side reactions reduce sulfur recovery and/or produce unwanted components that end up as ambient pollutant emissions. Therefore, it would be useful to combine the endothermic and exothermic process using an isothermal reactor offered by flameless oxidation combustion.

Approach

Critical review

We propose to conduct a critical review of the various approaches used for sulfur removal from the sour gas. The emphasis here will be on sulfur chemistry with due consideration to the fate of ammonia. Following the review, an experimental and a CFD numerical study of the flameless oxidation of the fuel will be conducted as follows:

CFD simulation

A numerical simulation study of the flame under normal and flameless oxidation of fuels in the furnace will be conducted using the available codes. Global features of the flow and thermal behavior will be obtained using the Fluent CFD and Chemkin computer codes. These codes provide detailed simulation of the flow, thermal and chemical behaviors (i.e., detailed chemistry) in the reactor flow using gas-phase reactants. The sulfur in the fuel is in gas phase, so we will be able to simulate and monitor the fate of sulfur during various stages of endothermic and exothermic reactions and over a range of temperature regimes, including those covered in the Claus furnace process. The simulation results will also guide the final design of the flameless furnace. The simulations will also help assist in the experimental program for data validation with the eventual goal of implementing the process for sulfur removal.

Experimental study

An experimental study of the flameless vs. normal flame combustion process for the conditions examined in the theoretical study, including that of Claus furnace, will be conducted. We will explore the operating conditions and the exhaust gas analysis under conditions of both flame and flameless modes to determine the extent of sulfur conversion under the two conditions over the temperatures that can simulate endothermic and exothermic conditions in the Claus furnace. The goal is to seek conditions that yield the highest sulfur recovery from a process. To some extent, these conditions will be based on the composition of the acid/sour gas, from sulfur-rich (> 50% H_2S) to lean (< 20% H_2S). It is expected that our fundamental information will contribute to the eventual design guidelines of an advanced sulfur recovery process furnace operating under flameless combustion mode.

Separate Sensible and Latent Cooling with Solar Energy

UMD Investigators: Reinhard Radermacher, Yunho Hwang
GRA: Ali Al-Alili
PI Investigator: Isoroku Kubo
Start Date: August 2007

1. Objective/Abstract

The main objective of this project is to design, fabricate and test a solar cooling system with the highest possible cooling COP measured to date. The approach involves combining a very efficient concentrating PV-T collector with separate sensible and latent cooling approach developed at CEEE. This solar cooling system is expected to operate under the UAE's harsh climate conditions.

2. Deliverables for the Completed Quarter

These are the accomplished tasks:

- Finished the shakedown test
- Charged optimization testing
- Started the actual test

3. Summary of Project Activities for the Completed Quarter

The focus of this quarter was to carry out a shakedown test of the complete experiment. Once the system operated as expected, a refrigerant charge optimization test was carried out to determine the charge that gives the highest coefficient of performance. After that, the actual testing was started and some time was spent on improving the energy and mass balances.

3.1 Vapor Compression Cycle Testing

A charge optimization testing was carried out in order to determine the charge that gives the highest coefficient of performance. The indoor and outdoor conditions are based on ASHRAE Test-A conditions. The optimal refrigerant charge was found to be about 1250 g, as shown in Figure 1.

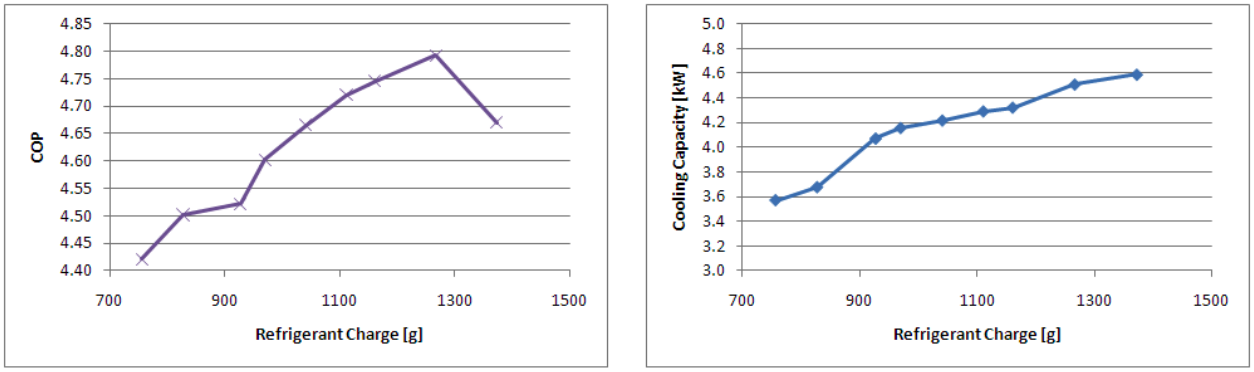

Figure 1. Charge optimization results.

3.2 Desiccant cycle testing

The first round of testing investigated the performance of the desiccant and sensible wheel performance. The testing was carried out at ARI- humid weather conditions. The following performance indices were used:

- Moisture Removal Capacity (MRC)

$$MRC = \dot{m_1} \Delta x_{1,2}$$

- Moisture Mass Balance (MMB)

$$MMB = \frac{\dot{m_1} \Delta x_{1,2}}{\dot{m_9} \Delta x_{8,9}}$$

- Total Energy Balance (TEB)

$$TEB = \frac{\dot{m_1} \Delta h_{1,2}}{\dot{m_9} \Delta h_{8,9}}$$

- Latent Coefficient of Performance (COP_{Lat})

$$COP_{Lat} = \frac{\dot{m_1} h_{fg} \Delta x_{1,2}}{\dot{m_9} \Delta h_{7,8}}$$

- Total Coefficient of Performance (COP_{tot})

$$COP_{tot} = \frac{m_1^{\bullet} \Delta h_{1,2}}{m_9^{\bullet} \Delta h_{7,8}}$$

The moisture removal capacity as a function of the wheel rotational speed is shown in Figure 2. As the temperature increases, the MRC increases. The figure shows that there is an optimal speed where the MRC value is maximum.

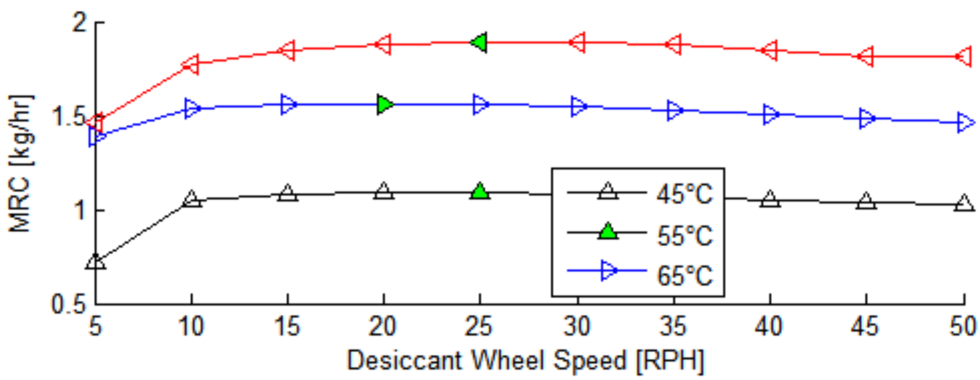

Figure 2. MRC at different regeneration temperatures.

Figure 3 shows the moisture mass balance which should be maintained within 5% based on ASHRAE standards.

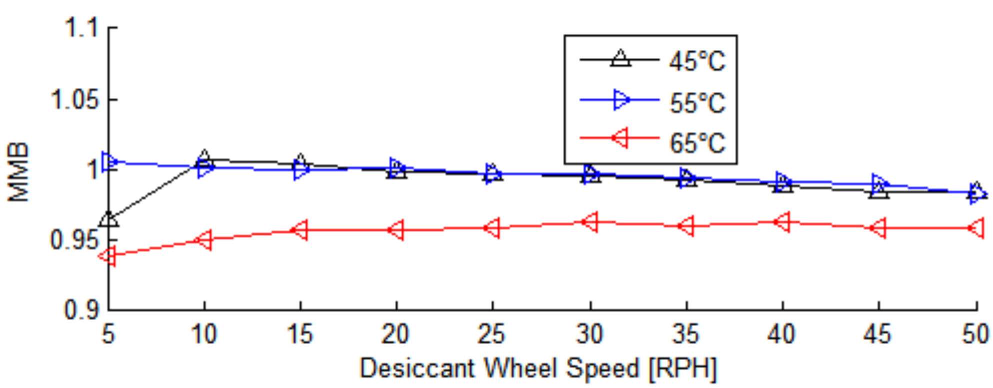

Figure 3. MMB at different regeneration temperatures.

Figure 4 shows the latent coefficient of performance of the desiccant wheel. It is the ratio of the latent capacity of the wheel to the heat provided to regeneration the wheel.

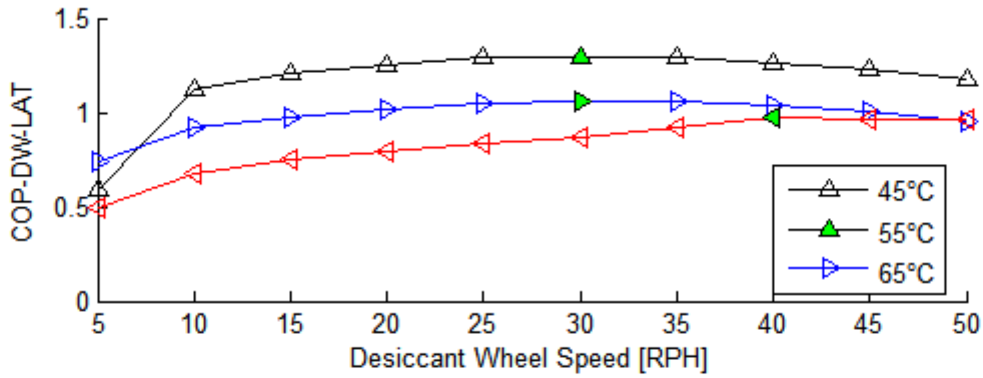

Figure 4. COP Latent of the desiccant wheel at different regeneration temperatures.

Figure 5 shows the total coefficient of performance. This figure shows that once the optimal speed is exceeded, the desiccant wheel speed
increases.

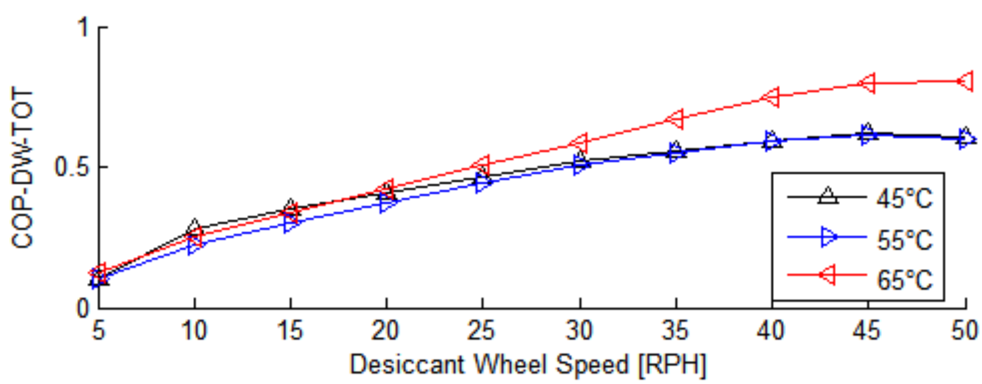

Figure 5. The total COP of the desiccant at different regeneration temperatures.

Figure 6 shows the total energy balance of the desiccant wheel. The goal is to maintain the energy balance within 10%. However, the figure shows that this limit is exceeded at lower rotational speeds. The reason is that the lower rotational speeds allow more time for heat lost from the circumference of the wheel.

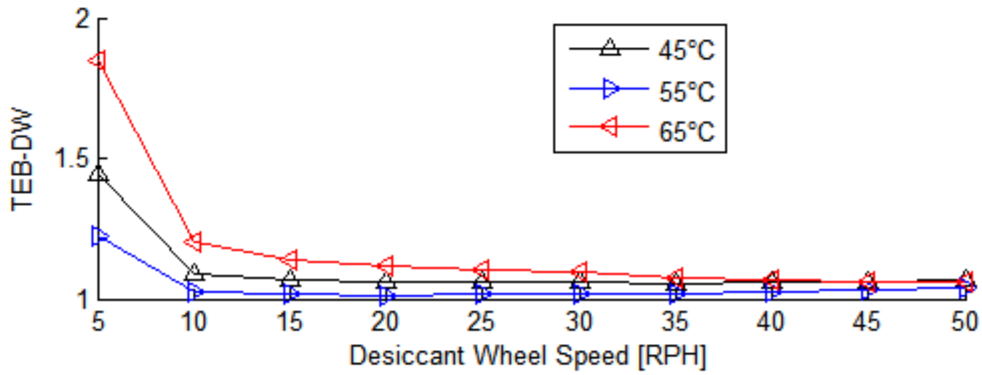

Figure 6. The total energy balance of the desiccant wheel.

4. Difficulties Encountered/Overcome

The exhaust duct collapses at higher mass flow rates due to higher negative pressure applied by the suction fan.

5. Planned Project Activities for the Next Quarter

The following activities are to be conducted in the next quarter:

- Finish the desiccant wheel cycle testing
- Start the complete cycle (VCC+DWC) testing

6. References

[1] Stine, W.B., Geyer, W.B., 2001, Power from the sun, www.powerfromthesun.net.
[2] Threlkeld,.J, Kuehn, T., Ramsy, J.,1998, Thermal Environmental Engineering, Prentice-Hall, Inc, USA
[3] http://www.nrel.gov/rredc/solar_data.html
[4] http://rredc.nrel.gov/solar/old_data/nsrdb/tmy2/State.html
[5] Notton, G., Poggi, P., Cristofari, C., 2006, Predicting hourly solar irradiations on inclined surfaces based on the horizontal measurements: Performances of the association of well-known mathematical models, *Energy Conversion and Management*, 47 1816–1829
[6] http://rredc.nrel.gov/solar/old_data/nsrdb/1991-2005/siteonthefly.cgi?id=724060
[7] ASHRAE, 1999, Applications Handbook, CH.32
[8] Kreith, F. and Kreider, J.F., 1978, Principles of solar engineering, *Hemisphere publishing corporation* Washington USA
[9] Kalogirou, S., 2004, Solar thermal collectors and applications, *Progress in Energy and Combustion Science* 30 pp. 231–295
[10] Goswami, Y., Kreith, F. and Kreider, J.F., 2000, Principles of solar engineering, *Taylor and Francis,* PA, USA,
[11] Duffie, J.A., Beckman, W.A., 1991, *Solar engineering of thermal processes*, Second edition, John Wiley & Sons, Inc., New York, ISBN: 0-471-51056-4.

[12] Pasupathy, A., Velraj, R., Seeniraj, R.V., 2008, Phase change material-based building architecture for thermal management in residential and commercial establishments, *Renewable and Sustainable Energy Reviews*, pp.39–64
[13] Dieng, A., Wang, R. , 2001 Literature Review on Solar Adsorption Technologies of Ice-making and Air Conditioning Purposes and Recent Developments in Solar Technology, *Renewable and Sustainable Energy Reviews* 5 pp.313–342
[14] Sumathy, K., Yeug, K, Yong, L., 2003, Technology Development in the Solar Adsorption Refrigeration Systems, *Progress in Energy and Combustion Science* 29 pp 301–327
[15] Roger, A. Messenger, J. V., 2005, Photovoltaic Systems Engineering, 2nd ed. Taylor & Francis
[16] http://www.nfpa.org/
[17] http://ieeexplore.ieee.org/iel5/7946/21930/01019771.pdf?arnumber=1019771
[18] TRANE, "Product Data: 4DCZ6036A through 4DCZ6060A" (2008), 22-1815-03
[19] METEONORM, "Global Meteorological Database for Engineers, Planners and Education,"(2007)

Waste Heat Utilization in the Petroleum Industry

UMD Investigators: **Reinhard Radermacher, Yunho Hwang**
GRAs: **Amir Mortazavi, Abdullah Alabdulkarem**
PI Investigators: **Saleh Al Hashimi, Peter Rodgers**
GRAs: **Sahil Popli, Alyas Ali Alshehhi**
Start Date: **October 2006**

1. Objective/Abstract

The main objective of this project is to minimize overall energy consumption of gas or oil processing plants and reduce their CO_2 emission by utilizing waste heat and/or improving cycle design with CO_2 capture and sequestration. Consideration will include the use of absorption chillers and steam cycles, among other options.

2. Deliverables for the Completed Quarter

The following were modeled or explored using HYSYS:

1. Optimization of six steam cycles with steam extraction for CO_2 regeneration.
2. Investigation of the power increase due to feed water preheating.
3. Development of a robust optimization technique for solving problems with uncertainty

3. Summary of Project Activities for the Completed Quarter

HYSYS and Matlab were used to optimize previously developed steam cycle configurations with steam extractions for CO_2 regeneration. Results show that the optimized steam cycle's power increased from 1.88% to 7.55%. Further, the increase in power due to feed water preheating was investigated.

Two configurations—the gas turbine combined cycle with double pressure steam cycle and the gas turbine triple combined cycle with double pressure steam cycle and absorption chillers—were optimized as an APCI LNG plant driver cycle. The best option according to our models consumes 38.2% less fuel than the baseline cycle.

3.1 Optimization of six steam cycles with steam extraction for CO_2 regeneration

The developed steam cycle configurations were optimized using GA of Matlab optimization toolbox. The objective function of the optimization is to increase power production of the steam cycles. The variables of the optimization are (1) steam mass flow rate, (2) steam superheat temperature, (3) steam pressure, and (4) steam split ratio in case of steam splitting configurations (partial steam extraction and parallel steam turbines configurations). The range of the optimization variables was ±20% of the baseline values, except for the steam pressure, where it was limited to just below the critical point pressure. The optimization's seven constraints with limits taken from the baseline model are listed as follows:

1) Temperature of the exhaust gas after HRSG ≥ 140°C
2) Extracted steam pressure ≥ 3 bar
3) Extracted steam load = 70.42 MW
4) Turbine outlet vapor quality ≥ 0.87
5) Economizer, evaporator, and superheater heat exchangers pinch temperatures ≥ 3 K

The results of the optimization are listed in Table 1. The difference in the gas turbine power is due to different back pressures. The exhaust gas in configurations with CCS need to be at a higher pressure to overcome the pressure drop resulting from the exhaust gas cooling heat exchangers and CO_2 absorber column. For example, the assumed exhaust pressure after the gas turbine is 1.55 bar for the “Diverting the Entire Steam Flow” configuration, whereas it is 1.16 bar for baseline NGCC without the CCS configuration. Higher exhaust pressure resulted in higher exhaust temperatures leaving the gas turbine. Thus, higher heat is available in the HRSG, which made steam cycles with CCS produce more power than steam cycles without CCS, but the total NGCC power consumption is different.

The optimization resulted in a steam cycle power increase from 1.88% to 7.55%. In all configurations the optimum boiler pressure and superheat temperature were increased as expected from Carnot cycle efficiency. The highest NGCC power-producing configuration was the “Diverting the Entire Steam Flow” configuration, producing 170.48 MW power. The second highest was the “Parallel Steam Turbines” configuration, producing 169.18 MW NGCC power.

Table 1. Optimization results of the developed configurations

		Baseline					
Configuration	GT Power (MW)	ST Power (MW)	m_{steam} (kg/s)	T_{sh} (°C)	P_{boiler} (bar)	Split Ratio	NGCC Power (MW)
BS NO CCS	119	70.09	61.11	540	120	-	189.09
Diverting the Entire Steam Flow	94.7	70.46	71.88	552	120	-	165.16
Partial Steam Extraction	94.7	68.11	70.94	552	120	0.44	162.81
Parallel Steam Turbines	94.7	69.96	71.75	552	120	0.453	164.66
Exhaust Gas Fired Stripper	93.57	54.73	46.81	556.7	120	-	148.3
Condenser as a Boiler and a Desorber (Higher T_{FG})	106.6	55.41	79.39	510.3	200	-	162.01
Condenser as a Boiler and a Desorber	94.7	60.93	79.39	565.9	210	-	155.63
	Optimum						
	ST Power (MW)	m_{steam} (kg/s)	T_{sh} (°C)	P_{boiler} (bar)	Split Ratio	CC Enhancement (MW)	CC Enhancement (%)
BS NO CCS	71.37	60.712	559.01	140.95	-	1.27	1.82
Diverting the Entire Steam Flow	75.78	71.47	608.26	219.96	-	5.32	7.55

Partial Steam Extraction	72.61	70	592.9	141	0.46	4.498	6.6
Parallel Steam Turbines	74.48	70.46	608.26	192.26	0.468	4.52	6.46
Exhaust Gas Fired Stripper	57.53	46.07	610.53	194.6	-	2.8	5.12
Condenser as a Boiler and a Desorber (Higher T_{FG})	58.62	74.09	584.16	220	-	3.21	5.78
Condenser as a Boiler and a Desorber	62.85	76.44	608.26	220	-	1.92	3.15

3.2 Using Waste Heat to Preheat the Water before HRSG

Three waste heat sources in the integrated CCS system were identified. The first one is the waste heat in the flue gas after the combined cycle. The second one is the waste heat in the regenerated CO_2 stream. The third one is the wasted cooling in the liquefied and pressurized CO_2. Many options were proposed for using the available waste heat as shown in Figure 1.

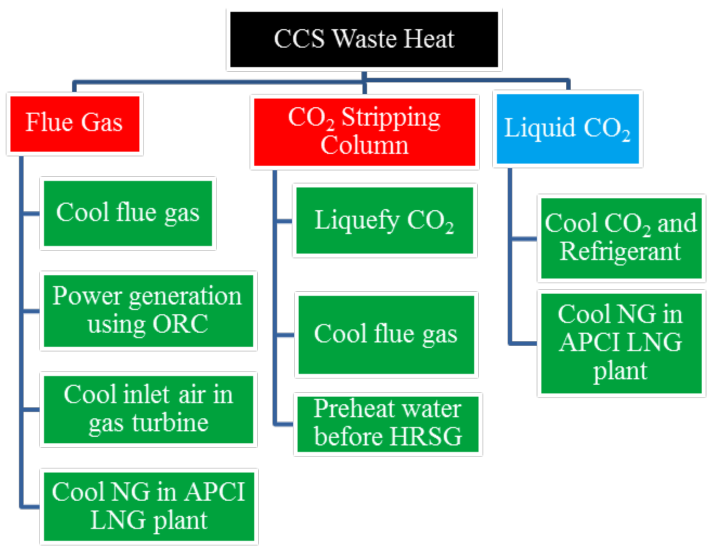

Figure 1. CCS waste heat classifications. Red: waste heat sources; Blue: cold sources; Green: potential uses for waste heat.

One of the proposed uses of the waste heat was to preheat the water before HRSG, which would cause the HRSG to generate more steam for equivalent heat. A preheater heat exchanger that uses a portion of the stripper condenser heat (23 MW at 105 °C to 80 °C) was placed between the HRSG and the pumps to preheat the water to 102 °C in all configurations except the "Condenser as a Boiler and a Desorber" configuration because the condensed water temperature was at 133 °C. The results in Table 2 show that the highest power increase was 7.65% in the "Exhaust Gas Fired Stripper" configuration because this configuration has the lowest condensing temperature (45°C) or feed water temperature to the HRSG without the preheater.

Table 2. Steam cycle power using preheater before HRSG

Configurations	Power w/o Preheater (MW)	Preheater Heat (MW)	Power w/ Preheater (MW)	Power Increase (MW)	Power Increase (%)
Diverting the Entire Steam Flow Configuration	75.78	3.84	77.25	1.46	1.93
Parallel Steam Turbines Configuration	74.48	4.66	76.02	1.55	2.08
Partial Steam Extraction Configuration	72.61	7.53	74.98	2.38	3.28
Exhaust Gas Fired Stripper Configuration	57.53	11.79	61.93	4.4	7.65

3.3 Developing robust optimization techniques

One of the barriers to the development of small remote gas fields is transportation of natural gas from these reservoirs to a specific market is that it is not economical to transport natural gas for long distances through a pipeline. On the other hand, it is not economical to build a stationary LNG plant for a small natural gas reservoir. One solution to this problem might be the development of mobile LNG plants. There are several uncertainties involved in the design of mobile LNG plants, including the natural gas composition (feed gas composition). It should be noted for a mobile LNG plant that the design should be insensitive to the natural gas composition of the gas field. Moreover, the mobile LNG plant should be energy efficient. The enhancement options of the first research task of this project could be implemented in design of mobile LNG plant based on APCI liquefaction technology. However, the big challenge is development of a refrigerant mixture that is both efficient and insensitive to the natural gas composition. Here, the efficient refrigerant mixture refers to a refrigerant mixture composition that leads to minimum amount of energy consumed per unit mass of produced LNG. To develop this refrigerant mixture optimization techniques should be employed. However, conventional optimization techniques cannot handle problems involving uncertainty. Robust optimization techniques would be the most suitable choice based on the design goal, which is operability of the mobile LNG plants for different natural gas compositions. However, to the best of our knowledge the current optimization techniques are either incapable of solving the optimization problem, which involves the simulation model of the LNG plant, or computationally prohibitive. We are currently addressing this issue by developing a novel robust optimization technique. The developed robust optimization technique will be used to develop a refrigerant mixture that is insensitive to the feed gas composition. This refrigerant will be applicable in both stationary APCI LNG plant dealing with different feed gas composition and mobile APCI LNG plants.

4. Difficulties Encountered/Overcome

None.

5. Planned Project Activities for the Next Quarter

The following activities are to be conducted in the next quarter:

- Use pinch analysis to evaluate further savings
- Integrate the proposed uses of the waste heat in the CCS plant
- Optimize mobile LNG plants using robust optimization

6. References

[1] Dopazo J. A., and Fernández-Seara J., 2010, "Experimental evaluation of a cascade refrigeration system prototype with CO_2 and NH_3 for freezing process applications," International Journal of Refrigeration, pp. 1-11.

[2] Venkatarathnam G., 2008, Cryogenic Mixed Refrigerant Processes, Springer-Verlag New York, LLC,.

[3] Paradowski H., Bamba M. O., and Bladanet C., 2004, "Propane Precooling Cycles for Increased LNG Train Capacity," 14th International Conference and Exhibition on Liquefied Natural Gas, pp. 1-18.

[4] Alefeld, G., Radermacher, R., 1994, "Heat conversion systems", CRC Press, Boca Raton.

[5] Al-Hamdan, Q.Z., Ebaid, M.S.Y., 2006, "Modeling and simulation of a gas turbine engine for power generation", ASME Journal of Engineering for Gas Turbines and Power, Vol. 128, pp. 302-311.

[6] LNG technology selection,

[7] http://www.fwc.com/publications/tech_papers/files/TariqLNG.pdf, Last access, June, 2008

[8] Haring, H., 2008, " Industrial Gas Processing", Wiley-VCH, Weinheim

[9] ASHRAE, 2002, "ASHRAE Refrigeration Handbook", American Society of Heating, Refrigeration and Air-Conditioning Engineers, Atlanta, GA, USA.

[10] ASHRAE, 2005, "ASHRAE Fundamentals Handbook", American Society of Heating, Refrigeration and Air-Conditioning Engineers, Atlanta, GA, USA.

[11] Brant, B., Brueske, S., Erickson, D.C., Papar, R., 1998, "New waste-heat refrigeration unit cuts flaring, reduces pollution", Oil & Gas Journal, May 18, pp.61-64.

[12] Brooks, F.J., 2000 "GE gas turbine performance characteristics", GE Power Systems Schenectady, NY, GER-3567H.

[13] Cohen, H., Rogers, G.F.C., Saravanamuttoo, H.I.H., 1996, "Gas turbine theory", 4th edition, Longman Scientific & Technical, Singapore.

[14] Erickson, D.C., 2000 "LPG recovery from reformer treat gas", US Patent 6,158,241.

[15] Erickson, D.C., Anand, G., Papar, R.A., Tang, J., 1998, "Refinery waste heat powered absorption refrigeration – cycle specification and design", Proceeding of the ASME Advanced Energy System Division, AES-Vol. 38, pp.391-402.

[16] Erickson, D.C., Kelly, F., 1998, "LPG recovery from refinery by waste heat powered absorption refrigeration", IECEC-98-079, 33rd Intersociety Engineering Conference on Energy Conversion, Colorado Springs, CO.

[17] Giampaolo, T., 2003, "The gas turbine handbook: principles and practices", 2nd edition, The Fairmont Press, Lilburn, GA.

[18] Herold, K.E.; Radermacher, R., Klein, S, 1996, "Absorption chillers and heat pumps", CRC Press, Boca Raton.

[19] Kim, T.S., Hwang, S.H., 2006, "Part load performance analysis of recuperated gas turbine considering engine configuration and operation strategy", Energy, Vol. 31, pp., 260-277.

[20] Klein, S.A., 2005, "Engineering Equation Solver" F-Chart Software.

[21] Kurz, R., 2005, "Gas turbine performance", 44th Turbomachinery Symposium, pp.131-146.

[22] Kurzke, J., 2003, "Model based gas turbine parameter corrections", GT2003-38234, Proceedings of 2003 ASME TURBO EXPO: Power for Land, Sea, & Air, Atlanta, GA, USA.

[23] Li, Y.G., Pilidis, P., Newby, M.A., 2006, “An adaptation approach for gas turbine design-point performance simulation”, Journal of Engineering for Gas Turbines and Power, Vol. 128, pp. 789-795.
[24] Orlando, J. A., 1996, “Cogeneration design guide”, American Society of Heating, Refrigeration and Air-Conditioning Engineers, Atlanta, GA.
[25] Pande, M., 1996, “Tools for fractionator design in ammonia-water absorption machines”, Master Thesis, University of Maryland, College Park.
[26] Walsh, P.P., Fletcher, P., 1998, “Gas turbine performance”, Blackwell Science, Oxford.

Appendix

Justification and Background

Waste heat utilization opportunities are abundant in the oil and gas industry. Proper use of waste heat could result in improved cycle efficiency, reduced energy usage, reduction in CO_2 emissions, and increased production capacity.

CEEE at the University of Maryland has extensive experience in the design and implementation of integrated combined cooling, heating, and power (CCHP) projects. The faculty at PI has experience in the design and operation of petroleum processing plants. Jointly the team is well equipped to address the challenge posed by this project.

Thrust 2
Energy-Efficient Transport Processes

Multidisciplinary Design and Characterization of Polymer Composite Seawater Heat Exchanger Module

PI Investigator: **Peter Rodgers**
UMD Investigators: **Avram Bar-Cohen, Satyandra K. Gupta, David Bigio, H.A. Bruck**
GRAs: **Juan Cevallos, F. Robinson, T. Hall, W. Pappas, A. Lederer**
Start Date: **Oct 2006**

1. Introduction

Heat exchangers are extensively used in all oil and gas processing operations with seawater as the preferred coolant in near-shore operations. The performance and cost effectiveness of conventional metallic heat exchangers in such environments are severely constrained by corrosion and scale deposits. Polymer heat exchangers, currently under investigation by the EERC team, offer a promising alternative to metallic heat exchangers for the fossil fuel industry. Recent advances in carbon-fiber polymer composites, yielding polymer materials with thermal conductivities equal to or higher than titanium, can be applied to the development of low-cost and low-weight compact heat exchangers for corrosive fluids. These attributes, combined with the low energy investment in the formation and fabrication of these polymer heat exchangers and their ease of manufacturing, appear to make near-term applications of seawater polymer heat exchangers viable. Numerical simulations and laboratory experiments, performed by the UMD/PI EERC team in the first phase of this research, strongly support these conclusions.

2. Milestones/Deliverables for the Completed Quarter

I. Several heat exchanger prototypes made by Fused Deposition Modeling were tested at the HX test rig at the University of Maryland (Task A1)
II. Developed and utilized thermomechanical finite element model to assess thermal and structural performance of a polymer composite heat exchanger module (A2)
III. Assessed the effects on geometric variation on the development of thermomechanical stresses in polymer composite heat exchangers (A2)
IV. Constructed model for moldability-based feasibility boundary (Task B1)
V. Removed features for efficient assessment of mold-filling feasibility of finned-plate geometries (Task B1)
VI. Developed a fiber orientation measurement methodology (Task B2)
VII. Prepared specimens with micro and nanoscale ingredients to study mixing effects in a Twin Screw Extruder to characterize the development of multi-scale structure and associated properties for these novel polymer composites for PHX applications (Task C1)
VIII. Frank Robinson successfully defended his M.S. thesis on “Thermomechanical Behavior of Polymer Composite Heat Exchangers”
IX. A paper entitled “Polymer Heat Exchangers – An Enabling Technology for Water and Energy Savings” was accepted at the 2011 International Mechanical Engineering Congress & Exposition in Denver, Colorado (Task A2)
X. A paper entitled “Modeling and Validation of Prototype Thermally Enhanced Polymer Heat Exchanger” was accepted at the 2011 International Mechanical Engineering Congress & Exposition in Denver, Colorado (Task A2)

XI. A paper entitled “An Integrated Approach to Design of Enhanced Polymer Heat Exchangers” was accepted for publication at the Journal of Mechanical Design (Task B1)

XII. Presented paper entitled “An Integrated Approach to Design of Enhanced Polymer Heat Exchangers” to DETC Conference to be held on August 29-31 2011 in Washington, DC (Task A2)

3. Summary of Project Activities for the Completed Quarter

3.1 Several polymer heat exchanger prototypes made with Fused Deposition Modeling were tested at the HX test rig at the University of Maryland (Task A1)

Several heat exchangers (HX) were built using Fused Deposition Modeling (FDM). The candidate materials chosen were polycarbonate, polyetherimide (ULTEM), and a filled polycarbonate resin with enhanced thermal conductivity. The geometry for these HXs was the webbed-tube heat exchanger (WTHX). The thermal performance of a WTHX for a gas/liquid application was discussed in previous progress reports. The WTHX was shown to provide the same heat transfer rate as a plate-fin HX but by using less mass; i.e., the WTHX transfers more heat per unit HX mass.

Figure 1 shows a 3D sketch of WTHX geometry, while Figure 2 shows dimensions of the initial WTHX design.

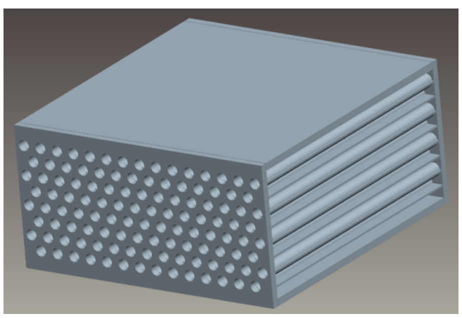

Figure 1. 3D Sketch of WTHX.

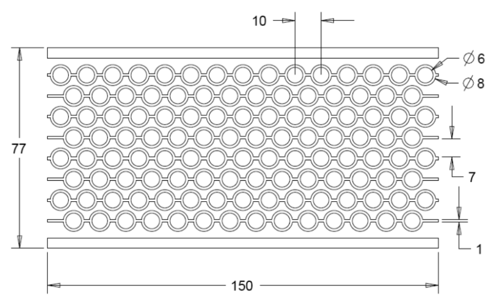

Figure 2. WTHX dimensions in mm.

In the previous progress report, it was reported that an optimum orientation to build the WTHX using FDM was chosen in order to minimize the amount of support material. The direction of layer addition was aligned with the water tubes axes, i.e., the direction perpendicular to the plane shown in Figure 2. Also, some features were added to the WTHX geometry to minimize the amount of support material even further. The features were 45° cones around the tube walls (shown in Figure 3), and 45° inside-chamfers at the intersection of the vertical walls and the ceiling. These features created a support structure for the tube sheet on top of the HX (see the front face of HX in Figure 1). The angle of the features allowed them to be built without support material. The resulting support structure is shown in Figure 4 below.

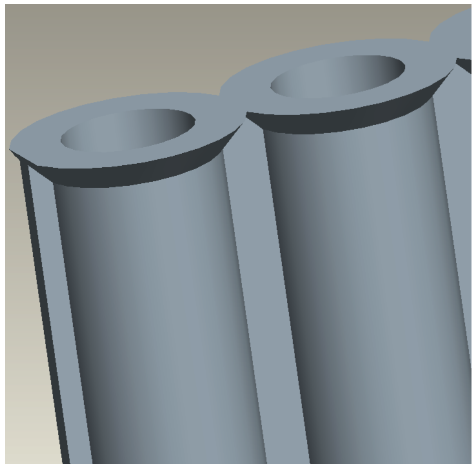
Figure 3. 45° cones around tube walls.

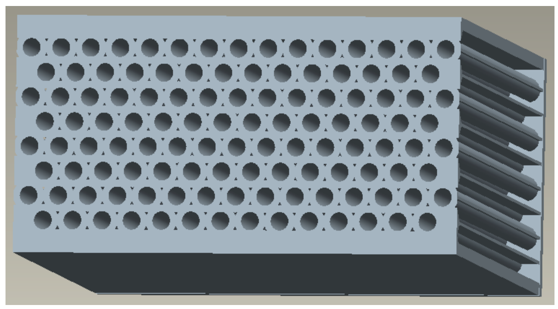
Figure 4. Supporting surface for tube sheet (gaps < 1.27 mm).

The WTHX shown in Figure 2 was tested for water leaks at flow rates between 40 and 60 cm^3/s at building pressure. The initial tests revealed significant water leaks from the tubes, specifically at regions where the tube joins the plate webbing. Figure 5 shows a picture of an ULTEM HX during testing. Water flows inside the tube from right to left in the picture, and water droplets accumulated in the corner between the tube and the webbing.

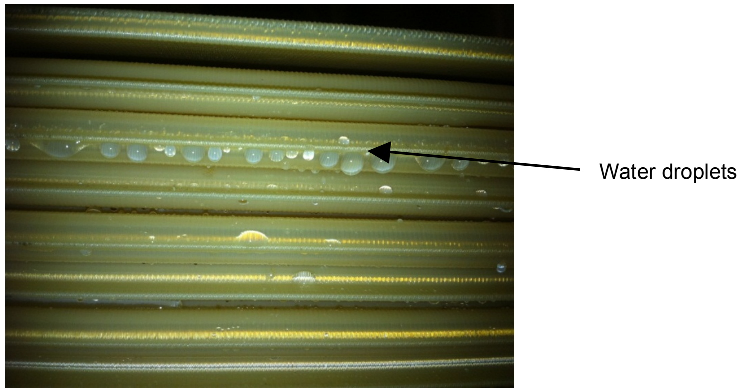

Figure 5. ULTEM HX tested for water leaks.

Stratasys, the company that built all the HXs for this experiment, redesigned the tool path used to build the WTHX geometry in order to create a continuous tool path, as opposed to two independent paths. Figure 6 shows sketches of the original and the optimized tool path. The optimized tool path makes one continuous path and minimizes the opportunity of porosity.

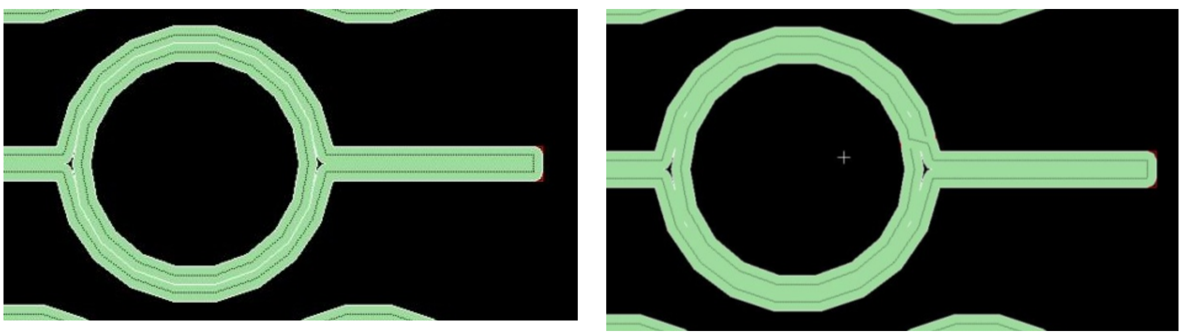

(a) Original tool path (b) New tool path

Figure 6. FDM tool path for WTHX geometry.

Using the optimized tool path, Stratasys used a smaller HX design to build two new HXs using unfilled and filled polycarbonate. The new design (shown in Figure 7) had larger spacing between tubes and between plates. This was done in order to facilitate any repairs needed for possible water leaks. Fortunately, the optimized tool path created a leak-free WTHX, and thermal tests followed.

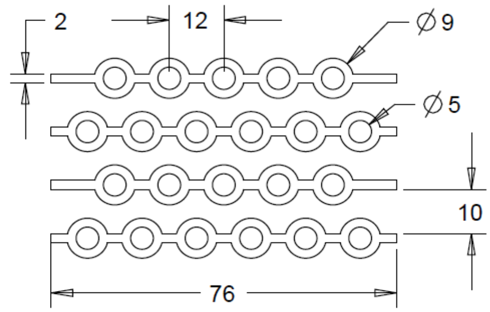

Figure 7. New WTHX geometry (tube length = 120 mm).

Testing of all HXs has commenced, and some preliminary data were collected using the HX test rig described in previous progress reports. Room air was heated to 120 °C at the HX inlet, while water at 27 °C was used to cool the air inside the WTHX. Water and air flow rates were recorded, as well as bulk temperatures at the inlet and outlet of each fluid stream.

The data recorded were used to calculate a heat transfer rate using the air-side temperature drop and flow rate. The water temperature rise was negligible for the range of data recorded so far, so the air-side temperature drop was preferred for heat transfer calculations. The heat transfer rate is a simple mass balance using the HX as a control volume and neglecting mass and energy losses:

$$\dot{q} = \dot{m} c_p \Delta T \tag{1}$$

Using the calculated heat transfer rate, the HX thermal conductance *UA* was calculated using the logarithmic-mean temperature difference (LMTD):

$$\dot{q} = UA \cdot LMTD \tag{2}$$

The thermal conductance was also calculated analytically using standard heat transfer correlations for simultaneously developing laminar flow to calculate the average heat transfer coefficients of both fluid streams. The effective thermal conductivity was left as a tuning parameter to fit to the experimental data. The *UA* was calculated as:

$$UA = \frac{1}{\frac{1}{(\eta_o hA)_h} + \frac{\ln\left(D_o/D_i\right)}{\pi k_w L} + \frac{1}{(hA)_c}} \tag{3}$$

The webbings were modeled as an extended surface, so a surface efficiency was applied to the air-side convective thermal resistance.

Preliminary results of the HX test data are shown in Figure 8. The plot shows the HX thermal conductance *UA* as a function of the air-side flow rate for the filled and unfilled polycarbonate HXs. The air-side temperature drop was 40 K on average, and the heat transfer rate was 65 W on average for the range of flow rates tested. The *UA* results reveal that no significant difference in thermal conductivity exists between the filled and unfilled polycarbonate materials in order to significantly affect the *UA*. This was somehow expected since the filled material was originally targeted by Stratasys to improve the electrical conductivity and not the thermal conductivity.

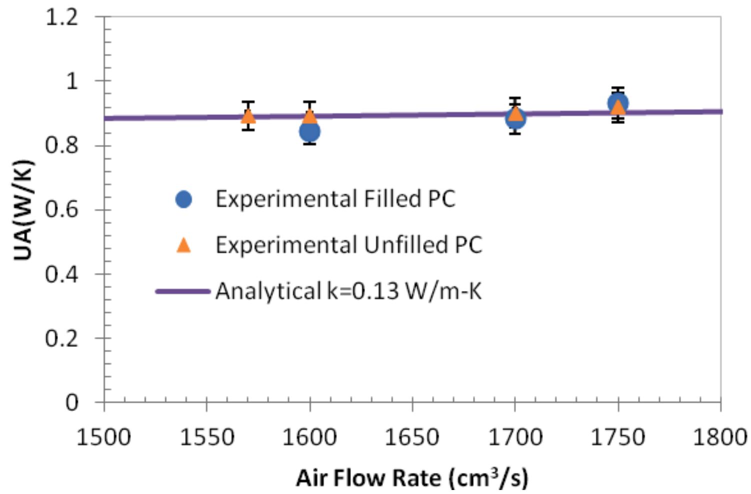

Figure 8. Experimental and analytical HX thermal conductance UA as a function of air flow rate (water flow rate: 40 cm³/s, air inlet T: 120 °C, water inlet T: 30 °C).

The experiments performed so far have revealed that a heat exchanger can be made using Fused Deposition Modeling successfully using both unfilled and filled resins, and that the resulting geometries can be built with no significant porosity to cause water leaks. The heat exchangers described here constitute the first occurrence of FDM-made heat exchanger. Testing will continue in the following quarter.

3.2 Develop and utilize thermomechanical finite element model to assess thermal and structural performance of a polymer composite heat exchanger module (A2)

Structural analysis was performed under combined pressure and convection loading to assess the effects of anisotropic thermomechanical properties on the stress distributions in the heat exchanger. Analysis was completed using a water flow rate of 60 cm^3/s, inlet temperature of 15°C and pressure of 500 kPa. The air flow rate was 3000 cm^3/s, the pressure was 500 kPa or 5000 kPa and the inlet temperature was 50°C or 150°C.

Figure 8 and Figure 9 show the x- and y-direction stresses normalized based on the yield strength of the polymer composite heat exchanger and titanium heat exchanger, respectively. The results reveal that – regardless of loading application – the maximum stress magnitudes are well below the expected yield stress of titanium (930 MPa). These results reveal that the titanium material is underutilized for these applications, and thus material substitution or geometric changes are required for better use of the material.

Titanium is energy intensive, costly and more difficult to manufacture than polymer composites, which could mean that polymer composites are a more practical material choice for these loading conditions. The easier-to-manufacture and less energy-intensive polymer composite experiences stresses that exceed its yield strength in the high temperature applications, but the stress levels for the moderate air inlet temperature of 50°C are within the acceptable range for the material. Thus, such an application appears to be a practical implementation of the polymer composite material from a structural standpoint.

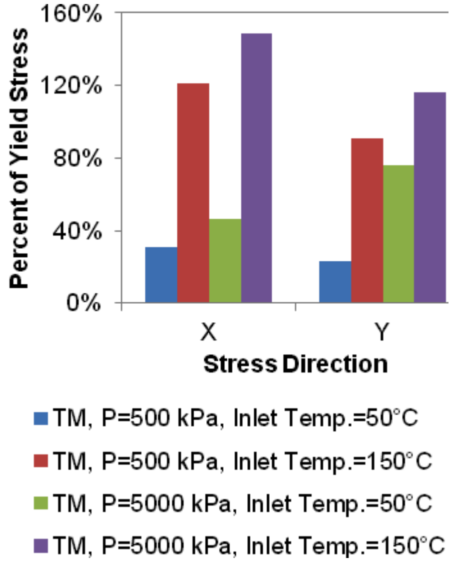

Figure 8. Normalized stresses in polymer composite heat exchanger.

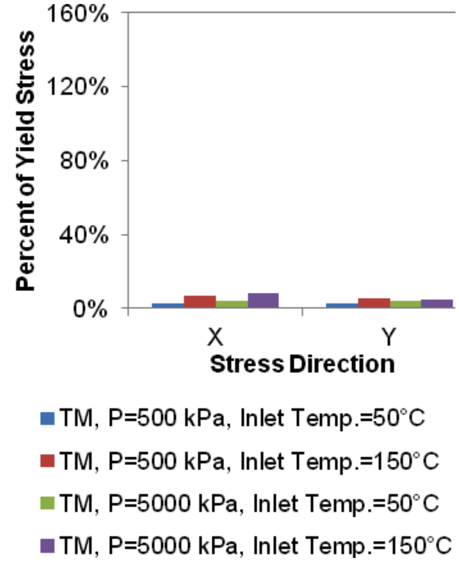

Figure 9. Normalized stresses in titanium heat exchanger.

3.3 Assess the effects on geometric variation on the development of thermomechanical stresses in polymer composite heat exchangers (A2)

The thickness of the fins and plates in the heat exchanger, which are uniformly sized, was varied in one case study to assess the effect of wall thickness on thermomechanical stress development in polymer composite heat exchangers. The directional thermomechanical stress was as high as 148% of the yield stress of the composite for the conditions studied for the baseline geometry. A similar study on the heat exchanger geometry was not performed for the titanium heat exchanger because the stresses seen in the titanium heat exchanger were approximately 10% of the yield stress.

The operating conditions studied for the PCHX geometric variation were as follows: air-side pressure of 5.0 MPa, air inlet temperature of 50°C and water-side pressure of 0.5 MPa. Of the operating conditions studied, these conditions represented conditions where the geometry is an important factor is stress development due to the high stress. The lower air-side inlet temperature meant that thermal stress development would not overshadow stress reductions resulting from increasing the plate thickness in the heat exchanger module.

The heat transfer characteristics of the fluid (i.e., local heat transfer coefficient and local fluid temperature) were not changed from the original analysis, although, assuming constant flow rate, the velocity of the fluid would increase with increasing wall thickness and the wetted area and hydraulic diameter would decrease. The properties of the fluid were not changed because these properties affect the temperature distribution (and thus, thermal stress distribution) in the heat exchanger and would have limited the conclusions made regarding the effect of the plate thickness on stress development.

By shaping the study without changing the convective properties, no discussion is provided regarding the effect of wall thickness on heat transfer rate. Based on one-dimensional conduction resistance and the low conductivity of the polymer composite, it is expected that the wall thickness is a significant contributor to the overall resistance of the heat exchanger. Nonetheless, more detailed variations of the geometry could lead to a heat exchanger design that reduces the

through wall thickness (and thus, conduction resistance) and increases the thickness in other areas to alleviate stress development.
Figure 10 provides the maximum directional stresses as a function of fin and plate thickness for air-side pressure of 5.0 MPa, air inlet temperature of 50°C and wate-rside pressure of 0.5 MPa. The thickness was varied from 1.5 to 4.5 mm in 0.5 mm increments; note that the baseline for previous results has been 2.5 mm.

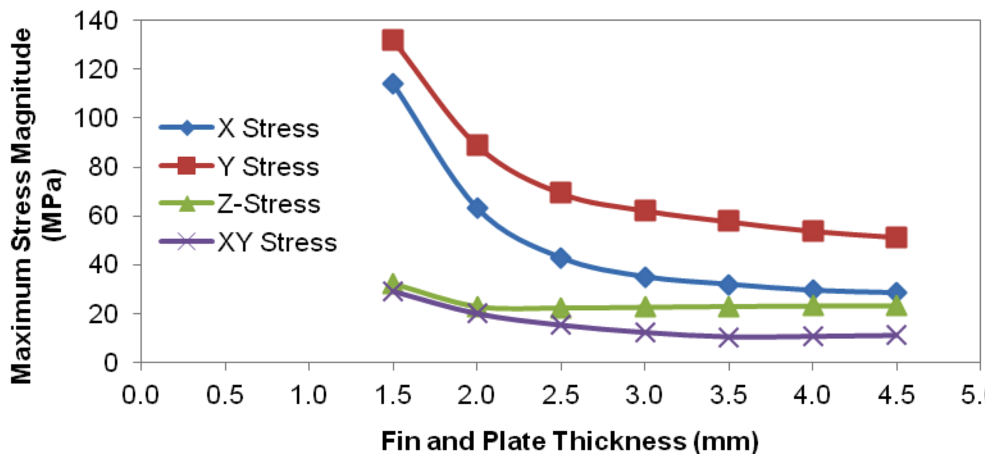

Figure 10. Maximum directional stress magnitude as a function of fin and plate thickness.

The results reveal that the fin and plate thickness significantly affect maximum directional stress magnitudes. The relative decreases in stress development decrease with increasing plate thickness. For example, in the x-direction, increasing the thickness from 1.5 mm to 2.0 mm decreases the stress 45%; increasing the thickness from 4.0 to 4.5 mm decreases the stress only 3%. A similar trend is seen for the y-, z- and xy-directional stress magnitudes.

The results also indicate that the assumed thickness for the present study (2.5 mm) provides a balance between high stress levels and higher mass of the heat exchanger. The diminishing reduction in stress magnitude indicates the importance of the thermal stress development in the anisotropic polymer composite heat exchanger. After the thickness has reached a certain level, only marginal reductions in stress magnitude are achieved by increasing the thickness further.

3.4 Explicit construction of moldability-based feasibility boundary

Motivation:

- Incorporating manufacturing feasibility during design phase is very important
- Optimal heat exchanger design often occurs at the minimum thickness that is feasible for mold filling
- Traditional metamodeling has limited accuracy in regions of interest
- Classification methods provide only an implicit approximation of the feasibility boundary

Action Plan:
Utilize a method of adaptive design of experiments and sequential sampling to closely identify the feasibility boundary across the design space while reducing the number of sample points required to develop this model.

Findings:
A feasibility boundary search algorithm was developed, as shown in Figure 11, to collect points along the feasibility boundary across the entire design space, as follows:

- Divide the design space of *n* parameters into a uniform grid of *n-1* parameters with a remaining search parameter
- Find initial point on the feasibility boundary with no history
- Use previous information to predict the location of the next feasibility boundary points and use adaptive control to refine the search behavior

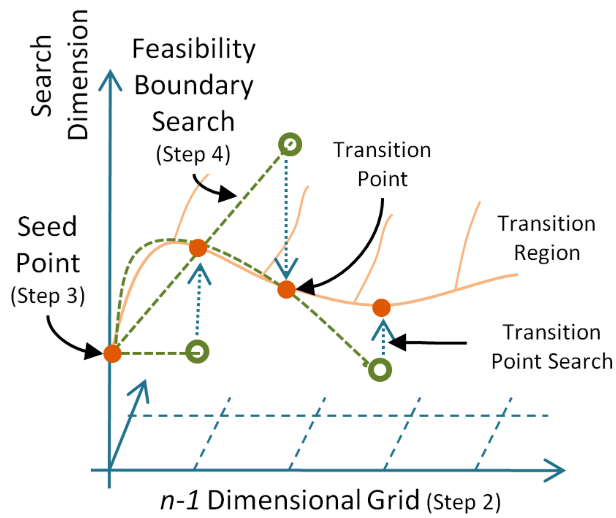

Figure 11. Overview of feasibility boundary search algorithm.

Based on the chosen design parameters, the design space was divided into 175 grid locations with the base thickness variable as the search dimension. 803 function evaluations were required to determine the feasibility boundary across the design space with an average of 4.59 search iterations per grid point.

Using the defined minimum search resolution of 0.002mm for spacing, a traditional exhaustive search would have required 350,000 total function evaluations to identify the feasibility boundary with the same accuracy, an increase by a factor of 436.

A set of 50 randomly selected test heat exchanger designs were used to evaluate the prediction performance of the developed method.

- 100% feasibility classification success
- 30 hours required for Moldflow® simulation of the 50 designs compared to 0.0469 of computation time for the developed model.

3.5 Feature removal for efficient assessment of mold-filling feasibility of finned-plate geometries

Motivation:
Parametric formulation of DoE for feasibility boundary construction limits flexibility

- Limited to relatively few parameters
- Additional prediction approach necessary for robust framework

Action Plan:
Utilize a model simplification technique for reducing the complexity of candidate heat exchanger designs and therefore reducing simulation time while introducing minimal error into simulation predictions and potentially utilizing metamodels for the simplified geometry to further reduce simulation time.

Findings:
A generalized flat plate mold filling metamodel was developed for predicting mold filling in a

simplified geometry with flexibility of overall geometry and processing conditions and is shown in Equation 4, where r is the filled radius, T is injection temperature, Q is injection flow rate, P is injection pressure, and H is the base thickness.

$$r(T,Q,P,H) = \begin{cases} 5.3493 \times 10^{-7} TQPH^{1.3358} & H \leq 2 \\ 6.9813 \times 10^{-7} TQPH^{1.0156} & 2 < H \leq 5 \\ 8.8125 \times 10^{-7} TQPH^{0.8723} & H > 5 \end{cases} \tag{4}$$

Using a disc-fin model to isolate the effects of fins on the overall filling behavior, the scaled thickness model shown in Equation 5 was developed to scale the simplified flat plate representation by the fin influence. A range of test cases were used to find the ideal value for k that minimized the model error, as shown in Figure 12.

$$H_{scaled} = k\left(\frac{V_{filled}}{\pi {r_{filled}}^2} - H_{orig}\right) + H_{orig} \tag{5}$$

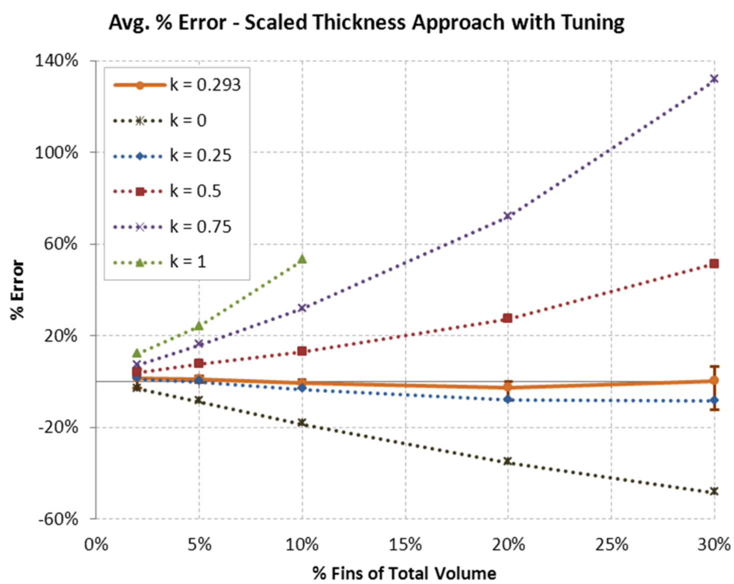

Figure 12. Tuning the scaled thickness model.

The developed model was applied to a set of randomly generated finned plate designs with percent fin volume of total volume ranging from 5 to 25%. The prediction error of these cases is shown in Figure 13, and it was concluded that the developed model is useful for cases when the percent fins of total volume is less than 20%.

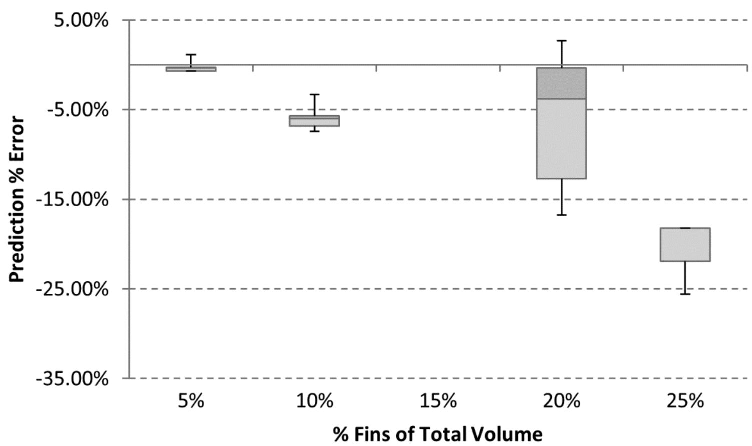

Figure 13. Flat plate simplification prediction error.

3.6 Development of a fiber orientation measurement methodology

Motivation:

- Fiber orientation plays an important role in overall material properties and therefore part performance
- FEA used to estimate fiber orientation
    - Utility of underlying models in thermally-enhanced applications is uncertain

Action Plan:

Develop fiber orientation measurement methodology for comparing Moldflow® predictions to measured behavior.

Findings:

We formulated a sectioning, polishing, and microscope imaging approach for collecting fiber orientation information from a variety of sample geometries. An example microscope image is shown in Figure 14. We also developed a fiber orientation image processing algorithm for extracting fiber orientation from microscope images and calculating tensor values for comparison with Moldflow® predictions.

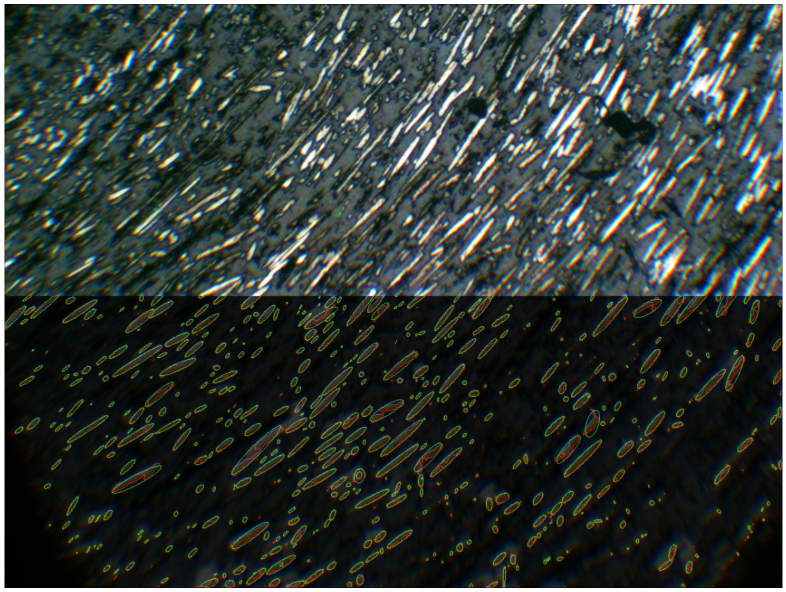

Figure 14. Example microscope image, with the lower half processed to extract fiber orientation.

A comparison framework was developed for analyzing the agreement between Moldflow® predictions and measured behavior. This was applied to an L-channel geometry that represented a sharp velocity change. Figure 15 shows a low-resolution comparison with the polymer flow entering the top of the geometry and exiting the left. 0.0 represents complete agreement (white) and 1.0 represents complete disagreement (black) between the Moldflow®-predicted and measured fiber orientation tensor values.

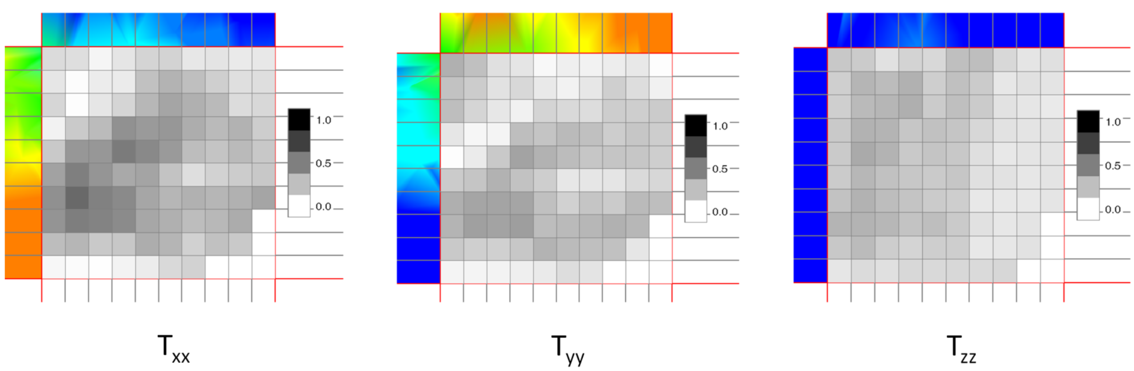

Figure 15. Low-resolution tensor comparison of corner region.

These results showed disagreement at the exit of the geometry and was analyzed with a higher resolution comparison shown in Figure 16.

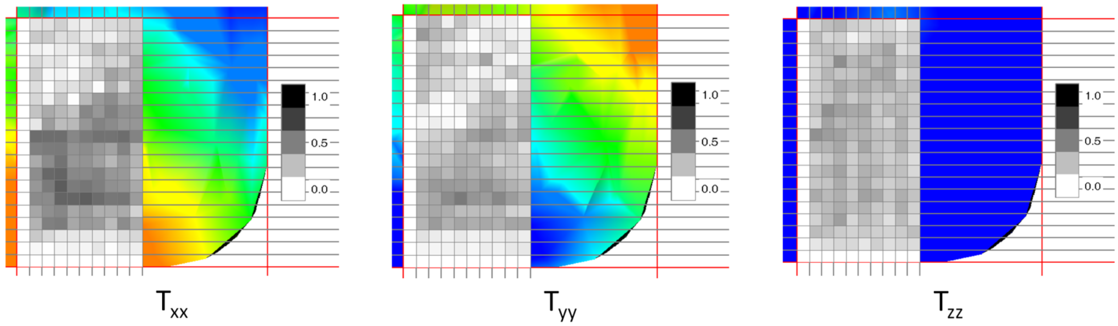

Figure 16. High-resolution tensor comparison of corner region.

Additional findings were as follows:

- The out-of-plane component, T_{zz} was not negligible in experimental findings and could lead to improved application results
- High agreement was observed at the mold wall
- Generally increasing uncertainty with increasing radius from the interior of the corner, especially at the exit

The comparison framework is useful for validating predictions and identifying situations when predictions may be unsuitable. Measured results can be incorporated into hybrid results to designer.

3.7 Characterization of mixing of multi-scale ingredients in TSE on structure-property relationships polymer composites for PHXs

Motivation:
Mixing of polymer composites is being conducted to enhance mechanical and thermal properties. We are determining whether specific throughput and screw speed have any effects on the structure and properties of the composites. The overall goal is to determine how to process polymer composites that will meet the mechanical and thermal demands of the polymer heat exchanger.

Action Plan:
Current samples being prepared and characterized are listed by weight percent as follows:

A1= 25% micro fibers only at 2.2 lb/hr and 35 rpm on wide kneading blocks
A2=15% micro fibers only at 2.2 lb/hr and 35 rpm on wide kneading blocks
A3=10% micro fibers only at 4.7 lb/hr and 110rpm on wide kneading blocks
A4=5% micro fibers only at 4.7 lb/hr and 110rpm on wide kneading blocks
B1=25% micro and 0.47% nano at 2.6 lb/hr and 60 rpm on narrow kneading blocks
B2=15% micro and 0.47% nano at 2.6 lb/hr and 60 rpm on narrow kneading blocks
B3=5% micro and 0.47% nano at 2.6 lb/hr and 60 rpm on narrow kneading blocks

PBT is the base polymer that is now being mixed with the micro- and nano-particles because of its superior thermal and mechanical properties compared to nylon. The first composite strips contained only micro carbon fibers. Fibers were fed through a mirco-feeder and entered through the mixing port. The variety of flow rates and screw speeds used helped determine which conditions produced optimal strips. This initial test was also conducted to have a comparison to the micro- and nano-composite.

A second batch of samples was prepared using a mix of micro-carbon fibers and nano-carbon pellets. The micro-fibers continued to be fed through the micro-feeder, but the nano-pellets were dropped by hand at specific rates for better consistency. Both the fibers and pellets enter through the mixing port.

All experiments were conducted on the 28 mm twin-screw co-rotating extruder we have used previously. For the pure carbon micro composites the 25% and 15% micro fill ran at 2.2 lb/hr and 35 rpm. The 10% and 5% micro fill ran at 4.7 lb/hr and 110 rpm. All the carbon micro and nano filled composites ran at 2.6 lb/hr and 60 rpm.

To characterize the relationship between mixing and the composition of the polymer composite, mechanical properties were obtained from tensile tests conducted on extruded strips of the micro- and micro-nano composites from which dog-bone specimens were prepared. Subsequent stress vs. strain curves could then be generated to obtain mechanical properties for comparison, shown in Figures 17-23.

The width of the middle of the dog-bone for the micro was 2.4 mm, whereas for the micro and nano was 1.9 mm. The dog-bones did not break because of the limit of the amount of force that can be applied with the give tensile testing equipment.

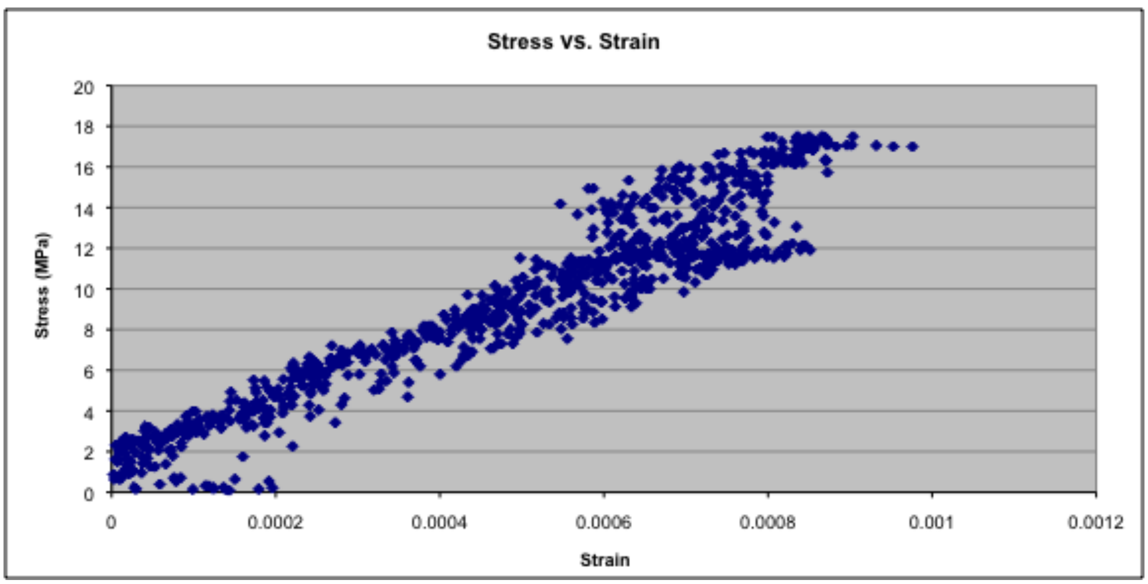

Figure 17. 25% Micro, Q= 2.2 lb/hr, N= 35 RPM.

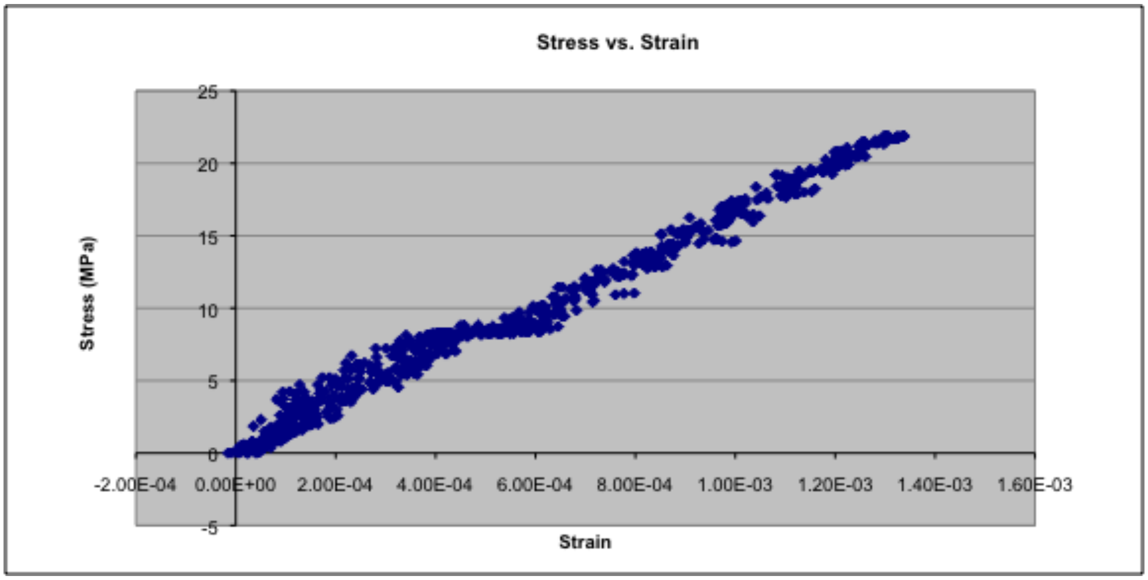

Figure 18. 25% Micro & 0.47% Nano, Q= 2.6 lb/hr, N= 60 RPM.

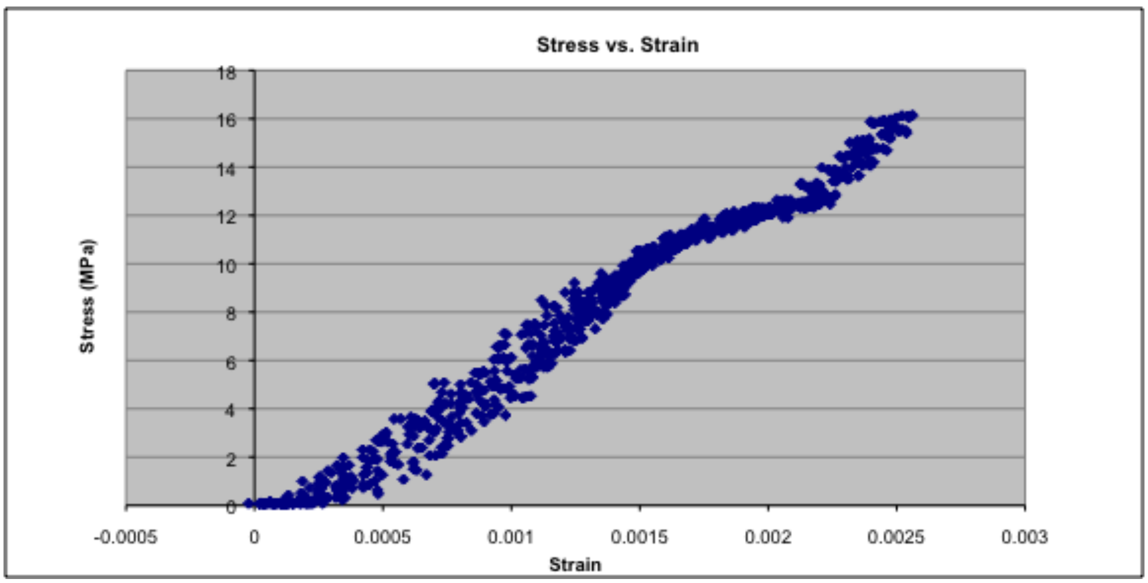

Figure 19. 15% Micro, Q= 2.2 lb/hr, N= 35 RPM.

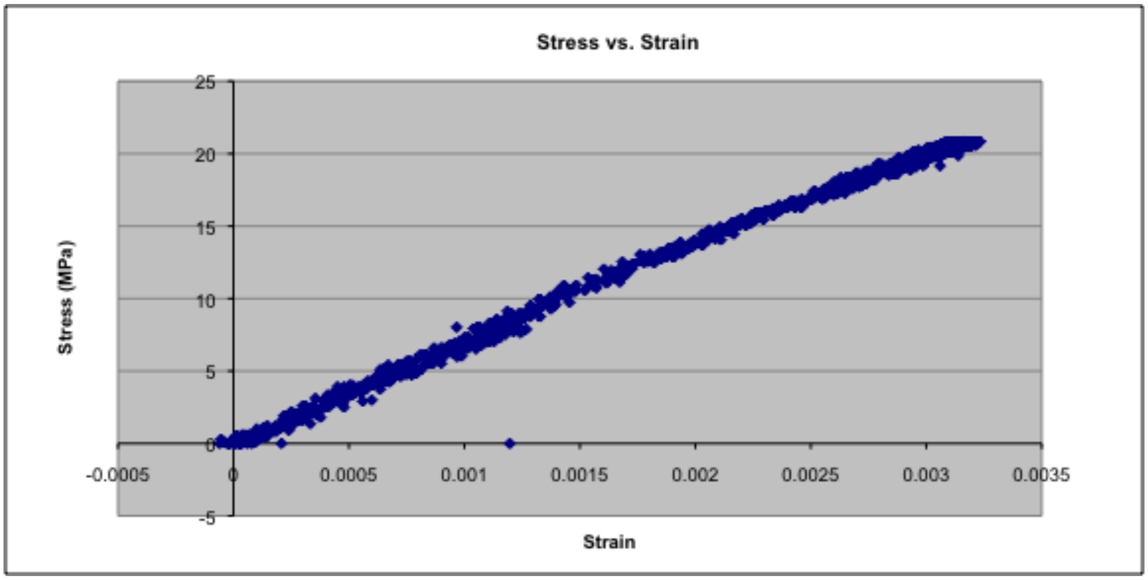

Figure 20. 15% Micro & 0.47% Nano, Q= 2.6 lb/hr, N= 60 RPM.

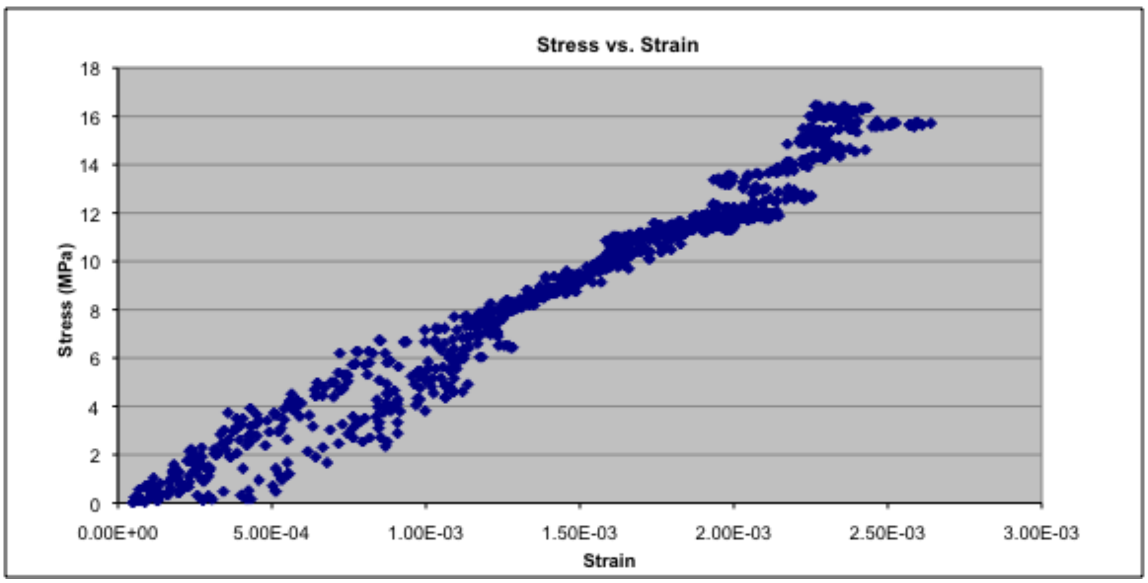

Figure 21. 10% Micro, Q= 4.7 lb/hr, N= 110 RPM.

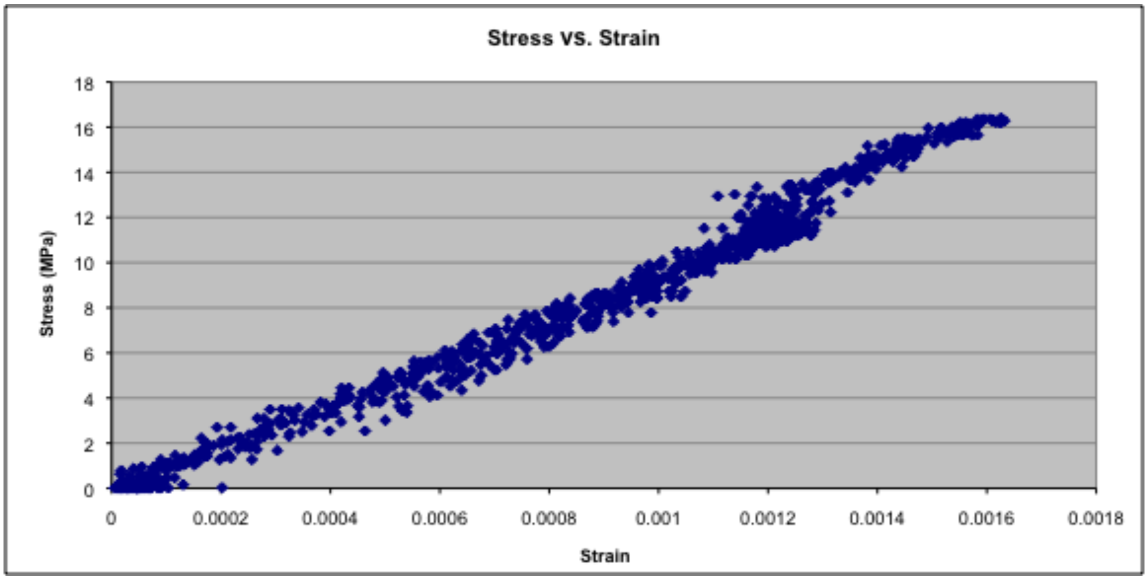

Figure 22. 5% Micro, Q= 4.7 lb/hr, N= 110 RPM.

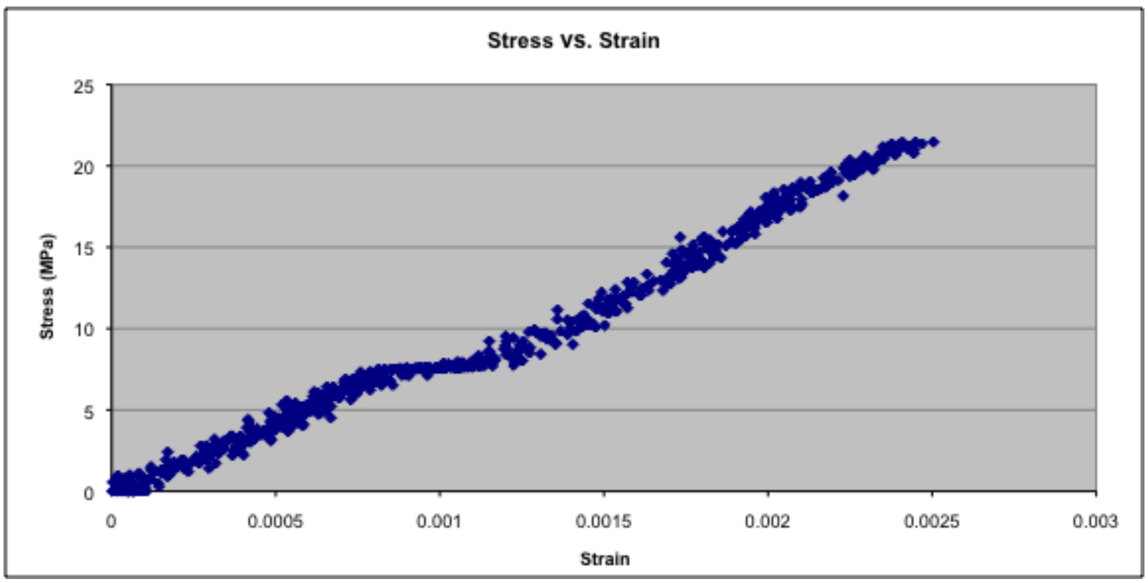

Figure 23. 5% Micro & 0.47% Nano, Q= 2.6 lb/hr, N= 60 RPM.

From these preliminary results, it can be seen that all of the specimens were fairly elastic. However there are some nonlinearities that may be attributed to the fillers or to the quality of the dog-bone specimen. The loading limits were 16-20 MPa, depending on the width of the specimen, which is well below the strength limit of PBT, which is 40-60 MPa. The apparent modulus was approximately 6-20 GPa. This is significantly higher than the modulus of unfilled PBT, which is approximately 2.6 GPa. In general, the 25 wt. % micro samples exhibited the best properties, but more characterization is necessary to correlate mixing with the mechanical properties of the composites.

Preliminary optical micrographs, shown in Figure 24, were also obtained from the microfiber filled composite that will be used to correlated structure with mixing and subsequent mechanical properties. For example, the alignment of fibers can be correlated to anisotropy and possible increases in the mechanical properties in the direction of the fibers.

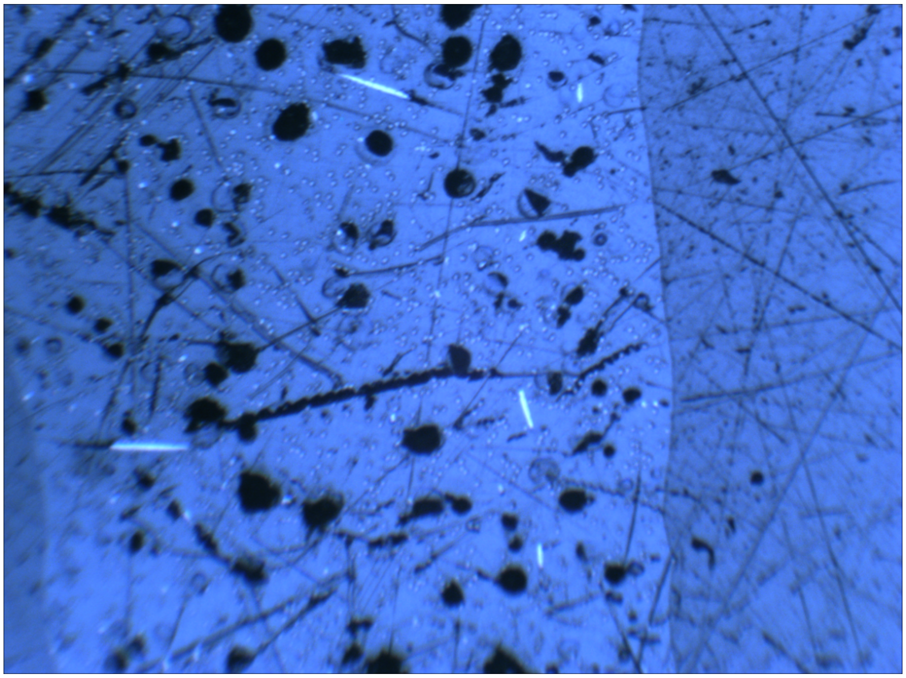

Figure 24. 15% Micro 5.2 lb/hr, 60rpm.

4. Difficulties Encountered/Overcome

None.

5. Planned Project Activities for the Next Quarter

- Test prototypes of new candidate PHX design in upgraded experimental test rig.
- A thesis entitled "Manufacturability Analysis of Thermally-Enhanced Polymer-Composite Heat Exchangers" was completed on August 4, 2011, and efforts will now be focused on submitting journal papers from that thesis.
- A thesis entitled "Thermomechanical Behavior of Polymer-Composite Heat Exchangers" was completed on August 4, 2011, and efforts will now be focused on submitting journal papers from that thesis.
- The next step for the mixing work is to test the first set of samples for anisotropies and thermal conductivity. A second set of sample material is being prepared that will be tested for strength, thermal conductivity, and other properties as they are determined necessary. Additional experiments will also focus on identifying the mixing conditions in the TSE for producing the best set of physical properties.
- Continue testing of prototypes of new candidate PHX design in upgraded experimental test rig.

6. References

[1] Bar-Cohen, A., Luckow, P., Cevallos, J.G., Gupta, S.K., 2010, Thermal Anisotropy in Injection Molded Polymer Composite Fins, International Heat Transfer Conference 14 at Washington DC

[2] Cevallos, J.G., Gupta, S.K., Bar-Cohen, A., Incorporating Moldability Considerations during the Design of Thermally Enhanced Polymer Heat Exchangers (under revisions)

[3] Cevallos, J.G., Bar-Cohen, A., Bergles, A.E., Gupta, S.K., Rodgers, P., Polymer Heat Exchangers – History, Opportunities, and Challenges (in progress)
[4] Luckow, P., A. Bar-Cohen, P. Rodgers, 2009, “Minimum Mass Polymer Seawater Heat Exchanger for LNG Applications,” accepted for publication, ASME TSEA, January 2010
[5] Cox, H.L., 1951, “The elasticity and strength of paper and other fibrous materials,” Brit. J. Appl. Phys., 3(3), pp. 72-79.
[6] Amado-Becker, A., Ramos-Grez, J., Yanez, M.J., Vargas, Y., and Gaete, L., 2008, “Elastic tensor stiffness coefficients for SLS Nylon 12 under different degrees of desensification as measured by ultrasonic technique,” Rapid Proto. J., 14(5), pp. 260-270.
[7] Halpin, J.C., and Kardos, J.L., 1976, “The Halpin-Tsai Equations: A Review,” J. Poly. Eng. and Sci., 16(5), pp. 344-352.
[8] Hahn, H.T., and Tsai, S.W., 1980, Introduction to Composite Materials, Technomic Publishing Co., Lancaster, PA.
[9] Pegoretti, A., Fambri, L., Zappini, G., and Bianchetti, M., 2001, “Finite element analysis of a glass fibre reinforced composite endodontic post,” Biomaterials, 23, pp. 2667-2682.
[10] Fu, S., and Lauke, B., 1997, “The elastic modulus of misaligned short-fiber-reinforced polymers,” Comp. Sci. and Tech., 58, pp. 389-400.
[11] Foye, R.L., 1972, “The Transverse Poisson’s Ratio of Composites,” J. Comp. Mater., 6(2), pp. 293-295.
[12] “Thermal Graph DKD,” Cytec Industries, Accessed 26 May 2010, http://www.cytec.com/engineered-materials/products/cfThermalGraphDKDX.htm.
[13] Robinson, F., Bruck, H., Gupta, S.K., and Bar-Cohen, A., 2010, “Saltwater Hygrothermal Aging Studies of Short Carbon Fiber Reinforced Polyamide 12,” ASME International Mechanical Engineering Congress & Exposition, Vancouver, British Columbia, Canada, November 12-18, 2010.

Appendix

Goals

The goal of the proposed 3-year EERC II polymer composite heat exchanger (PCHX) project is to develop the science and technology needed to underpin the systematic design of polymer-fiber composite heat exchanger modules that address the needs of the fossil fuel industry. The project team, lead by A. Bar-Cohen, brings together expertise in thermal science and technology (Bar-Cohen, Rodgers) with polymer composite molding and manufacturing (Gupta, Bigio). Design studies and molding simulations, as well as fabrication and testing of laboratory-scale polymer composite heat exchangers, during the first phase of this project, have provided the foundation for aggressive pursuit of such polymer composite heat exchangers.

Successful development of cost-effective, high-performance PCHX's will require a detailed understanding of the limitations imposed on the thermal performance, mechanical integrity, and cost of such heat exchange devices by the candidate polymer material; carbon fiber geometry, orientation, and concentration; thermal and mechanical anisotropy of the polymer-fiber composite; molding processes; thermal and structural failure mechanisms in the molded heat exchanger; and the energy investment in the fabrication and formation of the heat exchangers. The development and experimental as well as numerical validation of a multi-disciplinary computerized design methodology, along with the fabrication and testing of scaled polymer heat exchanger modules, would provide a unique knowledge-base from which low-life-cycle-cost heat exchange systems for the petroleum and gas industries could be developed.

Project Tasks

A. Thermal Design and Characterization of Polymer Composite Heat Exchanger Module
(Prof. Avram Bar-Cohen - UMD, Prof. Hugh Bruck- UMD, Prof. Peter Rodgers – PI)

1. ***Design and thermofluid evaluation of PHX concepts for LNG applications***, including sensitivity of thermal performance to key parameters, quantification of primary thermal and exergy figures-of-merit (metrics), comparison to conventional heat exchangers, and identification of least-mass/least-energy designs;

2. ***Detailed design, fabrication, and thermal characterization of least-energy PCHX module***, including mold fabrication for most promising design, assembly and instrumentation of laboratory prototype, analysis of thermal and structural performance under simulated LNG processing conditions;

3. ***Development of predictive models for anisotropic heat exchanger modules***, including use of molding CFD software for prediction of fiber orientation and effective thermal/ structural properties, numerical and analytical models for molded anisotropic fins, derivation of least-material anisotropic fin equations, determination of heat flow sensitivity to fiber geometry/concentration/orientation;

4. ***Evaluation of convective enhancement features in molded channels***, including identification of "best practices" in conventional heat exchangers, manufacturability analysis of candidate features with attention to mold complexity, part ejection, and warpage, polymer composite molding of 3-5 candidate enhanced channels; thermofluid characterization of candidate enhanced channels under simulated LNG processing conditions; and

5. ***Determination of seawater effects on polymer composite finned plates***, including design and molding of test samples, immersion in saltwater tanks at different temperatures and concentrations for pre-determined periods, surface/bulk imaging and mechanical characterization before and after immersion, analysis and correlation of effects.

B. Manufacturability Analysis and Mold Design for Polymer Composite Heat Exchanger Module (Prof. SK Gupta – UMD, Prof. HA Bruck - UMD)

1. *Development of an improved meta-model for mold filling predictions*: We plan to develop an improved meta-model for predicting mold filling for typical heat exchanger geometries. This meta-model will account for multiple gates with adjustable spacing. The data for developing this meta-model will be generated using mold flow simulations. We plan to utilize radial basis function based meta-models to provide the right balance of accuracy and computational speed.

2 *Creation of a computational framework for gate placement to optimize fiber orientation*: We plan to develop a computational framework for placing gates to optimize the fiber orientation, utilizing simulated fiber orientations to select the gates. The sensitivity of the gate locations on fiber orientation will be developed. Gradient-based optimization techniques will be used to optimize the fiber orientation. The optimization problem will incorporate the constraint satisfaction formulation of the weld-line locations to ensure that the fiber orientation formulation produces acceptable weld-lines.

3. *Generation of insert molding process models to incorporate connectors at the weld-lines*: In order to ensure that the weld lines do not compromise the structural integrity, we plan to embed metal connectors at the expected weld-lines locations. In order to accurately place these metal connectors in the structures, we plan to develop process models of the insert molding process and mold design templates for performing insert molding.

4. ***Develop key relationships for the dependence of fiber orientation on the flow geometry of the finned-plate PCHX module,*** in commercially available polymer composites, including the effect of carbon fiber length and diameter, for high and low fiber concentrations, for both base plate and fin passages in the mold, and the effect of fiber orientation/distribution on thermo-mechanical properties, verify relationships with suitable small scale experiments;

C. Polymer-Fiber Interactions in Polymer Composite Heat Exchanger Modules (Prof. David Bigio – UMD)

1. ***Determine achievable thermo-mechanical property enhancement*** through control of carbon fiber orientation, in the commercially available polymer composites, with attention to flow regimes, mixing processes in the flow of the melt, and heat exchanger module design, and verify experimentally;

2. ***Explore optimization of PCHX polymer composite properties through the creation of novel polymer composite compositions***, including multi-scale filler geometries, develop the molding methods for the desired geometries, create the novel composites and experimentally verify improved thermo-mechanical polymer composite properties.

Study on Microchannel-Based Absorber/Stripper and Electrostatic Precipitators for CO_2 Separation from Flue Gas

UMD Investigators: Serguei Dessiatoun, Amir Shooshtari, Michael Ohadi
GRAs: Christoph A. Dersch
PI Investigators: Afshin Goharzadeh, Mohamed Alshehhi

Start Date: Oct 2006

1. Objective/Abstract

This project is focused on research leading to the development of a high-efficiency CO_2 separation mechanism with application to a diverse range of processes in the oil and gas industry, including CO_2 separation separation/injection in petrochemical and refining processes, gas sweetening, and CO_2 capture for enhanced oil recovery applications.

The removal of acidic gases such as carbon dioxide from gas streams is an important process in the natural gas industry. In gas sweetening at least 4% by volume of raw natural gas consists of CO_2, which needs to be lowered to 2% to prevent pipeline corrosion, to avoid excess energy for transport, and to increase heating value. The separation of CO_2 from flue gases and its use for enhanced oil recovery and CO_2 sequestration applications is an increasing area of importance, as evidenced by the large investments in this area by ADNOC and its group companies, as well as affiliated government agencies in Abu Dhabi. A typical CO_2 separation process involves three stages: cooling down the flue gas; separating the solid particles and condensed water droplets; and finally capturing the CO_2 using the absorption process. The microchannel-based CO_2 separator being developed in this project, will significantly increase controllability of the thermal state of the reaction and the efficiency of the separation process while decreasing the reaction time and energy consumption, as well as potential substantial reduction of equipment footprint and the associated capital investment.

Flue gas also usually contains many contaminants in solid and liquid forms, the bulk of which are separated in gravity and inertia-driven feed gas separators. However, fine particles are carried on with the flow and can damage compressors, contaminate the gas absorption process, and reduce the quality of gas products. Electrostatic separation is one of the most effective techniques for separation of such particles and will be used in this project. The present project will address separation of droplets and particles using an EHD gas-liquid separation technique to remove liquid particles suspended in a moving gaseous medium, followed by the proposed microchannel-based separation of the CO_2 from the stream once the fine particles in the flow have been removed.

The project is being conducted jointly by the team at UMD and at PI. The team at PI is focusing on EHD separation process and absorption modeling, while the team at UMD has focused on the experimental work utilizing micro channel-based CO_2 separation and the absorption solution.

2. Executive Summary of Accomplishments in the Current Reporting Period

During this reporting period additional in-depth study of the processes and analysis of our experimental results contributed to our collective enhanced understanding of the physics and reaction kinetics. The team effort continued on advancement in two fronts, mathematical modeling and experimental study. The main focus of the collaborators at the Petroleum Institute has been in mathematical modeling of the absorption process in microchannels, and during this period the team focused on implementing the chemical absorption into computational model, which is still ongoing. The focus of collaborators at UMD has been on experimental study of the process and visualization study of the absorption of CO_2 in microchannels.

During this period, new sets of data on the effect of flow rate on the rate of absorption were collected. The results successfully demonstrated that reduction of flow rate enhances the absorption rate. Some of the major results collected in this period and the outline of the future work are presented in current report. In this reporting period, the collaborators from the PI and UMD continued joint reviews of the project progress and milestones and sharing idea through weekly audio conferences and exchange of emails.

3. Milestones/Deliverables Scheduled for the Completed Quarter

- Preliminary testing of the second-generation laboratory scale microchannel CO_2 separator
- Additional tests by varied CO_2 concentrations, gas flow rates and liquid flow rates

4. Summary of Project Activities for the Completed Quarter

Experimental setup:

We finished the fabrication of the second-generation microchannel reactor and installed it. Simultaneously we changed our setup, as shown in Figure 1.

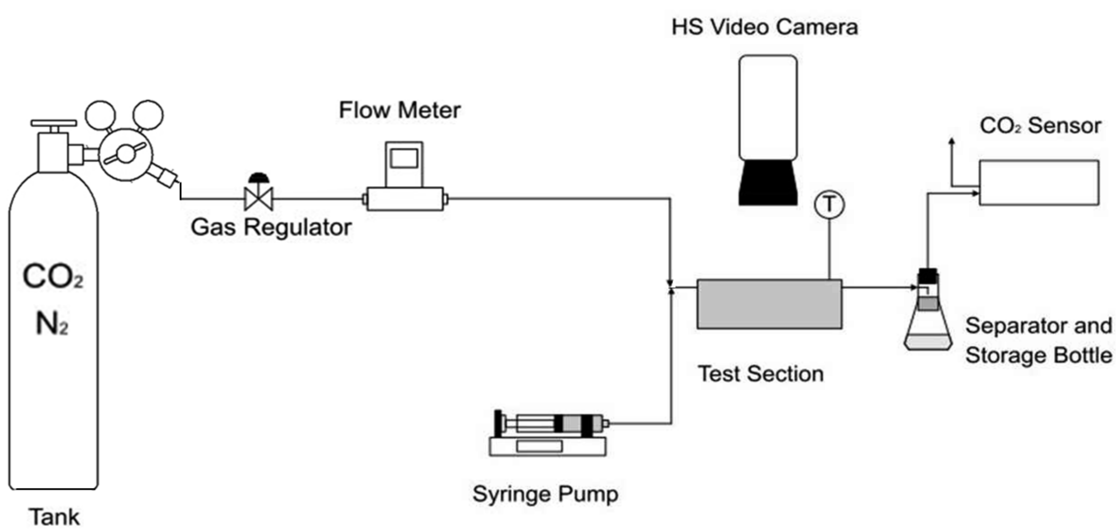

Figure 1. Schematic construction of the experimental setup.

To simplify the adjustment of the CO_2 concentration we are using 8L and 0.5L gas cylinders, which we fill with a mixture of CO_2 and N_2, before starting the experiment. The gas flow rate is measured by a Tylan FM-360 mass flow meter. For the liquid flow of the 20 wt% diethanolamine solution we still use the Harvard PHD 2000 syringe pump. The second-generation reactor has a thermocouple included, by which we are able to measure the temperature during the measurements. The integrated cooling loop is connected to a chiller.

The liquid/gas separator used is a plastic Erlenmeyer flask with a porous media. The flask serves as a reservoir for the diethanolamine solution CO_2 saturated. The gas phase, consisting of N_2 and traces of CO_2, is measured by a VAISALA CARBOCAP® Carbon Dioxide Module GMM111 with a range of 0-20% CO_2. Finally, the residual CO_2 and N_2 are released to the exhaust hood. During our experiments we observe and capture videos of the bubbles visible in the transparent tube reactor through the covering glass plate. All measurement points are connected to a computer-based evaluation unit.

Experimental Results:

The new setup configuration is now used to assess a new range of test conditions. Our objective of these experiments is to investigate the relation between:

- gas velocity / CO_2 absorption efficiency
- liquid velocity / CO_2 absorption efficiency
- CO_2 concentration / CO_2 absorption efficiency

We vary the gas flow with a valve and the liquid flow with the syringe pump. For the different gas mixtures we refill the gas cylinder each time. Our present test conditions are shown in the chart below:

Table 1. List of setup settings

Channel diameter	750 microns
Gas pressure	30 psi
CO_2 + N_2 concentration	5% 10% 15%
DEA concentration	20 wt %
Gas flow rates (mL/min)	5, 15, 25, 50, 75, 100
Liquid flow rates (mL/min)	1, 5, 10, 15

Effect of gas/liquid flow rates:

To get data for the effect of varying the gas and liquid flow rate, we vary the gas flow rate between 5, 15, 25, 50, 75 and 100 mL/min; and the liquid flow rate changes from 15, 10, 5 to 1 mL/min diethanolamine solution. Figure 3 shows our results of these tests. As can be seen, the absorption efficiency of CO_2 decreases with an increasing flow rate. A low flow rate of 5 or 15 mL/min provides a nearly complete absorption of the CO_2, but we lose almost 30% of efficiency when we raise the flow rate to 100mL/min. However, this is normal because a specific amount of diethanolamine solution can only absorb a specific amount of CO_2. Another point is that the residence time decreases with higher flow rates.

There is no significant change in removal efficiency at high liquid flow rates when the diethanolamine solution flow rate is varied. However, the absorption performance substantially decreases at low flow rates. Logically, a smaller amount of diethanolamine cannot absorb large amounts of CO_2. We would like to try to collect more data between 1mL/min and 5mL/ min in the future.

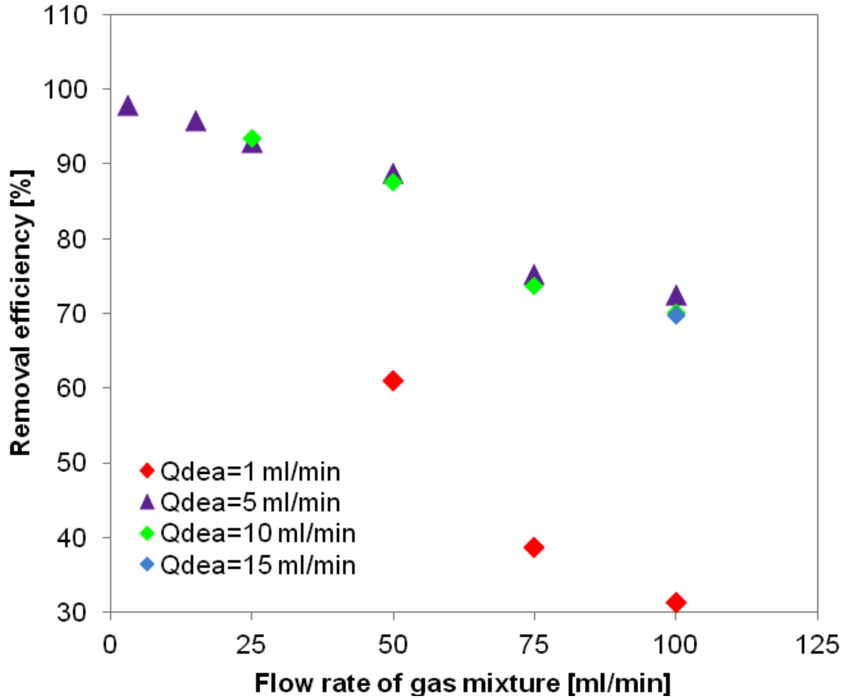

Figure 3. Relation between gas/liquid flow rates and CO_2 absorption efficiency.

<u>Effect of CO_2 concentration:</u>

In addition, we assessed the performance of absorption by changing the CO_2 concentration from 5% to 10% to 15% at diethanolamine solution flow rates of 5mL/min and 10 mL/min. Figure 4 shows, for example, that at a gas flow rate of 100mL/min, the absorption performance for the 15% CO_2 is better than for the 5% CO_2; this is illogical. A lesser amount of CO_2 should be absorbed better by the same amount of diethanolamine than a larger amount.

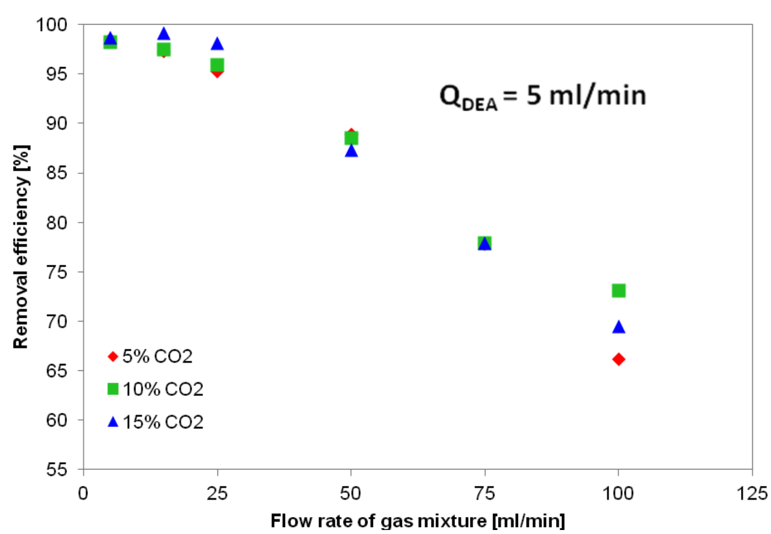

Figure 4. Relation between CO_2 concentration and CO_2 absorption efficiency.

To investigate the cause of this discrepancy we looked closer at the data. We calculated the error of the carbon dioxide sensor, which is given with ±(1,5% of range + 3% of reading), with the following equation:

$$X = \frac{y_{out} - y_{in}}{y_{in}} \times 100\% = f(y_{in}, y_{out}) \qquad (1)$$

$$U_x = \pm\sqrt{\left[U_{y_{in}}\left(\frac{\partial x}{\partial y_{in}}\right)\right]^2 + \left[U_{y_{out}}\left(\frac{\partial x}{\partial y_{out}}\right)\right]^2} \qquad (2)$$

$$U_{y_{in}} = \pm\left(\frac{1.5}{100} \times 20\% + \frac{3}{100} \times (y_{in})\right) \qquad (3)$$

$$U_{y_{out}} = \pm\left(\frac{1.5}{100} \times 20\% + \frac{3}{100} \times (y_{out})\right) \qquad (4)$$

The result demonstrates that we have a 2%-8% uncertainty in the CO_2 sensor reading value. This is illustrated in Figures 5 and 6.

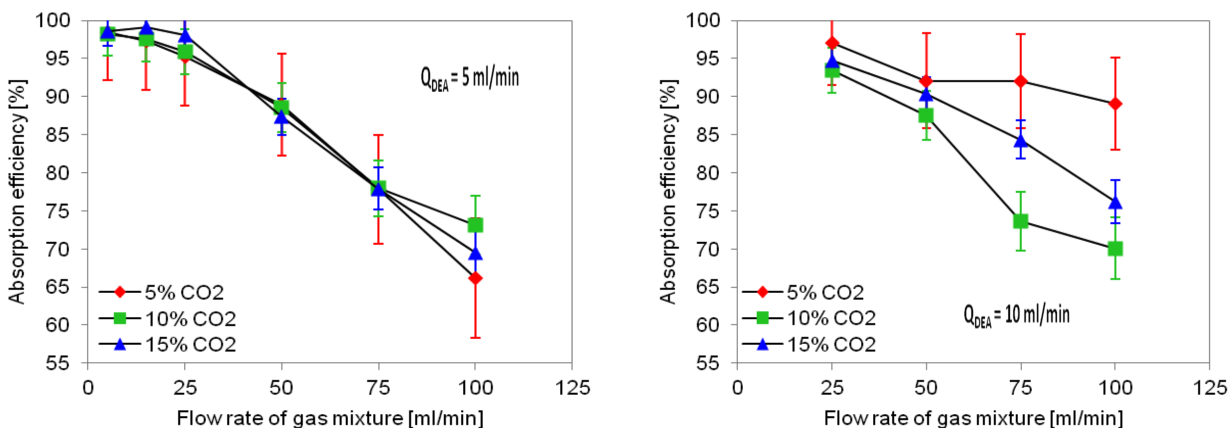

Figures 5 and 6. Relation between CO_2 concentration and CO_2 absorption efficiency for 5mL/min and 10mL/min. Includes CO_2 sensor error.

The uncertainties demonstrated in Figure 5 may explain the discrepancy. But, the uncertainty of the CO_2 sensor is not big enough to explain the differences in the 10mL/min chart (Figure 6). This observed trend could possibly be attributed to absorption occurring in the separator. Due to the large error illustrated by Figure 6, a new design is required for the separator in order to prevent absorption after the microchannel. This new design should also perhaps include a method of neutralizing the diethanolamine solution with acid.

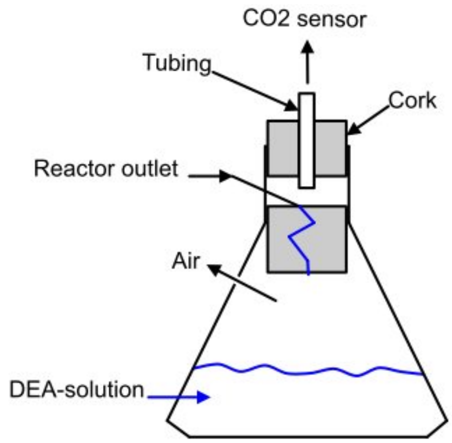

Figure 7. Present separator.

Mass transfer coefficient:

Another way to describe our data is to look at the volumetric mass transfer coefficient. This coefficient is calculated using the following equation:

$$k_L a = \frac{U_L}{l} \ln \frac{C^* - C_{CO_2(L),in}}{C^* - C_{CO_2(L),out}}$$

***U$_L$*:** liquid phase velocity (m/s)
***l*:** length of reactor
***C*:** concentration of CO_2 in liquid phase (mol/m^3)
***C**:** physical solubility of gas in liquid phase (mol/m^3)

The results are shown in Figure 8 and 9. A clear trend can be seen: with increasing CO_2 concentration the volumetric mass transfer coefficient also increases.

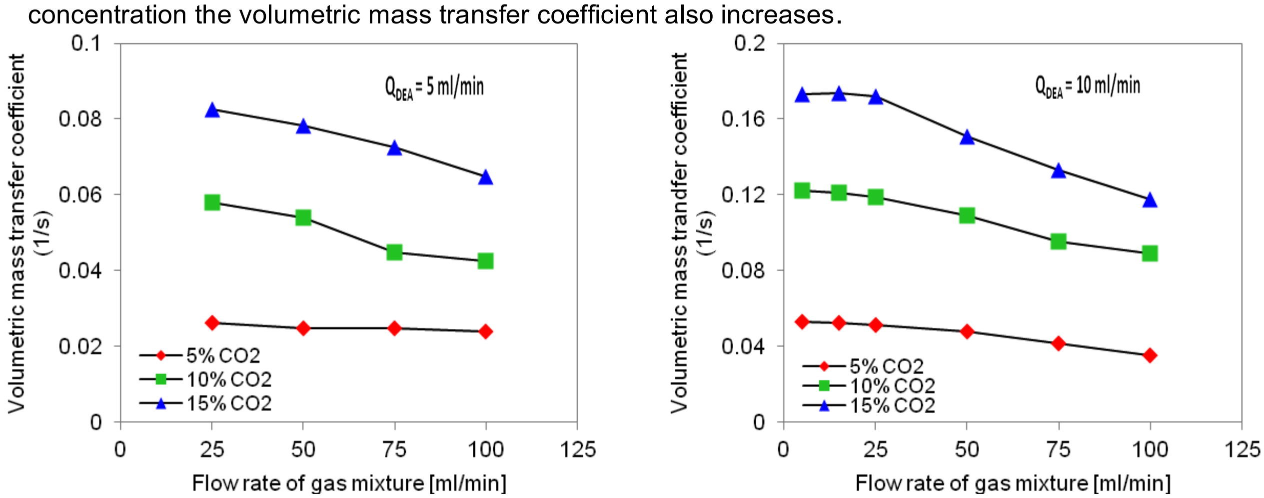

Figures 8 and 9. Relation between CO_2 concentration and volumetric mass transfer coefficient.

<u>Flow patterns:</u>

Moreover, we investigated the flow patterns visional using the captured videos. It is clearly evident that the bubble length enlarges with increasing flow rate. The flow patterns change from Taylor to Taylor-annular flow for flow rates larger than 50mL/min.

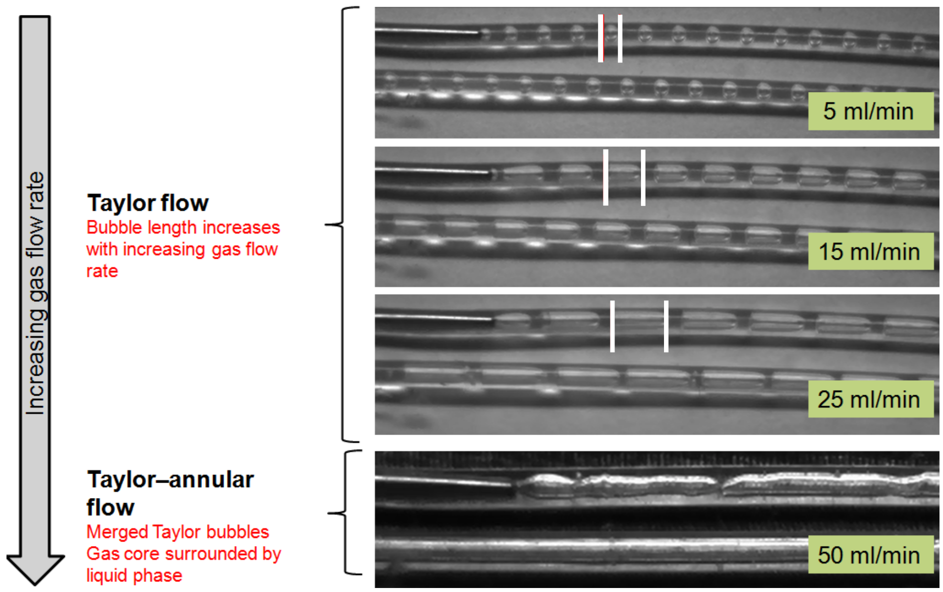

Figure 10. Flow patterns at different gas velocities; change from Taylor to Taylor-annular flow.

Analyzing the flow patterns of all our data, we then compared our data a flow chart from Chung and Kawaji (2004), shown in Figure 11. In future tests, we should go to higher flow rates, as well, to study the other flow regimes. Perhaps we can reduce the channel length and subsequently the channel diameter.

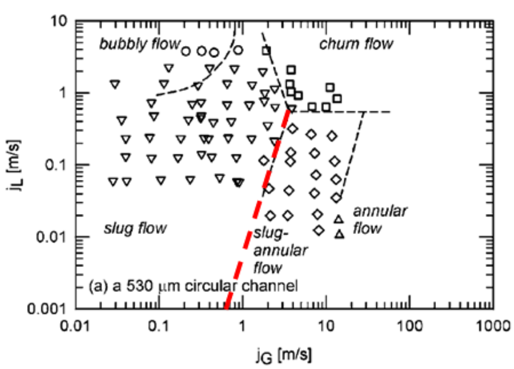

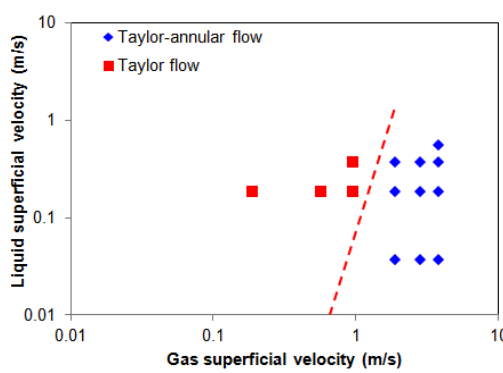

Figures 11 and 12. Flow chart from Chung and Kawaji [3]; our flow chart.

Summary of Results:

In this reporting period we investigated the effect of several flow rates for the liquid and the gas flow in the microchannel reactor. Almost all of the results fulfilled our expected trends: with an increasing gas flow rate, the absorption efficiency decreases, and with a decreasing diethanolamine solution flow rate, the absorption also decreases. We detected an unacceptable error range in all the absorption data and are considering a better separator design. Furthermore, we improved the description of efficiency by calculating the volumetric mass transfer coefficient. Recorded videos of the tests allow us to characterize their flow patterns, where we detected Taylor and Taylor-annular flow. We are now able to draw a flow pattern chart, comparable to one in the literature.

5. Difficulties Encountered/Overcome

None to report

6. Planned Project Activities for the Next Quarter

- Design a new separator to prevent additional absorption
- Investigate higher flow rates as well to study other flow regimes like annular flow, churn flow, bubbly flow
- Design improvement for a larger scale technology demonstrator unit (TDU)
- Parametric studies and performance characterization of the TDU

7. References

[1] *J. Yue et al. / Chemical Engineering Science 64 (2009) 3697 -- 3708*

[2] Gonzalo Va'zquez et al. J. Chem. Eng. Data 1996**,** 41, 806-808

[3] Chung, P.M.-Y. and Kawaji, M., 2004, "The Effect of Channel Diameter on Adiabatic Two-Phase Flow Characteritics in Microchannels", International Journal of Multiphase Flow, 30, pp. 735–761.

Appendix

Justification and Background

The development of environmentally friendly process in industry is one of the major goals that have to be achieved. One way to approach cleaner environment is capturing or minimizing harmful gas components before emission to the atmosphere. One of the main gases which contribute significantly in global warming is CO_2. Due to a necessity to develop more efficient techniques for CO_2 capturing, scientific research in this area has been expanded rapidly. Since in the past very little R&D was devoted to CO_2 capture and separation technologies, opportunities for revolutionary improvements in CO_2 separation technologies is very high To maintain its competiveness and bring environmental friendly industry to the region, ADNOC has adopted various policies and approached it via many plans including “zero-flare” policy, acquiring more energy efficient process and the agreement signed with MASDAR to develop CO_2 capture technology. CO_2 separated from flue gases will be re-injected in oil wells, increasing oil production.

One of the promising concepts which can lead to major technology advancement is microchannel-based absorption units with enhanced kinetics. The objective of this study is to develop a full process of CO_2 separation from flue gas with incorporating micro-channel absorption technology at laboratory scale. The project addresses various stages of separation process: separation of solid particles and condensed water droplets and CO_2 separation using absorption process. Microchannel absorption CO_2 separator developed in this project will, significantly, increase the efficiency of separation process while decreasing energy consumption involved in such operation. Moreover, development of such technology will lead to reduction of equipment’s size and, therefore, minimizing the footprint and cost of equipment. An electrostatic separator will be used prior to CO_2 separation to remove solid and liquid contaminants from flue gas. The ultimate objective is to design all separation stages such that the overall performance will be optimized.

Approach

Detailed analysis and identification of the phenomena and the design challenges involved in effective implementation of the mechanism. Parametric study of existing and improved separators. Design iterations, including numerical flow and field simulations, fabrication, and testing. Creation of database and engineering design correlations.

Three-Year Schedule

The schedule below reflects the revised scope approved by both sides

Year 1:

- Conduct literature review to understand the basic of mass transfer in micrreactor and separation of flue gas;
- Evaluate existing technologies and assess their applicability to CO_2 separation of flue gas;
- Repeat and implement some previous classical examples of microchannel separation to get familiarized with fundamentals and basic challenge;
- Analyze mixing in microchannels and possibility to use it in CO_2 separation;
- Continue improving efficiency of EHD separator for the fine liquid and solid particles;
- Conduct visualization study of liquid and solid particles migration in the electrical field.

Year 2:

- Continue on literature survey;
- Selection of the target alkanolamine;
- Simulate mixing and separation phenomena in microreactor via modeling and analytical means;
- Develop laboratory scale microchannel absorber and desorber for CO_2 separation;
- Conduct Experimental study and design optimization study;
- Continue on visualization study of liquid and solid particles migration in the electrical field.
-

Year 3:

- Conduct visualization study on absorption and desorption in microchannels;
- Design iterations and implementation;
- Parametric study of CO_2 separation process and experiment on different designs;
- Continue on simulation of mixing and separation phenomena in microreactor via modeling and analytical means;
- Present the best design to ADNOC group of companies;
- Develop design correlation;
- Prepare report.

Microreactors for Oil and Gas Processes Using Microchannel Technologies

UMD Investigators: **Serguei Dessiatoun, Amir Shooshtari**
GRA: **Meera Mahadevan**
PI Investigators: **Afshin Goharzadeh, Ebrahim Al-Hajri**
Start Date: **October 2006**

1. Objective/Abstract

Microfabrication techniques are increasingly used in gas and petrochemical engineering to realize structures with capabilities exceeding those of conventional macroscopic systems. In addition to already demonstrated chemical analysis applications, microfabricated chemical systems are expected to have a number of advantages for chemical synthesis, chemical kinetics studies, and process development. Chemical processing advantages from increased heat and mass transfer in small dimensions are demonstrated with model gas, liquid and multiphase reaction systems.

Different applications of microreactors and their impact on UAE industry economics have been evaluated in this quarter. The application of microreactors in the polymerization of ethylene and propylene is feasible and may provide significant economic benefits, and therefore will be considered for further investigation in the current project

2. Milestones/Deliverables Scheduled for the Completed Quarter

- Obtained useful kinetic data from batch scale polymerization with the produced catalyst.
- Initiated experiments in the microchannel reactor.

3. Summary of Project Activities for the Completed Quarter

Using the catalyst and silica nano particles produced, ethylene homopolymerization was carried out in batch and semibatch reactors to establish kinetics and polymer characteristics.

SEMI-BATCH POLYMERIZATION

- Catalyst : EBI/MAO
- Support : Nano SiO_2
- Monomer: Ethylene

Reactor Contents:
- Ethylene Pressure: 30 psig
- Temperature: 70 °C
- Using Henry Gesetz Equation: [Ethylene]: 0.233 mol/L
- Solvent: Toluene : 300 mL
- Mol-Zr/g-catalyst : 1.28 e-4 (approx. from other experiments)
- Run Time: 2 hrs

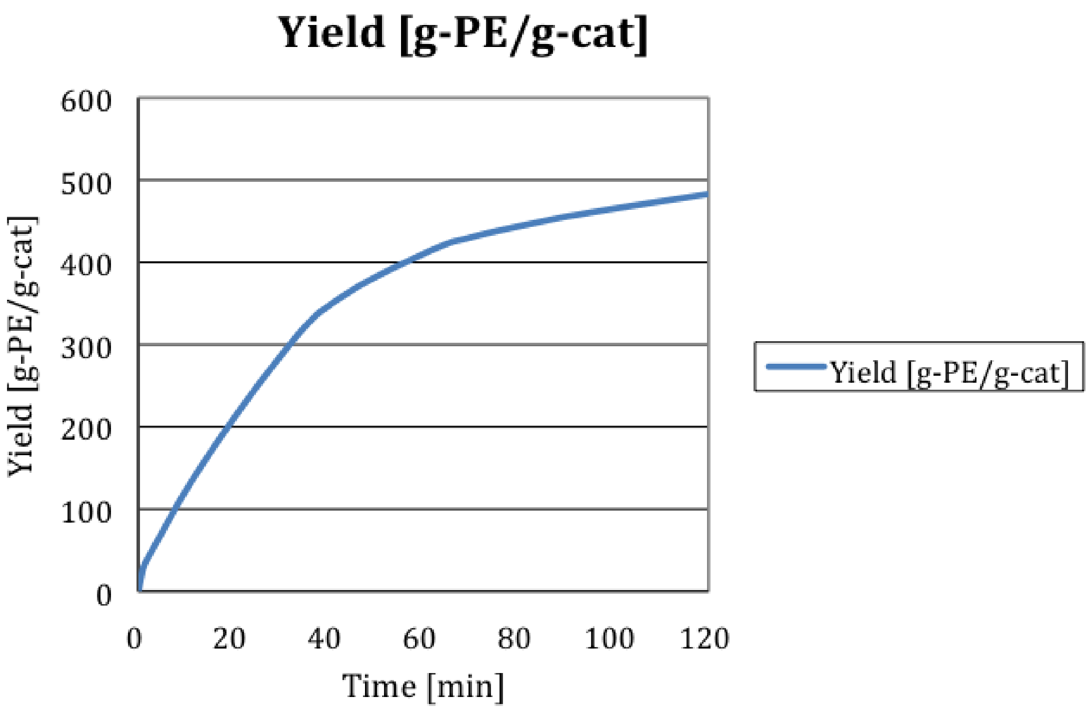
Yield [g-PE/g-cat]
600
500
400
300
200
100
0
0
20
40
60
80
100
120
Time [min]
Yield [g-PE/g-cat]
Yield [g-PE/g-cat]

Figure 1.

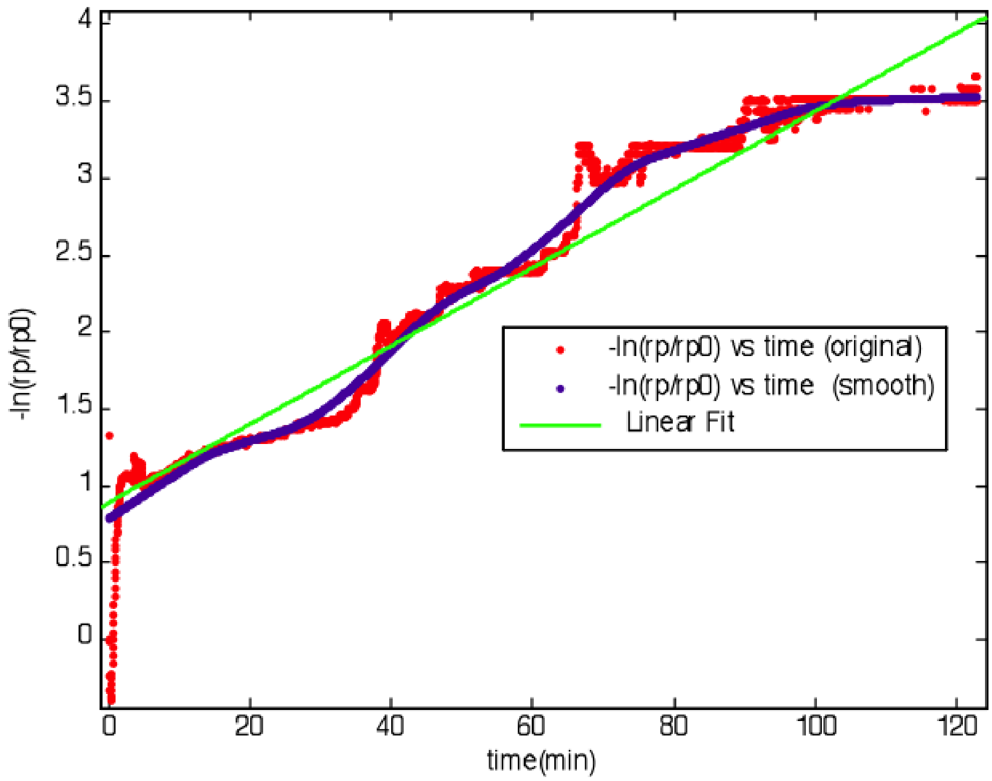

Figure 2.

$$R_p = k_p[M]_p f([C^*])w_m$$

$$R_p = k_p \eta [M]_b \psi [C_0^*] w_m$$

$$R_p = k_p \eta [M]_b \psi_0 [C_0^*]_0 e^{-k_d t} w_m$$

$$R_{p0} = k_p \eta_0 \psi_0 [M]_b [C_0^*]_0 w_m$$

$$\ln\left(\frac{R_p}{R_{p0}}\right) = -k_d t + \ln\left(\frac{\eta}{\eta_0}\right)$$

Rp- Rate of Polymerization (g-polymer/g-cat min)
kp- Propagation constant (L/mol.min)
C*- Active site concentration (mol-Zr/g-cat)
kd-deactivation constant
Ψ - catalyst site efficiency
η -effectiveness factor

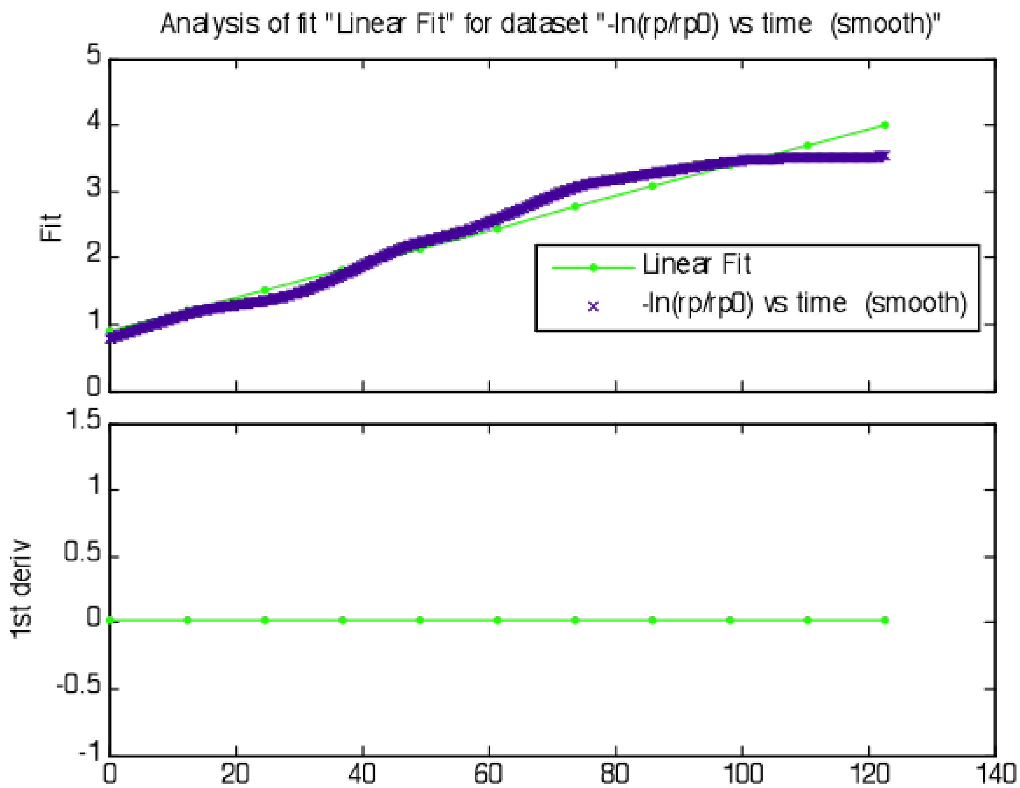

Figure 3.

$$\ln\left(\frac{R_p}{R_{p0}}\right) = -k_d t + \ln\left(\frac{\eta}{\eta_0}\right)$$

$$\frac{\eta}{\eta_0} = 0.72$$

$$k_d = 0.025 \text{ min}^{-1}$$

Batch Polymerization

- Catalyst : EBI/MAO
- Support : Nano SiO2
- Monomer: Ethylene

Reactor Contents:

- Ethylene Pressure: 30psig
- Temperature: 70C
- Using Henry Gesetz Equation : [Ethylene] (initial): 0.233 mol/L
- Solvent: Toluene : 300mL
- Mol-Zr/g-catalyst : 1.28e-4 (approx. from other experiments)
- Reaction Time: 32mins

$$gPE = ([M]_0 - [M]) w_m V_{toluene}$$

$$gCat = 0.05g$$

$$r_p = gPE / gCat.\min$$
$$[M] - mol / L$$
$$w_m - g / mol$$
$$[C^*] : mol(Zr) / gCat$$
$$k_p - L / mol.\min$$
$$k_d - \min^{-1}$$
$$r_p = -k_p [M][C_0^*] e^{-k_d t}$$
$$r_{p0} = -k_p [M_0][C_0^*] e^{-k_d t_0}$$
$$\ln\left(\frac{r_p}{r_{p0}} . \frac{[M_0]}{[M]}\right) = -k_d (t - t_0)$$

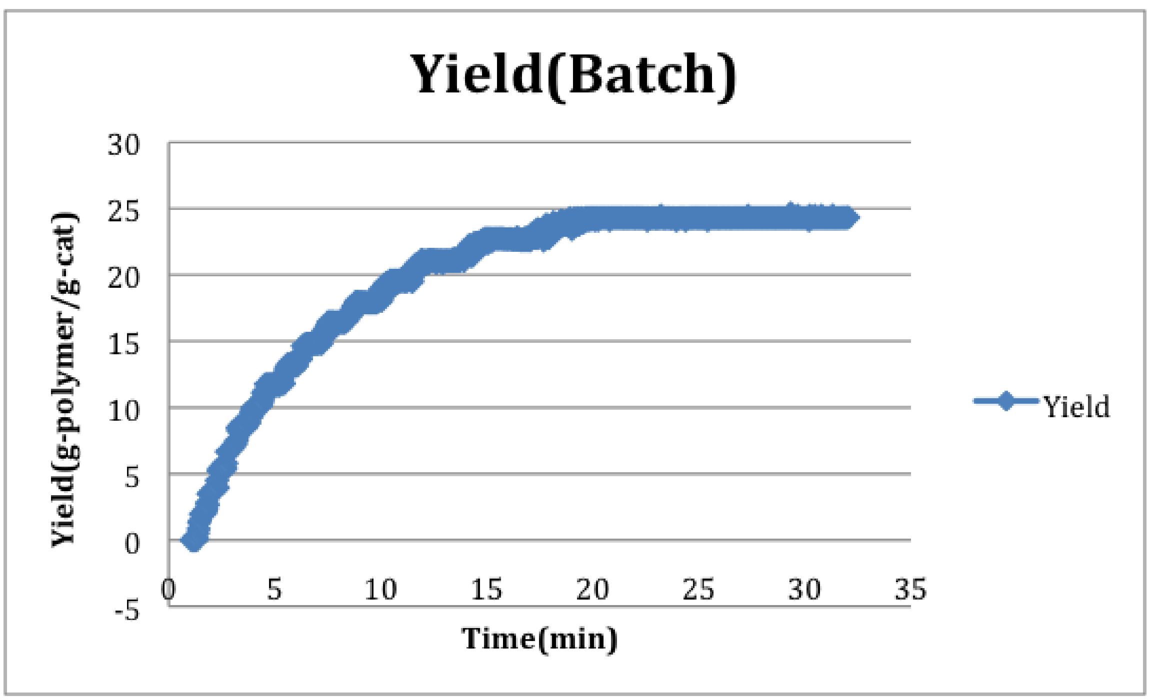

Figure 4.

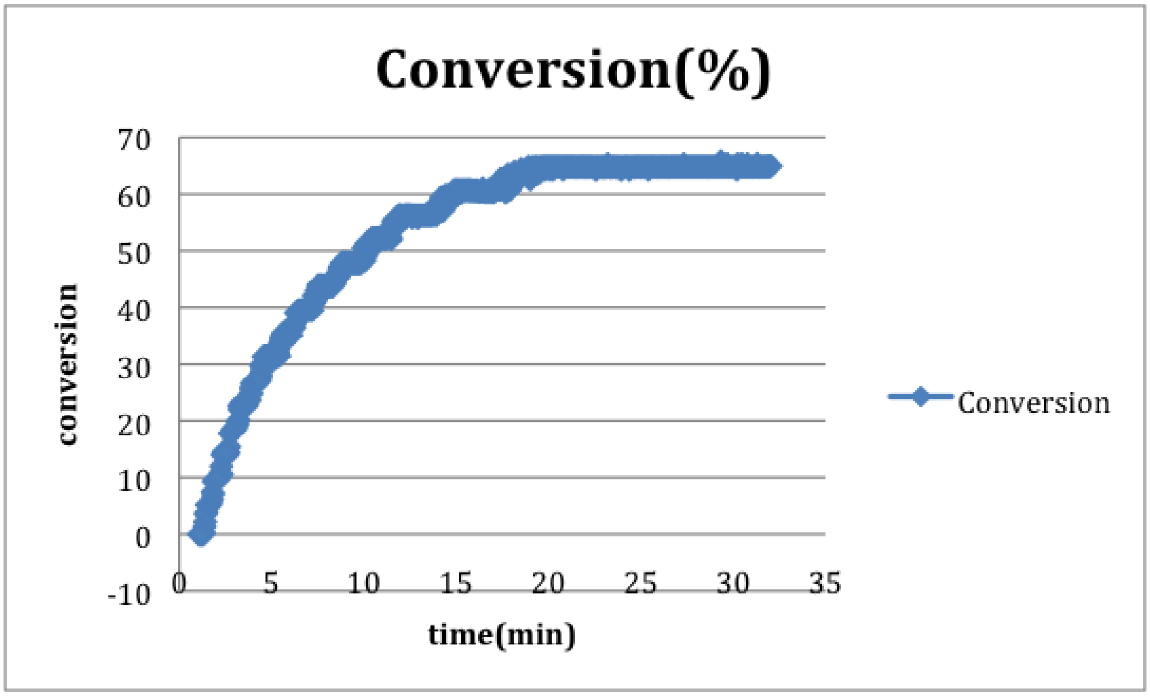

Figure 5.

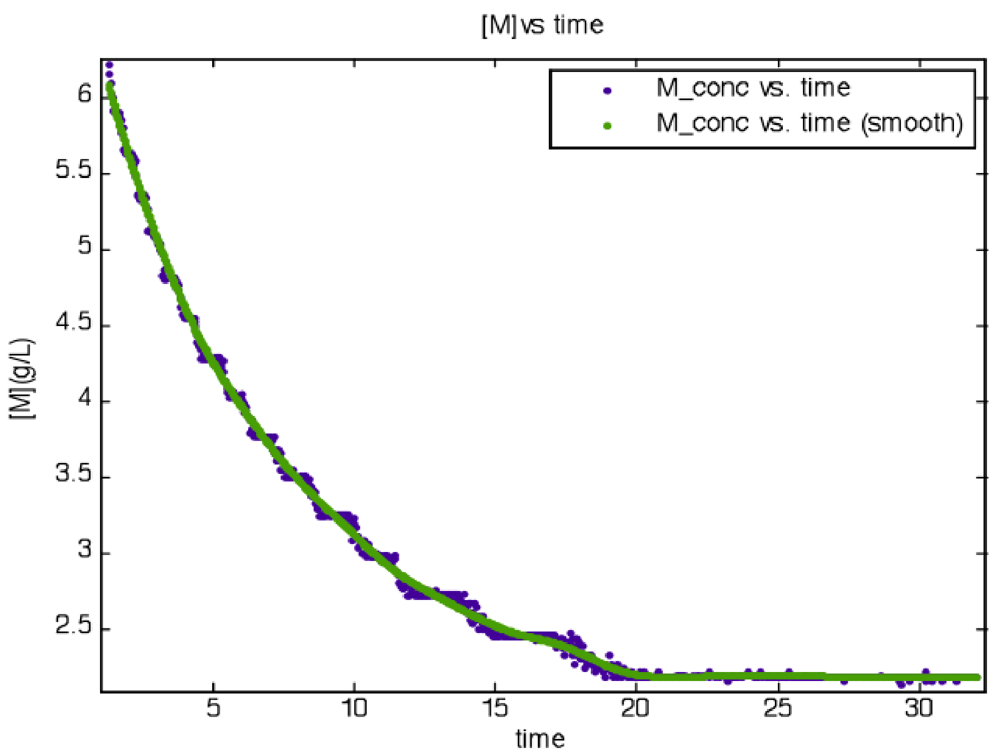

Figure 6.

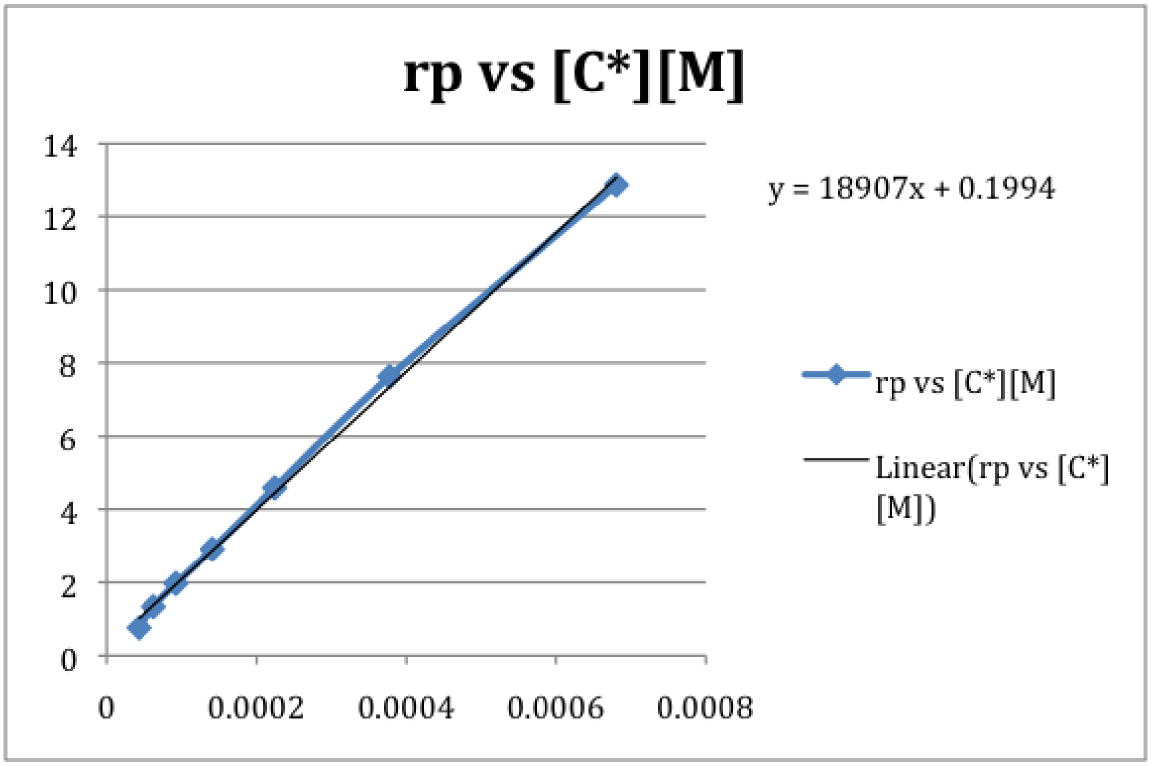

Figure 7.

Kp=18907 L/mol-min

These values of the kinetic constants are useful in modeling the experiments to be conducted in the microreactor set up.

SEM IMAGES OF SILICA SUPPORT, CATALYST, POLYETHYLENE PRODUCED

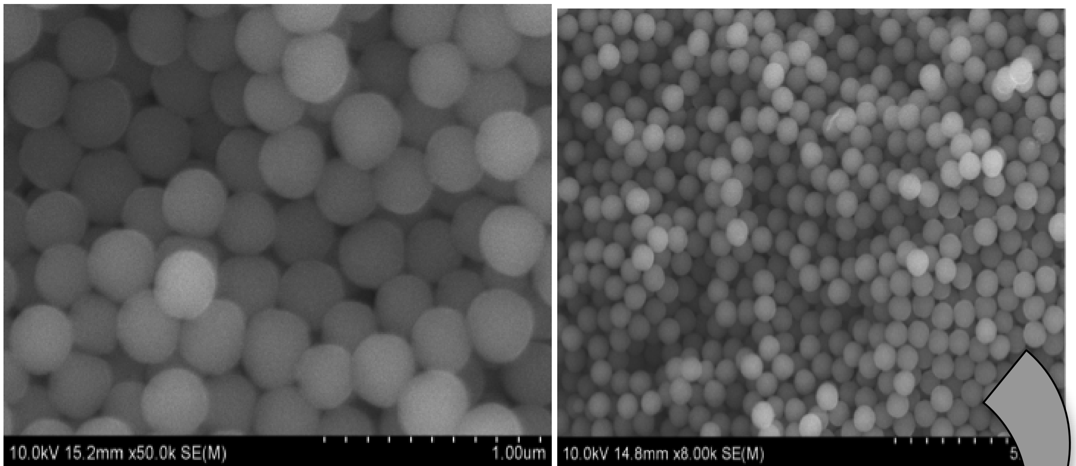

Figure 8. Silica nano-particles (300-400 nm).

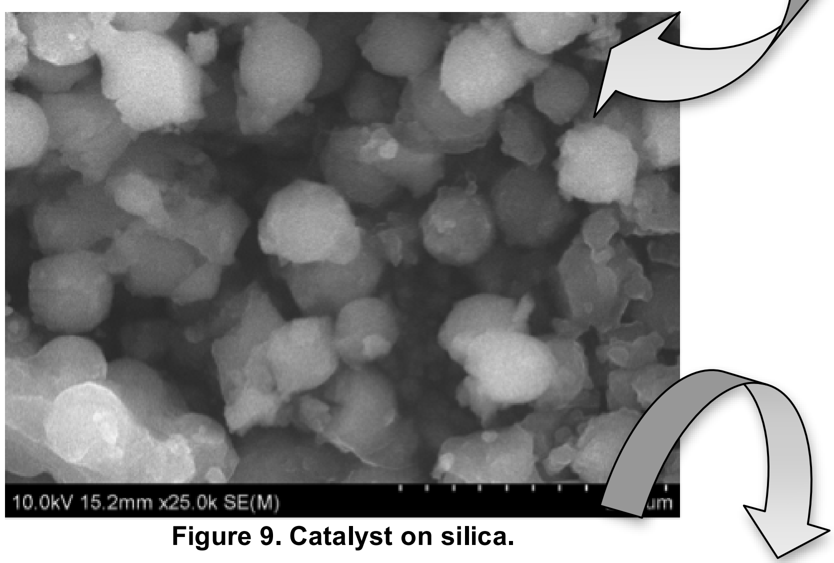

Figure 9. Catalyst on silica.

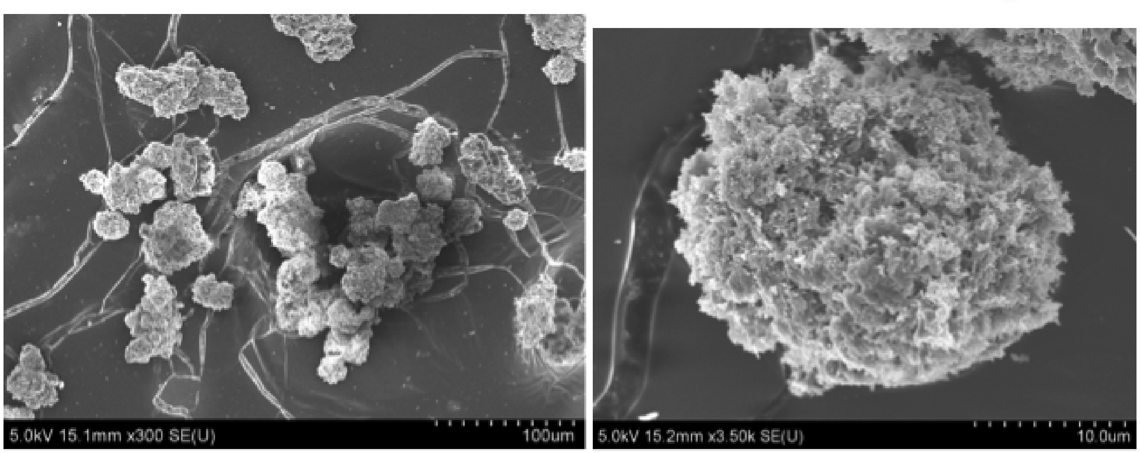

Figure 10. Polyethylene produced.

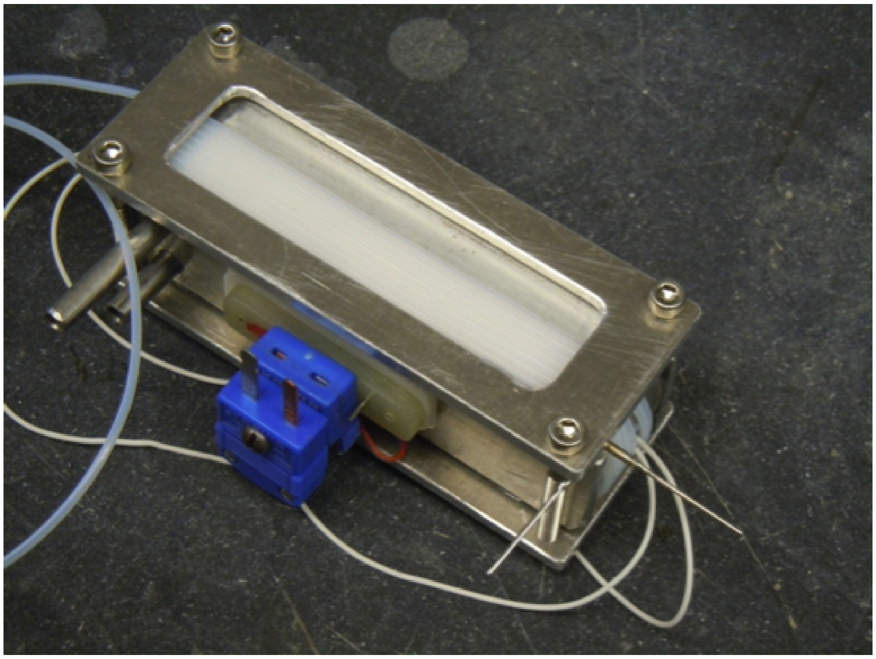
Figure 11.

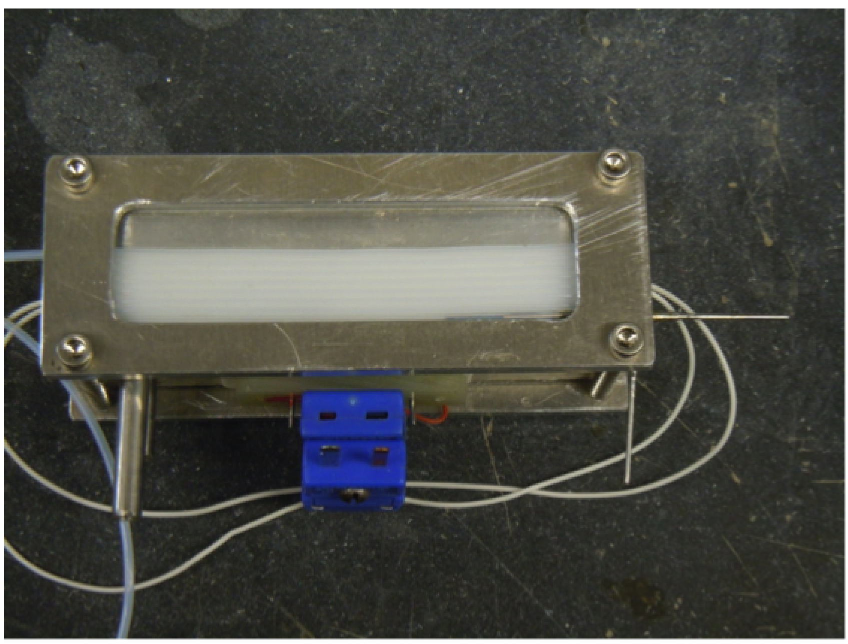
Figure 12.

Video snapshots of different flowrate analysis in the above microreactor setup to determine absorption of ethylene in toluene. Uniform Taylor bubbles were observed, which can be used to estimate mass transfer in the system.

4. References

[1] Development of a Microchannel In Situ Propellant Production System- September 2005 Prepared for the National Aeronautics and Space Administration Lyndon B. Johnson pace Center by KP Brooks, SD Rassat and WE TeGrotenhuis

[2] Catalytic synthesis of hydrogen peroxide in microreactors, Chemical Engineering Research and Design, volume 86, Issue 4, April 2008, Pages 410-415. S. Maehara, M. Taneda, K. Kusakabe

[3] Kinetics of hydrogen peroxide synthesis by direct combination of H2 and O2 in a microreactor, Catalysis Today, Volume 125, Issues 1-2, 15 July 2007, Pages 40-47 Yury Voloshin, Raghunath Halder, Adeniyi Lawal

[4] Auto-oxidation production of hydrogen peroxide via oxidation in a microreactor United States Patent 7416718, Sethi, Dalbir S. (Cranbury, NJ, US), Dada, Emmanuel A. (Bensalem, PA, US), Hammack, Kevin (League City, TX, US), Zhou, Xinliang (Sugar Land, TX, US)

[5] Experimental studies on hydrogenation of anthraquinone derivative in a microreactor Catalysis Today, Volume 125, Issues 1-2, 15 July 2007, Pages 48-55 Raghunath Halder, Adeniyi Lawal

[6] Chinese Journal of Chemical Engineering, 16(4) 503-516 (2008), "A State-of-the-Art Review of Mixing in Microfluidic Mixers" , Elmabruk A. Mansur, YE Mingxing , WANG Yundong and DAI Youyuan, The State Key Laboratory of Chemical Engineering, Department of Chemical Engineering, Tsinghua University,Beijing 100084, China.

[7] Morini, G.L., "Viscous heating in liquid flows in micro-channels", Int. J. Heat Mass Transfer, 48, 3637-3647 (2005).

[8] Judy, J., Maynes, D., Webb, B.W., "Characterization of frictional pressure drop for liquid flows through microchannels", Int. J. Heat Mass Transfer, 45, 3477-3489 (2002).

[9] Glasgow, I., Batton, J., Aubry, N., "Electroosmotic mixing in microchannels",Lab Chip, 4, 558-562 (2004).

[10] Engler, M., Kockmann, N., Kiefer, T., Woias, P., "Numerical and experimental investigations on liquid mixing in static micromixers",Chem. Eng. J., 101, 315-322 (2004).

[11] Yu, H.Y., Xiao, S.S., Chen, H., Fan, S.F., "Influence of flow velocity profile on mixing in micromixer", Nanotechnology and Precision Engineering (China), 3 (4), 290-294 (2005). (in Chinese).

[12] Bothe, D., Stemichb, C., Warnecke, H., "Fluid mixing in a T-shaped micro-mixer", Chem. Eng. Sci., 61, 2950-2958 (2006).

[13] Zhao, Y.C, Ying, Y., Chen, G.W., Yuan, Q., "Characterization of micro-mixing in T-shaped micro-mixer", J. Chem. Ind. Eng. (China),57, 1884-1890 (2006). (in Chinese).

[14] Goullet, A., Glasgow, I., Aubry, N., "Effects of microchannel geometry on pulsed flow mixing", Mech. Res. Commun., 33, 39-746 (2006).

[15] Johnson, T., Ross, D., Locascio, L., "Rapid microfluidic mixing",Anal. Chem., 74, 45-51 (2002).

[16] Seok Woo Lee, Dong Sung Kim2, Seung S. Lee, and Tai Hun Kwon, "SPLIT AND RECOMBINATION MICROMIXER BASED ON PDMS THREE-DIMENSIONAL MICRO STRUCTURE", Korea Advanced Institute of Science and Technology, Pohang University of Science and Technology.

[17] The Engineering ToolBox, "Thermal Conductivity of some common Materials", Online Resources, Tools and Basic Information for Engineering and Design of Technical Applications, Available at: http://www.engineeringtoolbox.com/thermal-conductivity-d_429.html Lass accessed on July 17, 2009

[18] DuPont Teflon fluoropolymer manufacturer, Fluoropolymer Typical Properties, available online at: http://www2.dupont.com/Teflon_Industrial/en_US/tech_info/techinfo_compare.html last accessed on July 17, 2009
[19] Rodgers P, 2009, “MEEG376 Core measurements Uncertainty analysis”, The Petroleum Institute, spring 2009
[20] A.Y. Tonkovich, S. Perry, D. Qiu, T. LaPlante, W.A. Rogers, Microchannel process technology for compact methane steam reforming. Velocys, Inc., Technology Development, 7950 Corporate Drive, Plain City, OH 43064, USA. Y.Wang (Battelle, Pacific Northwest National Laboratory, Richland, WA 99352, USA)
[21] “The discovery and progress of MgCl2-supported TiCl4 catalysts”. N. Kashiwa, J. Polym. Sci. A: Polym. Chem. 42 (1–8) (2004) 1.
[22] J.J.A. Dusseault, C.C. Hsu, J. Macromol. Sci. Rev. Macromol. Chem. Phys. C 33 (2) (1993) 103.
[23] S. Kojoh, T. Fujita, N. Kashiwa, Recent Res. Dev. Polym. Sci. 5 (2001) 43.
[24] J.T.M. Pater, G. Weickert, J. Loos, W.P.M. van Swaaij, Chem. Eng. Sci. 56 (2001) 4107.
[25] J.T.M. Pater, G.Weickert,W.P.M. van Swaaij, J. Appl. Polym. Sci. 87 (2003) 1421.
[26] G.Weickert, G.B. Meier, J.T.M. Pater, K.R.Westerterp, Chem. Eng. Sci. 54 (1999) 3291.
[27] L. Noristi, E. Marchetti, G. Baruzzi, P. Sgarzi, J. Polym. Sci. A: Polym. Chem. 32 (1994) 3047.
[28] X. Zheng, J. Loos, Morphology evolution in the early stages of olefin polymerization, Macromol. Symp., 236, 249-258, (2006).
[29] X. Zheng, M.S. Pimplapure, G. Weickert, J. Loos, Influence of porosity on the fragmentation of Ziegler-Natta catalysts in the early stages of propylene polymerization, e-Polym., 028, 1-10, (2006).
[30] M. Bartke, in: J.R. Severn, J.C. Chadwick (Eds.), Tailor-Made Polymers. Via Immobilization of Alpha-Olefin Polymerization Catalyst, Wiley–VCH Verlag GmbH & Co. KGaA,Weinheim, 2008.
[31] G. Cecchin, E. Marchetti, G. Baruzzi, Macromol. Chem. Phys. 202 (2001) 1987.
[32] Adiwinata G., Prashant M., Panagiotis D. C., Fault-tolerant control of a polyethylene reactor, Journal of Process Control 17 (2007) 439–451

Thrust 3
Energy System Management

Integration of Engineering and Business Decisions for Robust Optimization of Petrochemical Systems

UMD Investigators: Shapour Azarm, P.K. Kannan
PI Investigators: Ali Almansoori, Ali Elkamel
UMD GRA: Weiwei Hu
PI GRA: Adeel Butt
Acknowledgements: Zhichao Wang, Khaled Saleh
Start Date: Oct 2006

1. Objective/Abstract

The overall objective of this project is to develop a framework for integrating engineering and business decisions. In this quarter, our research efforts continued to extend the dashboard-based Decision Support System (DSS) by considering the crude oil processing units in the refinery. A preliminary Matlab-based model was developed that included crude distillation, catalytic reforming, hydro treating and other important operations. This model allows the dashboard-based DSS framework to consider costs and revenues in the crude distillation process for profit calculation. Additionally, the previous HYSYS simulation model was improved with a heat exchanger network design to recover the extra energy generated from the reactor. Several other revisions/changes were also made in the HYSYS model to reflect practical operational considerations. Finally, for the invited book chapter on "Multi-Objective Optimization: Techniques and Applications in Chemical Engineering," a preliminary draft was completed during this quarter. The book chapter summarizes two multi-objective robust optimization methods and an online approximation technique. A new objective robustness measure was defined for the first time to restrict only downside variation in the objective functions. The methodologies in the book chapter and the newly defined robustness measure can potentially benefit the operational optimization under uncertainty for oil and petrochemical industries.

2. Deliverables for the Completed Quarter

- Completed a preliminary draft for a book chapter in "Multi-Objective Optimization: Techniques and Applications in Chemical Engineering":
  - Summarized two important multi-objective robust optimization methods and an online approximation technique.
  - Defined a new objective robustness measure to restrict only downside variation in objective functions.

- Developed a preliminary model to simulate crude distillation/separation process, which can be integrated later with the dashboard:
  - Developed a series of crude oil processing modules, e.g., crude distillation, catalytic reforming, hydro treating, and etc., in Matlab.
  - Connected different crude oil processing modules and derived a profit function.
  - A blending module is under preparation and will be developed soon.

- Improved the HYSYS reactor-distillation model with heat integration :
  - Developed a heat exchanger network to recover the energy from reaction gases and used it for heating feed streams.
  - Revised the previous HYSYS model by applying 'adjust operation' to ensure the reactor-distillation process to be working within practical operating conditions.

- Progress on recent joint publications:

  Journal Papers:

  [1] Hu, W., M. Li, Azarm, S. and Almansoori, A., 2011, "Multi-Objective Robust Optimization Under Interval Uncertainty Using Online Approximation and Constraint Cuts," Journal of Mechanical Design, 133(6), pp. 061002-1 to 061002-9.

  [2] Hu, W., A. Almansoori, Kannan, P.K., Azarm, S. and Wang, Z. 2010, "Corporate Dashboards for Integrated Business and Engineering Decisions in Oil Refineries: an Agent-Based Approach" Decision Support Systems, revised and submitted.

  [3] Hu, W., Azarm, S. and Almansoori, 2011, "Approximation Assisted Multi-objective collaborative Robust Optimization (AA-McRO) under Interval Uncertainty," submitted to Structural of Multidisciplinary Optimization (reviews are back and the paper is under major revisions).

  Book Chapter:

  [4] Hu, W., Butt, A., Azarm, S., Almansoori, A. and A. Elkamel, 2011, *Robust Multi-Objective Genetic Algorithm under Interval Uncertainty*, in *Multi-Objective Optimization: Techniques and Applications in Chemical Engineering*, in progress.

  Working Paper:

  [5] Hu, W., Azarm, S. and Almansoori, A., 2011, "Uncertain Interval Reduction Approach with Multi-Objective Robust Optimization with Online Approximation," under preparation.

  Working Conference Proceeding:

  [6] Butt, A., Almansoori, A., Elkamel, A., Hu, W., Wang, Z., Kannan, P.K. and Azarm, S., "An Agent-Based Approach to an Integrated Corporate Dashboard for Oil Refinery," 2012 Canadian Operational Research Society (CORS) International Joint Conference, June 12-13. (Abstract was originally submitted to 2011 Canadian Society of Chemical Engineering Conference)

3. Summary of Project Activities for the Completed Quarter

Project meetings held during the ninth quarter were as follows:

Three teleconference meetings were held between PI and UMD research collaborators on July 7, August 1 and September 21, with Adobe Connection. Highlights of these meetings include:

(1) Mr. Adeel Butt (PI graduate student) came to Maryland for a six-week internship. His research training plan was focused on refinery simulation model development and optimization implementation.
(2) A working plan for the proposed book chapter in “Multi-Objective Optimization: Techniques and Applications in Chemical Engineering” was developed and presented.
(3) Research progress on a simple oil refinery model development was discussed. A set of GAMS codes was converted to Matlab files which represented various units in the refinery. Efforts made to connect these files together to simulate an oil refinery process.
(4) Status on joint publications was discussed. A journal paper based on the dashboard model was revised and re-submitted to the Journal of Decision Support Systems. A second journal paper based on a multi-disciplinary optimization technique with a chemical engineering example was submitted to Structure and Multidisciplinary Optimization, respectively.

Research efforts in this quarter included the following:

Completing a preliminary draft for the book chapter in "Multi-Objective Optimization: Techniques and Applications in Chemical Engineering"

Our research efforts in this quarter focused on a book chapter, titled "Robust Multi-Objective Genetic Algorithm (R-MOGA) under Interval Uncertainty." The R-MOGA method was developed as a collaborative research effort between UMD and PI team. The book chapter consists of six main sections: 1. Introduction; 2. Background and Definition; 3. Robust Multi-Objective Genetic Algorithm (R-MOGA); 4. Approximation Assisted R-MOGA; 5. Numerical and Chemical Engineering Examples and 6. Conclusion. The draft of the book chapter was scheduled to be completed in October 2011, while the final manuscript is planned to be submitted in November, 2011. An abstract for this chapter was submitted earlier.

The book chapter will discuss two optimization methods and an online approximation technique. The two optimization methods include a previous robust multi-objective optimization method and its improved version developed by our group. The online approximation technique was developed to reduce computational cost in optimization. One motivation in developing the robust multi-objective optimization methods was fact that the oil and petrochemical systems/processes typically include multiple objectives: e.g., maximizing profit and maximizing product quality. Furthermore, the operational conditions and parameters in these processes are often uncertain and hard to predict. On the other hand, a challenge in solving the oil and petrochemical process optimization problems lies in its computational cost. It is well known that computer models for process simulations are becoming increasingly complex, which results in extended and sometimes intractable computations when optimization is conducted based on such models. To overcome this difficulty, an online approximation method was developed and integrated with the robust multi-objective optimization framework. The combination of robust multi-objective optimization and online approximation allows the decision makers to efficiently obtain optimal decision variables for an oil refinery process.

In many earlier robust optimization methods, both upside and downside variations in the objective functions were restricted. However, a simple change in the robust optimization approach can be made so that only downside variation in the objective function is restricted. For example, when minimizing the utility cost in the refinery, if the uncertainty leads to a decrease in the utility, the decision maker is typically indifferent to such a variation. In view of this point, we present a newly defined objective robustness (as in the book chapter) next.

In a multi-objective optimization problem, it is assumed that both decision variables and parameters can have uncertainty. A design solution has a nominal value for the decision variables and parameters, as denoted by **x** and **p** (a bold letter representing a vector). However, the actual values for the decision variables and parameters may be uncertain and varied around the nominal values. Let $\Delta\mathbf{x}$ and $\Delta\mathbf{p}$ represent the uncertainty in **x** and **p**, respectively; the range (lower and upper bounds) is presumed known such as $\Delta\mathbf{x} \in [\Delta\mathbf{x}^l, \Delta\mathbf{x}^u]$ and $\Delta\mathbf{p} \in [\Delta\mathbf{p}^l, \Delta\mathbf{p}^u]$. Due to the interval uncertainty, the value for the objective function may also change. Typically, it is undesirable for an objective function value to increase if it should be minimized. Let $\Delta\mathbf{f}^+$ denote the increase in the design objectives, which can be calculated based on the formulation as shown in Eq. (1):

$$\begin{aligned}\Delta\mathbf{f}^+ &= [\mathbf{f}(\mathbf{x}+\Delta\mathbf{x}, \mathbf{p}+\Delta\mathbf{p}) - \mathbf{f}(\mathbf{x},\mathbf{p})]^+ \\ &= \begin{cases} \mathbf{0}, \text{ if } \mathbf{f}(\mathbf{x}+\Delta\mathbf{x}, \mathbf{p}+\Delta\mathbf{p}) \le \mathbf{f}(\mathbf{x},\mathbf{p}) \\ \mathbf{f}(\mathbf{x}+\Delta\mathbf{x}, \mathbf{p}+\Delta\mathbf{p}) - \mathbf{f}(\mathbf{x},\mathbf{p}), \text{ otherwise} \end{cases} \end{aligned} \tag{1}$$

where $\mathbf{f}(\mathbf{x}+\Delta\mathbf{x}, \mathbf{p}+\Delta\mathbf{p})$ and $\mathbf{f}(\mathbf{x}, \mathbf{p})$ represent the actual and nominal values for the objective functions. Note $\Delta\mathbf{f}^{+}$ is also a vector whose elements represent the variation in each objective function in multi-objective optimization. To measure the variation in all design objectives with a single value, we define $\|\Delta\mathbf{f}^{+}\|$ as the Euclidean norm of $\Delta\mathbf{f}^{+}$. In solving a multi-objective optimization problem under interval uncertainty, it is important that not only are the design solutions obtained optimal, but also that the increases on all its objectives are acceptable. In achieving this goal, the decision maker can specify a positive scalar value η_f called Acceptable Objective Variation Range (AOVR), such that the maximum Euclidean norm of the design objective vector, i.e., max$\|\Delta\mathbf{f}^{+}\|_{\max}$ is smaller than η_f. This condition can be formulated as a constraint function as shown in Eq. (2):

$$\max\left\|\Delta\mathbf{f}^{+}\right\| \le \eta_f \tag{2}$$

Since $\Delta\mathbf{f}^{+}$ represents an increase in objective functions, the inequality constraint in Eq. (2) ensures such an increase is always acceptable. A representation of objective robustness in a multi-objective optimization problem with interval uncertainty is shown in a 2-D space in Figure 1. The uncertainty space in Figure 1(a) has two axes defined by Δx and Δp, where the gray area represents the uncertain interval. Any point inside the gray area in the uncertainty space corresponds to the uncertainty: e.g., the zero point represents the nominal design solution; i.e., $(\mathbf{x}, \mathbf{p})$, in Figure 1 (a). The gray area in Figure 1 (a) is mapped to the objective variation space on the right-hand side where the zero point (origin) represents the nominal value for design objectives: i.e., $\mathbf{f}(\mathbf{x}, \mathbf{p})$, in Figure 1 (b). It can be seen that the maximum Euclidean norm of the design objective vector is the distance from the nominal point to the farthest point on the mapped objective variation range in Figure 1 (b). The dash-lined circle denotes the AOVR whose radius is equal to η_f.

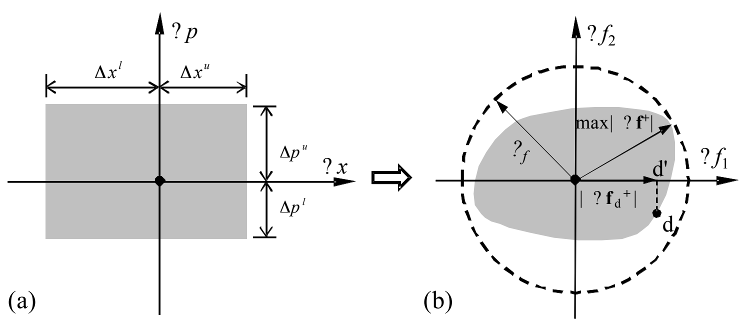

Figure 1. Objective robustness in multi-objective optimization with interval uncertainty.

Since we are only concerned with the increase (positive variation) in objective functions but indifferent to any decrease, any point in the third quadrant in the mapped objective variation range in Figure 1 (b) is ignored when measuring the furthest point. However, to calculate the Euclidean norm for a point in the second and forth quadrant, the point should be projected to the positive axis. For example, point d′ is the projection of point d in Figure 1 (b). The Euclidean norm for point d, i.e., $\|\Delta\mathbf{f}_{\mathrm{d}}^{+}\|$, is represented by the horizontal line segment along axis Δf_1. Likewise, all points in the second and forth quadrant of the mapped objective variation range (gray area) in Figure 1 (b) can be projected. In this way, in searching the furthest point, only the first quadrant needs to be considered. Figure 1 shows the case in which the furthest point on the mapped objective variation range is located in the first quadrant in the objective variation space. Since max$\|\Delta\mathbf{f}^{+}\| \le \eta_f$ is satisfied, the current nominal design is said to be objectively robust.

In the book chapter, a chemical engineering case study is used to demonstrate the method. The purpose is to use this case study to show the general procedure of applying multi-objective optimization to obtain robust optimal solutions in an efficient manner. This case study was targeted at a crude oil processing unit in a typical oil refinery. In the next section, the development of the case study model is presented.

Developing a preliminary model to simulate the crude distillation/separation process

Crude oil processing is an important and challenging operation in any oil refinery. The ultimate goal in crude processing is to ensure such an operation to be efficient and cost-effective in order to maximize the profit for a given amount of crude input. Today's oil refineries are becoming increasingly complex with a combination of various technologies for product quality improvement, energy savings and emission controls. For this reason, determining the most cost-effective operating conditions for an oil refinery can be a very difficult task.

There are many process configurations for crude distillation. The most common ones includes crude distillation unit (CDU), Fluid Catalytic Cracking (FCC), and hydro cracking. Additionally, other process technologies such as catalytic reforming, hydro-treating and sulfur recovery are widely adopted to comply with stringent environment and product quality regulations. Figure 2 shows the schematic of a typical oil refinery (a nomenclature is provided at the end of this report). The flow diagram was developed using the commercial oil refinery simulation software PetroPlan. The flow diagram depicts various unit processes and flows of intermediate product streams. For simplicity, the diagram does not include the facilities that provide utilities such as steam, cooling water and electricity. Also, the storage facilities such as the crude oil tank and intermediate product storage tank are not shown.

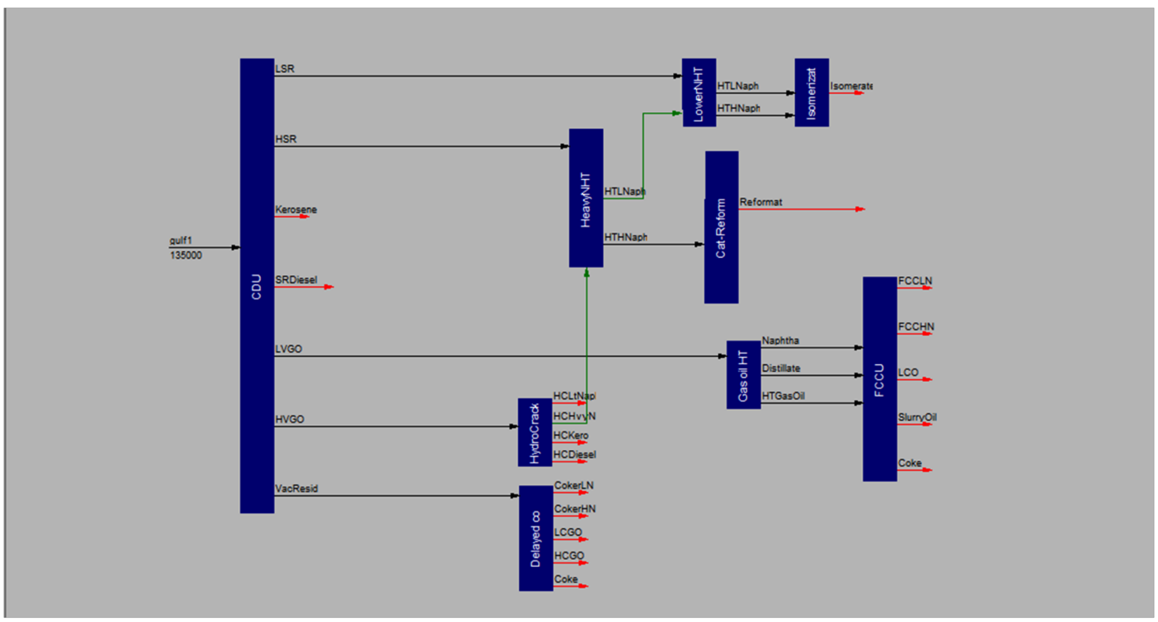

Figure 2. Flow diagram of a series of typical crude oil refining units

The crude processing model as shown in Figure 2 was simulated using Matlab based on the built-in property library and functional relationships defined in PetroPlan. The profit models and physical property calculation models for each block are also included in the library files of the software. For example, the assay (composition and material property) data of various type of crude oil can be obtained from a built-in spreadsheet in PetroPlan. It is assumed that 'Gulf' crude is the primary feedstock to the CDU as shown in Figure 2. The flow rate of the crude oil input is assumed to be fixed at 135,000 BPD (barrels per day). In Figure 2 the properties of outlet product streams from each block can be calculated from the inlet feed stream. For example, the flow rate of the intermediate product streams from the CDU block such as kerosene, Straight Run (SR) diesel can be calculated according to the crude oil feed flow rate and the cut point temperatures. The blocks are solved in the order indicated by the user. It is up to the user to decide this sequence so that each block's feeds are calculated by the preceding blocks.

The rates and properties of the streams flowing from one refinery block (process unit, mixer, splitter, etc.) to another as well as the streams going to sales are calculated. Profit is calculated from feedstock and product prices taking into account utility and other costs. The formulation of profit is given in Eq. (3):

$$profit = \sum_{i \in SI} F_i c_i - \sum_{k \in SK} F_k c_k - \sum_{r \in SR} C_r \qquad (3)$$

where c_i is the unit price of products and c_k is the unit cost of feed material. F_i and F_k are the quantities of product sales and crude oil feed flow rate, respectively. C_r represents other costs such as the capital cost, operating and utility costs, labor cost, inventory cost and so on. SI denotes different types of products, and SK represents various components of feeding stream. SR includes the resources that the process requires: e.g., human resources, cooling water, and electricity.

Improving the HYSYS reactor-distillation model with heat integration

Heat integration is an effective approach to reduce energy consumption and cost in the reactor-distillation process. The previous reactor-distillation model was improved by partially recovering the heat generated from the reactor through a heat exchanger network design, as shown in Figure 3.

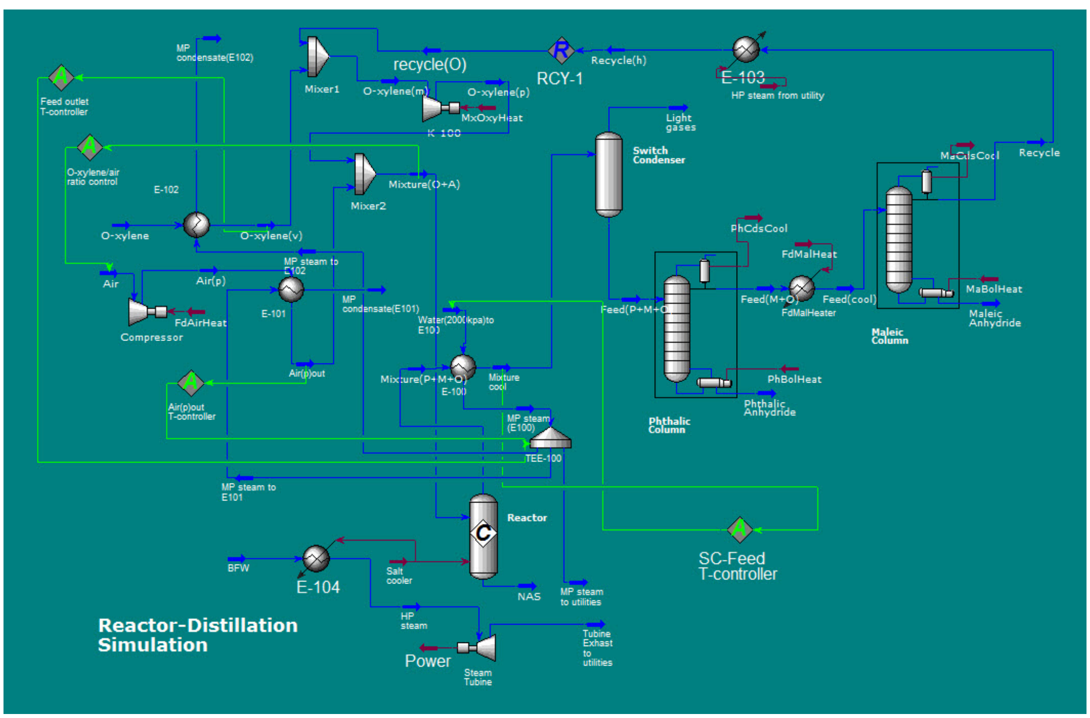

Figure 3. A heat-integrated reactor-distillation model

In the reactor-distillation simulation model in Figure 3, the feedstock of o-xylene and air are preheated to ensure complete vaporization before it enters the reactor. In the previous model, the preheating was defined as a simple heating process which requires external energy input. In the improved model, the heaters for both air and o-xylene are replaced by heat exchangers using medium pressure steam as a heating source. This steam is produced by utilizing the heat of reaction gases exiting from the reactor, which puts a limit on the exit temperatures of both o-xylene feed and air. Therefore, an adjust operation is applied to avoid the temperature mismatch in heat exchangers, as shown in Figure 3.

The reaction is highly exothermic and is controlled at a temperature of 370 ^{0}C at the exit. The remaining reaction heat is recovered by a salt cooler, a special type of salt composition used in the industry. The heat recovered by the salt cooler is used to produce high-pressure steam, which is used to produce power. In the actual process, the steam is totally condensed in vacuum condenser at the exit of steam turbine to recover maximum amount energy. But since this model does not present the actual scenario, the current model will not consider such a case.

Adjust operation is also applied on the mixture of o-xylene/air to the reactor, in order to control the o-xylene/air ratio between 6 to 10 mol%. The lower flammability limit of O-xylene to air is 1 mol%, and upper flammability limit is 6 mol%. For safety considerations, it is necessary that process conditions comply with that limit. Furthermore, it is also necessary that the percentage of O-xylene content in the reactor does not exceed 10 mol% because beyond this limit the catalyst will no longer operate at the desired selectivity and the reaction could become oxygen starved, forming a significant amount of CO and other undesired by-products.

In the model shown in Figure 3, the switch condenser is defined as a network of heat exchangers and a separator. For simplicity we use a simple separator to represent the switch condenser with an adjusted inlet temperature of 85 ^{0}C. According to the simulation results, production capacity may be increased when the inlet temperature is controlled to be equal to or less than 70 ^{0}C. This can be achieved by considering the condenser as real or near to real. The ratio of medium pressure steam to o-xylene heat exchanger and air heat exchanger is adjusted to control the outlet temperatures of these heat exchangers (5 ^{0}C approach is considered). The remaining steam can be exported as utilities.

4. Difficulties Encountered/Overcome

Because an Aspen license was unavailable (including HYSYS that is used for the engineering simulation model in dashboard), it was decided to extend the refinery process simulation with Matlab. In this quarter, we focused on developing simulation models for a series of crude processing units such as crude distillation, catalytic reforming, and hydro-treating. Developing such models required definitions of physical properties of different streams and correlations between various flows. Such information was obtained from the built-in library and spreadsheets in the commercial refinery simulation software PetroPlan. After successful completion of Matlab codes for each unit in the process, they were connected through a single executable file as per the sequence in the flow sheet. Currently, the crude processing model does not consider blending of intermediate products from different units; a MATLAB model for the blender is in progress.

5. Planned Project Activities for the Next Quarter

- Develop a Matlab-based simulation model for blending of intermediate flow streams from different process units.
- Connect the blending model with the crude oil process simulation models.
- Refine the case study with an integration of the crude oil refinery simulation model within the dashboard-based DSS framework.
- Finalize and submit the book chapter.

6. References

[1] Aspen HYSYS, 2009, http://www.aspentech.com, Aspen Technology.
[2] Deb, K., 2001, “Multi-Objective Optimization using Evoluionary Algorithms,” John Wiley & Sons, Ltd, New York.
[3] Douglas, J.M., 1988, “Conceptual Design of Chemical Processes”, McGraw-Hill, New York, USA.
[4] Forbes, R.J., 1948, “Short History of the Art of Distillation”, Brill, Leiden, Holland.
[5] Gargeya, V., 2005, “Plant Level Performance Measurement: An Exploratory Case Study of a Pharmaceutical Encapsulation Company”, Technovation, 25(12), pp.1457-1467.
[6] Gattu, G., Palavajjhala, S., and Robertson, D., 2003, “Are Oil Refineries Ready for Non-Linear Control and Optimization?” International Symposium on Process Systems Engineering and Control, Mumbai, India.
[7] Grossmann, I. E., 2005, “Enterprise-Wide Optimization: A New Frontier in Process Systems Engineering,” AIChE Journal, 51(7), pp. 1846-1857.
[8] Halemane K. P., Grossmann I. E., 1983, “Optimal Process Design under Uncertainty,” AIChE Journal, 29(3), pp. 425-433.
[9] Hu, W., M. Li, Azarm, S. and Almansoori, A., 2011, "Multi-Objective Robust Optimization Under Interval Uncertainty Using Online Approximation and Constraint Cuts," Journal of Mechanical Design, 133(6), p. 061002.
[10] Jackson, J., Hofmann, J., Wassick, J. and Grossmann, I., 2003, “A nonlinear multi-period process optimization model for production planning in multi-plant facilities”, Proceedings FOCAPO2003, pp. 281-284..
[11] Janak, L., Lin, X. and Floudas, C. A., 2007, “A New Robust Optimization Approach for Scheduling Under Uncertainty: II. Uncertainty with Known Probability Distribution,” Computers and Chemical Engineering, 31(3), pp. 171-195.
[12] Kaplan, R. and Norton, D., 1996, “Using the Balanced Scorecard As a Strategic Management System”, Harvard Business Review, 74(1), pp. 75-85.
[13] Kleijnen, J. and Smits, M., 2003, “Performance metrics in supply chain management”. Journal of the Operational Research Society, 54(5), pp. 507–514.
[14] Koehler, J.R., Owen, A.B., 1996, "Computer Experiments," Handbook of Statistics, Elsevier Science, New York. pp. 261-308.
[15] Lin, X., Janak, S. L. and Floudas, C. A., 2004, “A New Robust Optimization Approach for Scheduling Under Uncertainty: I. Bounded Uncertainty,” Computers and Chemical Engineering, 28(6-7), pp. 1069-1085.
[16] Linnhoff, B., Townsend, W., Boland, D., Hewitt, F., Thomas, E., Guy, R. and Marsland, H., 1982, “User Guide on Process Integration for the Efficient Use of Energy,” IChemE, UK.
[17] Li, M., and Azarm, S., 2008, "Multiobjective Collaborative Robust Optimization with Interval Uncertainty and Interdisciplinary Uncertainty Propagation," Journal of Mechanical Design, 130(8), p. 081402.
[18] Micheletto, S. R., Carvalho, M. C. A. and Pinto, J. M., 2008, “Operational Optimization of the Utility System of an Oil Refinery,” Computers and Chemical Engineering, 32(1-2), pp. 170-185.
[19] Netlogo, http://ccl.northwestern.edu/netlogo/, Sep., 2011.
[20] PetroPlan, http://www.ingeniousinc.com/proplan-main.php, Sep., 2011.
[21] Pinto, J., Joly, M. and Moro, L., 2000, “Planning and scheduling models for refinery operations”, Computers and Chemical Engineering, 24(9), pp. 2259–2276.
[22] Sahdev, M., Jain, K., Srivastava, P., “Petroleum Refinery Planning and optimization Using Linear Programming”, The Chemical Engineers' Resource Page, http://www.cheresources.com/refinery_planning_optimization.shtml
[23] Simpson, T. W., and Mistree, F., 2001, “Kriging Models for Global Approximation in Simulation-Based Multidisciplinary Design Optimization," AIAA Journal, 39(12), pp. 2233-2241.
[24] Suresh, S. Pitty, Li, W., Adhitya, A., Srinivasan, R., Karimi, A., 2008, “Decision support for integrated refinery supply chains”, Computer and Chemical Engineering, 32, pp. 2767–2786.
[25] Z. Wang, S. Azarm, and P. K. Kannan, 2011, “Strategic Design Decisions for Uncertain

Market Systems Using an Agent Based Approach," Journal of Mechanical Design," 133(4), p. 041003

Appendix

Justification and Background

Many oil, gas and petrochemical systems involve numerous coupled subsystems. These systems and their subsystems usually have uncertain inputs and thus it can be difficult to make the “best” engineering and business decisions in terms of independent operations of these complex systems. It becomes even more difficult to make those decisions when the system consists of many units or plants producing different products. This difficulty presents an opportunity taken on in this project. A review of mainstream literature has revealed that previous models in management of petrochemical systems have been based on either engineering or business decisions but not both. There is a significant gap in the literature as to how these two types of decisions should be devised and integrated. To address this important gap, the focus of this investigation is to develop an integrated robust decision support framework considering both engineering and business models under uncertain conditions. Our overall objective has several underlying research questions, including: (i) how to develop business models that include management decisions in a multi-unit organization and at the same time account for engineering aspects; (ii) how to determine the relative importance and effects of uncertain system and/or subsystem input parameters on subsystem and/or system outputs (e.g., system performance); (iii) how to define a set of metrics, by way of a dashboard, that will serve as a visualization tool to keep track of a company’s financial status in view of competition and market systems and provide for easy communication between various levels in the company, and (iii) how to extend our current single-level robust optimization method to multi-subsystem problems and maintain reasonable computational complexity for the method. These underlying questions and corresponding investigations will be organized into tasks throughout the time frame allocated to the project. The details of these tasks are explained in the next section.

Approach

There are two main tasks in this investigation as detailed in the following.

<u>Task 1 (PI):</u>
Develop and implement engineering analysis models, in a Matlab (or Matlab compatible) environment, for a crude distillation unit case study model.

- Task 1.1: Develop a multi-input multi-output analysis model for a representative petrochemical system with corresponding subsystem analysis models.
- Task 1.2: Extend the analysis model in Task 1.1 to include: (i) additional complexity, (ii) subsystem details and uncertainty to include reasonable representation of engineering side of a plant. The ultimate goal is to develop an integrated multi-subsystem petrochemical analysis model for a plant or a group of units in a plant.

<u>Task 2 (UMD):</u>
Develop and implement a Robust Decision Support System (RDSS).

Engineering Tasks

- Task 2.1: Develop a single level (all-at-once) approximation-assisted robust optimization technique that is able to significantly reduce the computational efforts of making robust decisions.
- Task 2.2: Demonstrate an application of the approach from Task 2.1 with a case study in petrochemical systems which will be developed by PI as a part of Task 1.
- Task 2.3: Develop an approximation assisted multi-objective multi-disciplinary robust optimization approach, which is an extension to Task 2.1.

- Task 2.4: Demonstrate an application of the approach from Task 2.3 with a case study in petrochemical systems which will be developed by PI as part of Task 1.

Business Tasks

- Task 2.5: Develop business models in Netlogo and/or Matlab and solve a simplified refinery supply chain optimization problem with Matlab.
- Task 2.6: Develop a Dashboard and test the robustness and sensitivity of the Dashboard's elements for the model in Task 2.5.

Integration Tasks

- Task 2.7: Inspect engineering and business problems to determine coupling variables between two problems.
- Task 2.8: Integrate Tasks 2.1 to 2.4 with Tasks 2.5 to 2.6 to formulate a refinery optimization problem that considers both engineering and business objectives and constraints.
- Task 2.9: make the supply chain management problem more realistic by considering more decision levels, more finished products and a wider market, and by increasing the size of the refinery's internal network and then repeat Task 2.8.
- Task 2.10: Verify and validate the integrated model.

Nomenclature

LSR = Lower straight run
HSR = Higher straight run
SRDiesel = Straight run diesel
LVGO = light vacuum gas oil
HVGO = Heavy vacuum gas oil
VacResid = Vacuum residue.
CokerLN = Coker lower naphtha
CokerHN = Coker higher naphtha
LCGO = Lower coker gas oil
HCGO = Higher coker gas oil
HCKero = Hydrocraked kerosine
HCdiesel = Hydrocraked diesel
Gas oil HT = Gas oil hydrotreater
HTGasOil = hydrotreated gas oil
FCCU = fluid catalytic cracking unit
FCCLN = fluid catalytic cracked lower naphtha
FCCHN = fluid catalytic cracked higher naphtha
LCO = lower cracked oil
HeavyNHT = heavy naphtha hydrotreater
HTLNaph = hydrotreated lower naphtha

Dynamics and Control of Drill Strings

UMD Investigator: Balakumar Balachandran
PI Investigators: Hamad Karki and Youssef Abdelmagid
GRA: Chien-Min Liao (started in Spring 2007)
Other Participants: Nicholas Vlajic
Start Date: Oct 2006

1. Objectives/Abstract

Drill-string dynamics need to be better understood to understand drill string failures, control drill string motions, and steer them to their appropriate locations in oil wells. Although a considerable amount of work has been carried out on understanding drill-string vibrations (for example, Leine and van Campen, 2002; Melakhessou *et al*., 2003; Spanos *et al*., 2003; Liao *et al*., 2009), the nonlinear dynamics of this system are only partially understood given that the drill string can undergo axial, torsional, and lateral vibrations, and operational difficulties include sticking, buckling, and fatiguing of strings. In addition, the prior models focus on either bending or torsional or axial motions. Hence, it is important to consider coupled axial-bending-torsional vibrations and contact instability in oil and gas well drilling. A better understanding of these vibrations can help keep the drill string close to the center of the borehole and help realize near-circular bores during drilling operations.

The overall goal of the proposed research is to understand the nonlinear dynamics of the drill string and develop a control-theoretic framework for its stabilization, enabling energy efficient drilling with longer lifespan for the equipment. Specific research objectives of this project are the following: i) building on Phase I efforts, develop and study control-oriented models for the drill strings through analytical and numerical means, ii) investigate the control of an under-actuated nonlinear system (drill string) with complex interactions with the environment, and iii) use the drill-string test-beds constructed at the Petroleum Institute (PI) & the University of Maryland (UMD) to validate the analytical findings and suggest possible strategies to mitigate drill-string failures in fixed and floating platform environments.

2. Summary of Results

In the previous report, the investigators presented experimental results from the scaled vertical drill string experimental apparatus in the absence of external forces from the borehole, or outer shell. Under these conditions, the researchers were able to experimentally study geometric nonlinearities, which are expected to influence the dynamics of horizontal and curved drill strings. In the current report, the authors numerically investigate the response of the drill string in the absence of the external forces. The numerical integration results obtained for the string and rotor trajectories have similar features to the trajectories observed in the experiments. In parallel, the scaled experimental setup used to study horizontal and curved drilling is shown, and preliminary experimental results are also reported here.

The rest of this section is organized as follows. In Section 2.1, model predictions of the drill-string dynamics obtained by using the three-degree-of-freedom model and no contact are given. In Section 2.2, modifications made to enhance the experimental apparatus and to study horizontal drilling are explained with corresponding data. In Section 2.3, an outline of future work is provided.

2.1 Model Predictions for Drill-String Dynamics

As a continuation of previous work, the three-degree-of-freedom model, which was presented in an earlier report, is further studied here. This model consists of two parts, one involving the dynamics of the string and the other involving the contact condition between rotor and shell. Since the focus is on the drill-string dynamics, the contact model is not included in these simulations. This corresponds to a physical setting where the drill string is in pure rotation without any contact with the outer shell.

2.1.1 Simulation Results

A series of rotor trajectories obtained for different driving speeds are shown in Figure 1. As observed in experiments and shown in Figure 1(a), the rotor orbits the origin for low rotational speeds. With an increase in the driving speed, as shown in Figure 1(b), the rotor begins to make elliptical orbits that are associated with a combined torsion and lateral vibration. As the driving speed is increased further, the rotor exhibits an erratic pattern, as illustrated in Figure 1(c). Within certain driving speed ranges, the rotor trajectory no longer exhibits erratic motions, as shown by the results illustrated in Figures 1(d) and (e). However, above a threshold driving speed, the rotor moves between a series of orbits and exhibits features similar to the earlier erratic motions illustrated in Figure 1(f). It is noted that the rotor trajectories presented in Figures 1(c) and 1(f) show similar features, although they were obtained for different driving speeds.

The results obtained through numerical integrations and experiments share similar rotor trajectory features, as the driving speed is increased. In general, in both experiments and simulations, the rotor orbits the origin at low rotating speeds and has a small radius of rotation. As the driving speed is increased, the radius of the orbit is increased. Furthermore, in the numerical simulations, rotor response follows regular orbits for certain driving speeds. This aspect has also been previously reported in the context of experimental results, but needs to be further investigated.

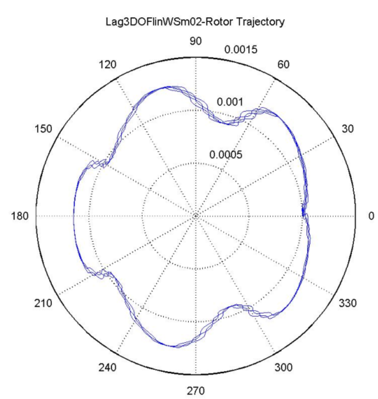

(a)

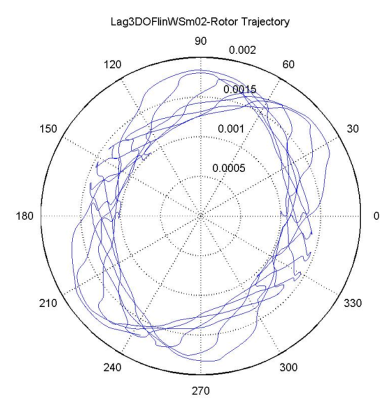

(b)

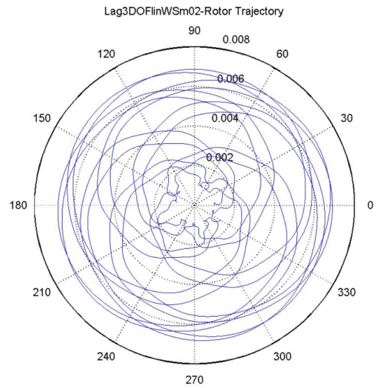

(c)

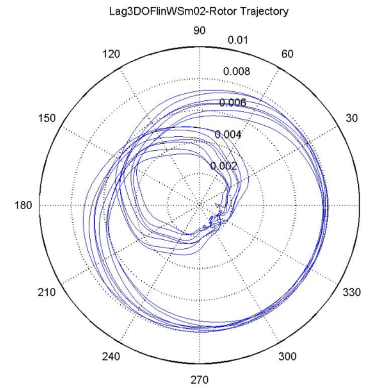

(d)

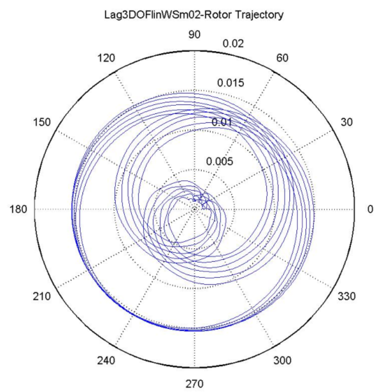

(e)

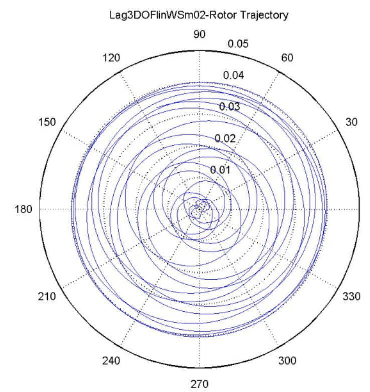

(f)

Figure 1. Rotor response trajectories for different driving speeds: (a) 10 rpm, (b) 20 rpm, (c) 42 rpm, (d) 44 rpm, (e) 52 rpm, and (f) 55 rpm.

2.2 Horizontal Drill String Experimental Apparatus

The focus of the experimental research has transitioned from studying vertical drill strings and wellbore force interactions to studies of horizontal drill strings. In the current section, the authors outline the experimental arrangement being used for studying horizontal drilling and include preliminary data.

2.2.1 Experimental Arrangement

A photograph of the horizontal drill string experimental arrangement is shown in Figure 2. In the current configuration, the drill string has been removed from the acrylic tubes that represent the borehole. Additionally, a shorter section of drill string is being examined in contrast to the string structure presented in the November 2010 report. The current structure allows investigators to study the dynamics of the drill string specific to a curved configuration in the absence of force interactions. The wellbore force interactions for a curved structure will be taken into consideration at a later date. The assembly at the vertical end of the string is referred to as the "Top Assembly," which has been explained in the July 2011 report. At the opposite end, the drill string, which extends from the top assembly, is inserted into an apparatus at the horizontal end that is referred to as the “Bottom Assembly,” which will be discussed further.

A photograph of the bottom assembly with annotations is shown in Figure 3. The drill string is inserted into a rotary encoder and extends beyond to a roller bearing. By using the encoder at the base of the string in conjunction with the encoder at the top assembly, torsion motions of the string may be recorded using a data acquisition system. An actuator is mounted transverse to the end of the drill string, and when extended, the end effector compresses the drill string into the brake-pad assembly. This actuator can then be used as a brake, or used to excite torsion vibrations arising from stick-slip motions.

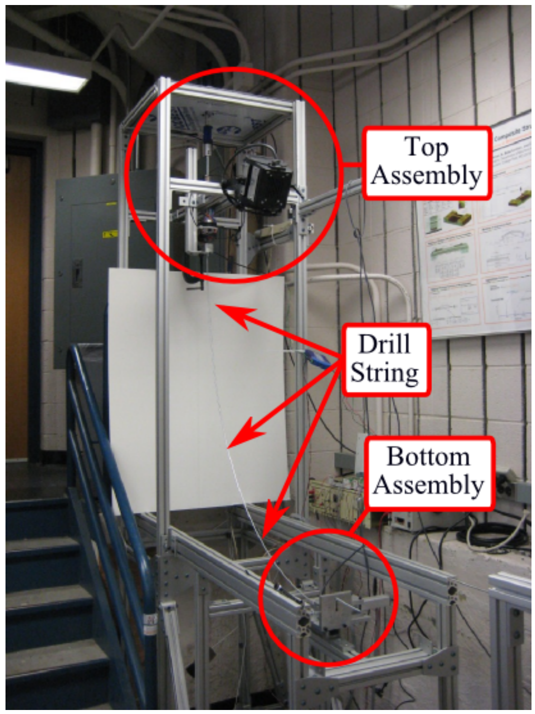

Figure 2. A photograph of the horizontal drill-string apparatus.

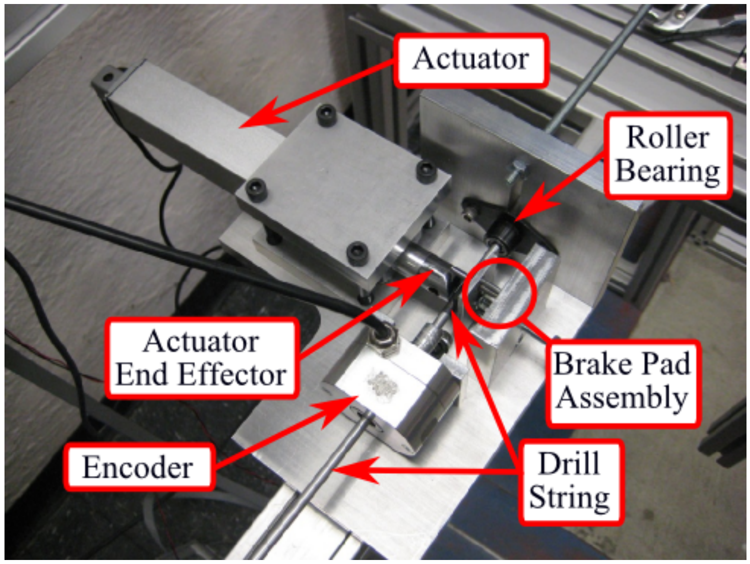

Figure 3. Photograph of the bottom assembly used to actuate and measure vibrations of the drill string.

2.2.2 Preliminary Experimental Results

In the current experiments, the actuator is not used; rather, only the readings from the top and bottom encoders are collected while the string is subject to rotation from the top assembly. The torsion motions of the string may be extracted using the information obtained from both encoders. Typical data obtained from the encoders during an operation are given in Figures 4(a) and (b). The data are collected in the form of 11-bit Gray code and then converted into a decimal equivalent, whose values range between 0 and 360 degrees. Afterwards, the signal is filtered by using a third-order lowpass Butterworth filter. For all the data collected, the cut-off frequency is set to be three times the driving speed. In order to better examine the filtered data, a closeup section of Figure 4(a) between four and five seconds is provided in Figure 4(b). The data given in Figure 4(a) and (b) were recorded for a driving speed of 1 Hz (equivalent to 60 revolutions per minute). The amplitude of vibration in this case is around 3 degrees with a DC offset of 1.5 degrees. It is noted that these vibrations arise from the curvature of the string and do not originate from an unbalanced mass or interaction forces as seen in the vertical drill-string experiments.

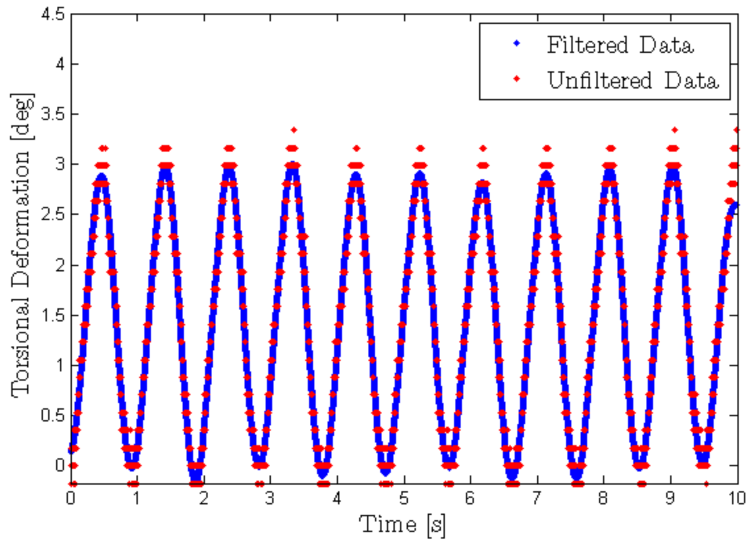

(a)

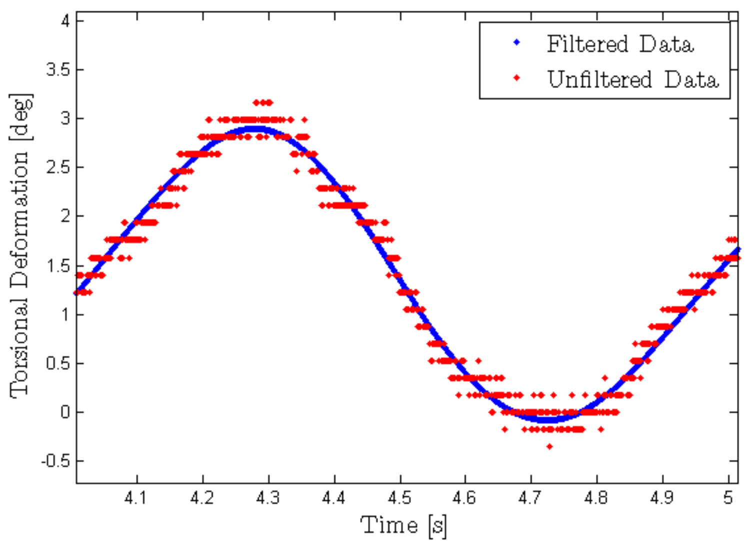

(b)

Figure 4. Experimental data obtained of the torsional vibrations of the curved drill-string apparatus.

2.2.3 Future Experiments

Future experiments will attempt to replicate stick-slip vibrations that will be generated by using the actuator in the bottom assembly. Additionally, the bottom assembly will be retrofitted with a linear bearing and a 10 lb shaker that will be used to prescribe the axial motion of the end of the drill string. Both actuators will be used to replicate the dynamics an actual drill bit would be subject to in a field operation. By using the encoders and strain gages, the response of the drill string may be measured. Furthermore, a video camera will also be mounted to record to the motions of the drill string along the curved section. A gradient-based image processing technique can then be used to gather the position during operations. This image processing procedure has been effective in earlier experiments.

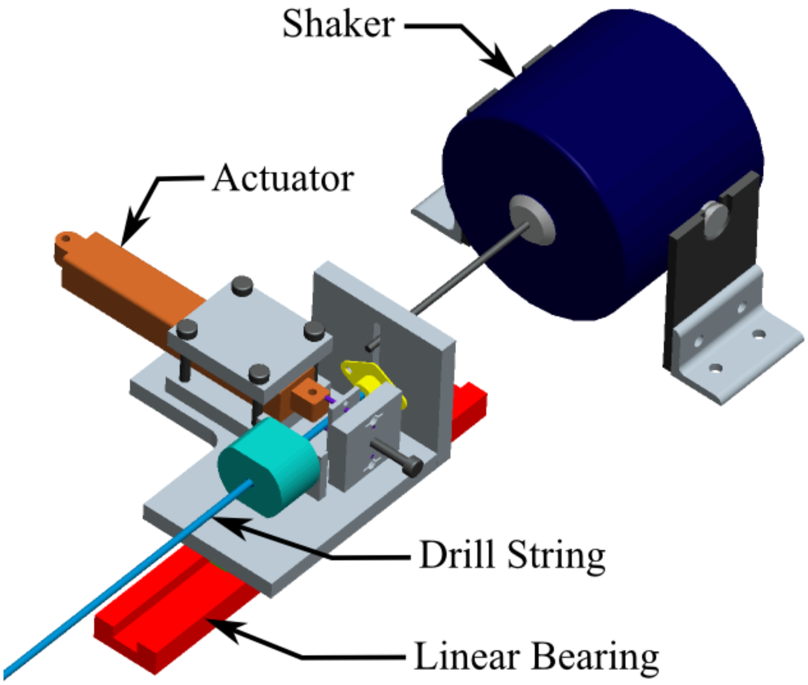

Figure 5. The bottom assembly will be modified in future experiments with a linear bearing and a shaker in an attempt to better replicate the forces the drill bit experiences while in operation.

3. Discussion and Future Work

Numerical simulations presented in this report are in good agreement with experimental results observed in earlier reports. Results from both numerical and experimental studies indicate that, even when neglecting external forces, nonlinear effects exist in the vertical configuration and are likely due to the geometry of the drill string. System geometric nonlinearities are expected to be even more pronounced in the curved configurations.

The current scope of the research now includes horizontal drill strings that will be studied with an experimental apparatus. This apparatus has been presented along with preliminary results in this report. In addition to the curved nature of the string, a further novelty of the experiment is the bottom assembly. This mechanism allows researchers to better recreate the forces an actual drill bit may experience while in operation. Future reports are to contain findings and results pertaining to horizontal drilling studies.

4. References

[1] Akgun, F. 2004, “A Finite Element Model for Analyzing Horizontal Well BHA Behavior,” J. of Petrol. Sci & Eng., Vol. 42, pp. 121-132.

[2] Bednarz, S., 2004, “Design and Exploitation Problems of Drill Strings in Directional Drilling,” Acta Montanistica Slovaca, Vol. 9, pp. 152-155.

[3] Downtown, G., 2009, "*New Directions in Rotary Steerable Drilling"*, Oilfield Review, pp. 18-29.
[4] Feng, Z., and Zhang, X., (2002). "Rubbing phenomena in rotor-stator contact". Chaos, Solutions, & Fractals, 14(2), August, pp. 257–267.
[5] Leine, R. I., van Campen, D. H., and Keultjes, W. J. G. (2002). "Stick-Slip Whirl Interaction in Drill String Dynamics," *ASME Journal of Vibration and Acoustics*, Vol. 124 (2), pp. 209-220.
[6] Liao, C.-M., Balachandran, B., and Karkoub, M., (2009). "Drill-String Dynamics: Reduced Order Models," Proceedings of ASME IMECE 2009, Nov. 13-19 Lake Buena Vista, FL, USA, 2009; Paper No. IMECE2009-10339.
[7] Melakhessou, H., Berlioz, A., and Ferraris, G. (2003). "A Nonlinear Well-Drillstring Interaction Model," *ASME Journal of Vibration and Acoustics*, Vol. 125, pp. 46-52.
[8] Mihajlović, N., van Veggel, A. A., van de Wouw, N., and Nijmeijer, H. (2004) "Analysis of Friction-Induced Limit Cycling in an Experimental Drill-String System," *ASME Journal of Dynamic Systems, Measurement, and Control*, Vol. 126(4), pp. 709-720.
[9] Mihajlović, N., van de Wouw, N., Rosielle, P.C.J.N., and Nijmeijer, H. (2007) "Interaction between torsionalal and lateral vibrations in flexible rotor systems with discontinuous friction," *Nonlinear Dynamics*, Vol. 50, pp. 679-699.
[10] Nayfeh, A. H. and Balachandran, B. (1995, 2006). Applied Nonlinear Dynamics: Analytical, Computational, and Experimental Methods, Wiley, New York.
[11] Spanos, P. D., Chevallier, A. M., Politis, N. P., and Payne, M. L. (2003). "Oil and Gas Well Drilling: A Vibrations Perspective," *Shock and Vibration Digest* Vol. 35(2), pp. 85-103.
[12] Short, J. A. "Introduction to Directional and Horizontal Drilling " Pennwell Pub, 1993.
[13] Singh, S. P. and Balachandran B. (2009). "Rolling Rub Translations of a Flexibility Connected Disk," pre-print.
[14] Vlajic, N., Liao, C.-M., Karki, H., & Balachandran, B. (2011) "Stick-Slip and Whirl Motions of Drill Strings: Numerical and Experimental Studies," Proceedings of the 2011 ASME IDETC 2009, August 29-31, Washington, D.C., Paper No. DETC2011-47949.

Appendix

Approach

A combined analytical, numerical, and experimental approach is being pursued at the University of Maryland and the Petroleum Institute. Specifically, the drill string is being modeled as a reduced-order nonlinear dynamical system. Appropriate attention is also to be paid to the interactions with the environment. The experiments at UMD and PI are tailored to address specific aspects of the drill-string dynamics as well as complement each other. Actuator and sensor choices are also to be explored to determine how best to control the system dynamics, in particular, through the rotational speed. The studies will be initiated with drill strings located on fixed platforms, and later extended to other situations.

Three-Year Schedule

Phase II:

January 1, 2009 to December 31, 2009: Carry out quantitative comparisons between experimental results and predictions of reduced-order models for open-loop studies; understand stick-slip interactions and explore continuum mechanics based drill-string models for fixed platform environments; examine different configurations including horizontal drilling

January 1, 2010 to December 31, 2010: Construct control schemes; carry out experimental, analytical, and numerical studies; and identify appropriate schemes; study horizontal drilling configurations through experiments and analysis

January 1, 2011 to December 31, 2011: Continue horizontal drilling studies; carry out experiments, analysis, and numerical efforts.

January 1, 2012 to May 1, 2012: Compile results obtained for drill-string operations in vertical and horizontal configurations and provide guidelines for enhancing operations.

Studies on Mobile Sensor Platforms

UMD Investigators: **Balakumar Balachandran, Nikil Chopra**
GRAs: **Rubyca Jaai**
PI Investigator: **Hamad Karki, Sai Cheong Fok**
GRAs: **Hesham Ishmail (ADNOC Fellow)**
Start Date: **April 2009**

1. Objective/Abstract

Mobile sensor platforms can be employed in a variety of operations including environmental and structural health monitoring operations in harsh and remote environments. In the proposed work, cooperating sensor platforms are to be studied for potential use in oil storage tanks, which are periodically tested for corrosion, cracks, and leaks, and oil pipelines. These platforms are envisioned for estimating geometrical profile parameters, such as the tank bottom thickness. To this end, simultaneous localization and mapping (SLAM) algorithms (also known in the literature as concurrent mapping and localization (CML) algorithms) for co-operating sensor platforms operating in harsh environments are being investigated. The SLAM algorithms can provide the solution to autonomous inspection to determine locations of faults in structures such as oil tanks and pipelines.

The overall objective of this project will be to carry out a combined analytical, numerical, and experimental effort to develop mobile sensor platforms and appropriate simultaneous localization and mapping (SLAM) algorithms for cooperative sensor platforms to operate in a harsh environment. Research objectives are the following: i) develop SLAM algorithms based platforms taking into account system constraints such as constrained communication, the type of sensors considered, allowable dynamics, and factors such as sensor failures and reliability of the considered sensors and ii) carry out experimental and supporting simulation studies by using mobile platform test platforms at the University of Maryland and the Petroleum Institute.

In this report, results of experiments and simulations carried out to demonstrate SLAM are presented. In Section 2, experimental and simulation results are presented, and an outline of the future work is provided in Section 3.

2. Summary of Results

In this report, results obtained from experiments carried out to demonstrate SLAM are presented. Additionally, simulation work completed on the feature extraction and the data association algorithms are also discussed.

2.1 Experimental Setup

As mentioned in the previous report, the experimental setup has been constructed to collect data in order to demonstrate the working of simultaneous localization and mapping algorithms. The setup includes mobile platforms, a scaled version of a corridor like environment using plexiglass structures, and cameras to track the mobile platforms movements during experiments. The image processing to extract the path and environment information to track one or more mobile platforms has also been coded. The mobile sensor platform is equipped with encoders and can be controlled by using Matlab (Simulink). In addition to the available sensors, a Kinect sensor has been added to the mobile agent. The Kinect sensor can be utilized to extract three-dimensional information of the environment, as the sensor provides an image of the environment with depth information for each pixel in the image. The three-dimensional information of the environment can then be used to build three-dimensional maps. Furthermore, the Kinect sensor is equipped with a three-axis accelerometer. Adding a motor to rotate the Kinect provides the ability to capture parts of the environment not in the field of view without requiring the mobile agent to change its path. The depth data, feature matching, and the accelerometer data can then be used to form a complete picture of the environment. A battery powered Kinect sensor has been added to the mobile platform as shown in Figure 1.

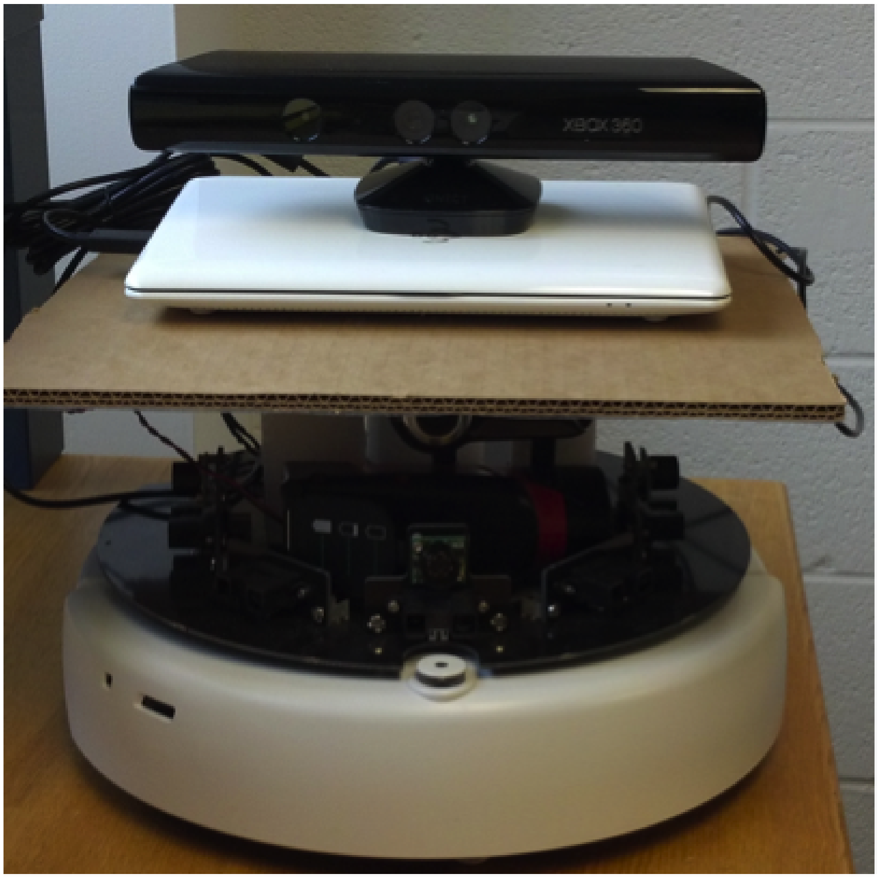

Figure 1. Mobile agent with battery powered Kinect sensor.

A representative Kinect data set is shown in Figure 2. In Figure 2b, the depth of each pixel in the image shown in Figure 2a is provided. The Kinect sensor is capable of sensing depths from around 0.5m to 4m. The depth data is shown by using a color map, where the red color is used to indicate the region nearest to the Kinect sensor, and blue color denotes the areas furthest from the sensor.

Figure 2a. RGB image obtained from the Kinect sensor.

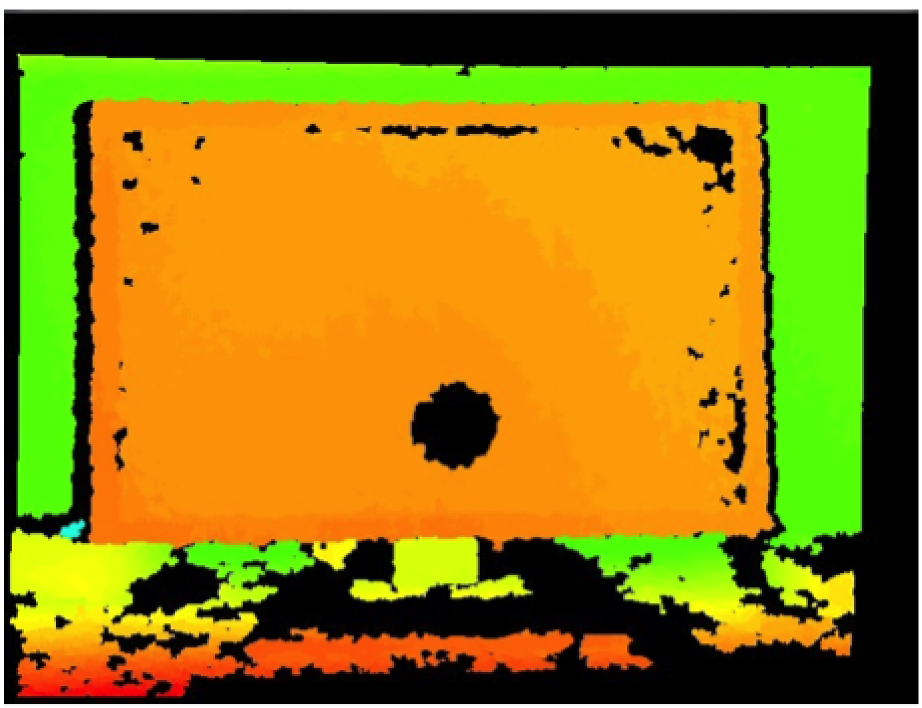

Figure 2b. Colorized depth map corresponding to Figure 2a.

2.3 Simulation Results

Simulation results obtained using a particle filtering-based estimation algorithm known as fastSLAM are shown in Figure 3. The particle filter estimation is a Monte Carlo-based method that is applicable to nonlinear systems. Furthermore, it does not require the conservative assumption that the noise in the motion and measurement models be modeled as a Gaussian distribution. One of the disadvantages of using the particle filter in the SLAM problem is that as the map size grows, the number of calculations required also increases exponentially. Hence, a modified solution known as the fastSLAM algorithm was proposed by (Montemerlo, *et al.,* 2002), wherein the robot position over time is estimated using a particle filter, while the estimates of the map features or landmarks are calculated using the extended Kalman filter. The robot pose being a vector of fixed dimensions at all times does not cause the calculation time to increase exponentially. Point landmarks with unknown data association were used in the simulation. The results are based on nearest neighbor matching of the point landmarks carried out using a gating technique. Data association using the gating technique is based on the distance between landmarks observed (Dissanayake *et al*., 2001). With every new measurement, the landmark's position is estimated and its distance from each of the other landmarks already present in the map is computed. The distance calculations are based on the Mahalanobis distance. If the nearest neighbor is at a distance that is less than a predefined threshold, the measurement is associated with the nearest neighbor. A certain minimum number of associations are required for any landmark to become a valid landmark in the map.

In order to implement the data association, two lists of landmarks are maintained. One list contains the landmarks that have already been validated (i.e., have the required number of data associations). The other list contains potential landmarks with less than the required number of data associations. The measurements that are not associated with any previous landmarks are placed in the list of potential landmarks until they reach the required minimum number of associated measurements. Additionally, if any member of the potential landmarks does not reach the threshold for validation within a certain number of measurements, it is removed from the list.

In Figure 3, the simulation results obtained using fastSLAM and the data association technique described above are shown. One hundred particles were used to represent the robot pose, and the extended Kalman filter was used for the landmarks. The blue line indicates the user input path for the mobile agent. The mobile agent is assumed to be a two wheel, differential drive system. Additional constraints on the mobile agent motion such as maximum steering angle and maximum steering rate possible were applied to the simulation. The green triangle shows the actual position of the mobile agent and the red triangle shows the estimated position. The green markers show the positions of the landmarks, and the red markers show the estimates of the landmark positions with uncertainty. The spread in the red markers shows the amount of uncertainty in the estimate, which reduces with the number of times that the landmarks are observed.

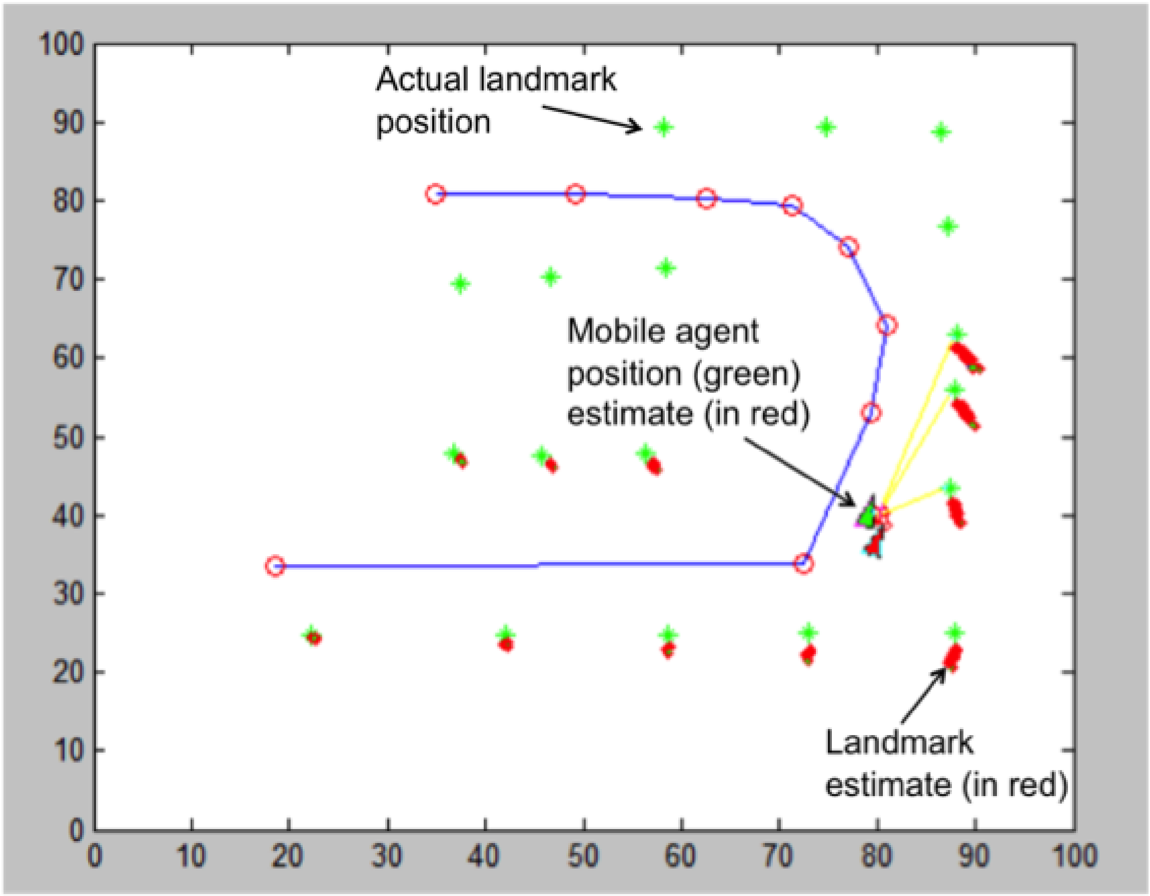

Figure 3. Simulation results with data association for point landmarks.

2.4 Interactions

A paper abstract titled “Simultaneous Localization and Mapping with Consideration of Robot System Dynamics” has been submitted to SPIE Smart Structures/NDE for review.

3. Planned Project Activities for the Next Quarter

Future work includes performing experiments and collecting data of the environment with different sensors such as laser sensors and the Kinect sensor to construct three-dimensional maps using various SLAM algorithms. In addition, a motion model taking into account the dynamics of the mobile agent will be constructed, and its effect on the various SLAM algorithms will be analyzed. The experimental test setup of a scaled pipeline structure will be used to demonstrate the applicability of the SLAM algorithms for inspection purposes.

4. References

[1] Arras, K.O., 2003, "Feature-Based Robot Navigation in Known and Unknown Environments", Ph.D. dissertation, Nr. 2765, Swiss Federal Institute of Technology Lausanne, Autonomous Systems Lab, June.

[2] Bay, H., Ess, A., Tuytelaars, T., and Gool, L. V., 2008, "SURF: Speeded Up Robust Features," Computer Vision and Image Understanding, vol. 110, no. 3, pp. 346-359.

[3] Dissanayake, M.W., Newman, P., Clark, S., Durrant-Whyte, H.F., and M. Csorba, 2001, “A Solution to the Simultaneous Localization and Map Building (SLAM) Problem,” Robotics and Automation, IEEE Transactions on, Vol.17, No.3, pp. 229–241, June.

[4] Dudek, G., Jenkin, M., Milios, E. and Wilkes, D., 1996, “A Taxonomy for Multi-Agent Robotics,” Autonomous Robots, vol. 3, no. 4.
[5] Durrant-Whyte, H. and Bailey, T., 2006, “Simultaneous Localization and Mapping: Part I," IEEE Robotics & Automation Magazine, Vol.13, no.2, pp. 99-110, June.
[6] Durrant-Whyte, H. and Bailey, T., 2006b, “Simultaneous Localization and Mapping: Part II State of the Art," IEEE Robotics & Automation Magazine, Vol.13, no.3, pp. 108-117, 2006.
[7] Garulli, A., Giannitrapani, A., Rossi, A., and Vicino, A., 2005, “Mobile robot SLAM for line-based environment representation,” 44th IEEE Conference on Decision and Control, 2005 and 2005 European Control Conference. CDC-ECC '05., pp. 2041 – 2046, December.
[8] Lemaire, T. and Lacroix, S., 2007, "SLAM with Panoramic Vision," Journal of Field Robotics, vol. 24, no. 1-2, pp. 91-111, February.
[9] Montemerlo, M., Thrun, S., Koller, D., and Wegbreit, B., 2002, “FastSLAM: A Factored Solution to the Simultaneous Localization and Mapping Problem," in Proceedings of the AAAI National Conference on Artificial Intelligence, AAAI, (Edmonton, Canada).
[10] Neira J., and Tardós, J.D., 2001, “Data Association in Stochastic Mapping Using the Joint Compatibility Test”, IEEE Trans. Robotics and Automation, vol. 17, no. 6, pp. 890-897.
[11] Smith, R., Self, M., and Cheeseman, P., 1990, “Estimating Uncertain Spatial Relationships in Robotics”, pp. 167-193, Springer-Verlag New York, Inc., New York, NY, USA.
[12] Tardós , J. D., Neira, J., Newman, P. M., and Leonard, J. J., 2002, “Robust mapping and localization in indoor environments using sonar data,” International Journal of Robotics Research, vol. 21, pp. 311—330.
[13] Thrun, S., 2003, “Robotic Mapping: A Survey,” in Exploring Artificial Intelligence in the New Millennium, G. Lakemeyer and B. Nebel, eds., pp. 1-35, Morgan Kaufmann Publishers Inc., San Francisco, CA, USA.
[14] Thrun, S., Burgard, W., and Fox, D., 2006, “Probabilistic Robotics,” MIT Press.
[15] Yap, T.N., and Shelton C.R., 2009, "SLAM in Large Indoor Environments with Low-Cost, Noisy, and Sparse Sonars," Proceedings of the IEEE International Conference on Robotics and Automation, pp. 1395-1401.
[16] Zhang, S., Xie, L., and Adams, M., 2005, “An Efficient Data Association Approach to Simultaneous Localization and Map Building,” International Journal of Robotics Research, vol. 24, pp. 49-60.

Appendix

SLAM and its Components

The basic aim of the simultaneous localization and mapping (SLAM) algorithm is to make a mobile platform autonomous by providing the capability to navigate through an unknown environment from an initially unknown location. This is achieved by iteratively building a consistent map of the environment and by simultaneously determining its location within the map (Durrant-Whyte and Bailey, 2006). Therefore, SLAM is the process by which a mobile platform can build a map of the environment and at the same time use this map to compute the platform's location within the map (Thrun, 2003). This ability is useful particularly in applications such as search and rescue, inspection and surveillance, and exploration, which require accurate localization within unknown environments. For example, in the inspection problem, by using SLAM techniques, the mobile sensor platform can determine locations of faults thereby providing an autonomous solution and reducing the need for external sensors to perform the same task.

In the SLAM problem, an agent or a mobile sensor platform traverses an unknown area and uses relative sensing information between the agent and the surrounding environment. The data collected from the experiment includes the following:

i) Encoder or inertial measurement unit (IMU) data providing information on the mobile agent's movements
ii) Sensor data measuring the relative distance and angle between the mobile agent and the environment (using sensors such as laser, ultrasonic, camera and so on).

The solution to the SLAM problem involves the implementation of a probabilistic framework to analyze experimental data and build a map that constitutes the locations of landmarks or features in the surrounding environment as well the platform's position within the map. This is due to the presence of noise in the sensor data. The steps in a typical SLAM implementation are as follows. The encoder or IMU data are processed to get the relative motion (distance and angle) moved by the mobile agent with respect to its last position. A motion model describing the evolution of the position (x, y, and heading angle) of the mobile agent with time and the relative motion data is built. The relative motion data are used in an estimation algorithm such as the extended Kalman filter along with the motion model to predict the position of the mobile agent at every time step. The sensor measurements of the environment are processed by using feature extraction algorithms to identify distinct landmarks. At every time step, a data association algorithm is used to determine if the identified features are new or already present in the map. The relative positions of previously identified landmarks are used to update the map and the position of the mobile agent. New landmarks are added to the map for future processing. A block diagram of the important steps in SLAM implementation is shown in the figure below.

Well known solutions to the SLAM problem include the use of the extended Kalman filter (EKF) algorithm to estimate the positions of landmarks and the pose (i.e., position and heading) of the robot as Gaussian distributions or particle filters that allow for non-Gaussian representations or their combinations (known as FastSLAM) (Smith *et al*., 1990, Montemerlo *et al*., 2002).

Before fusing new sensor data into the SLAM map, new measurements are associated with existing map landmarks by using data association algorithms such as joint compatibility and nearest neighbor (Neira and Tardos, 2001, Zhang *et al.*, 2005). The problem is that incorrect data association can cause divergence of the map estimates. Additionally, the incorrect data association can lead to failure in the localization of the mobile platform within the map. Practical SLAM solutions are therefore vulnerable to incorrect association of observations to landmarks. Additionally, it is necessary to solve the loop-closure problem that occurs when a mobile platform returns to observe landmarks that were previously observed after a long route and the algorithm must recognize that this has occurred by correctly associating new measurements to landmarks that were observed at the beginning of the robot path. The association problem is compounded in environments that are not simple points (Durrant-Whyte and Bailey, 2006b).

Feature extraction is another component of the SLAM problem that is critical. In environments that are not simple, correct data association also involves representing the environment by features extracted from the sensors provided on the mobile platform. Some examples include extracting line features in indoor environments typically from sonar and laser sensors (Tardos *et al.*, 2002; Garulli *et al.*, 2005), and extracting corners and scale invariant features from stereo camera data using techniques from computer vision (Bay *et al.*, 2008; Lemaire *et al.*, 2007).

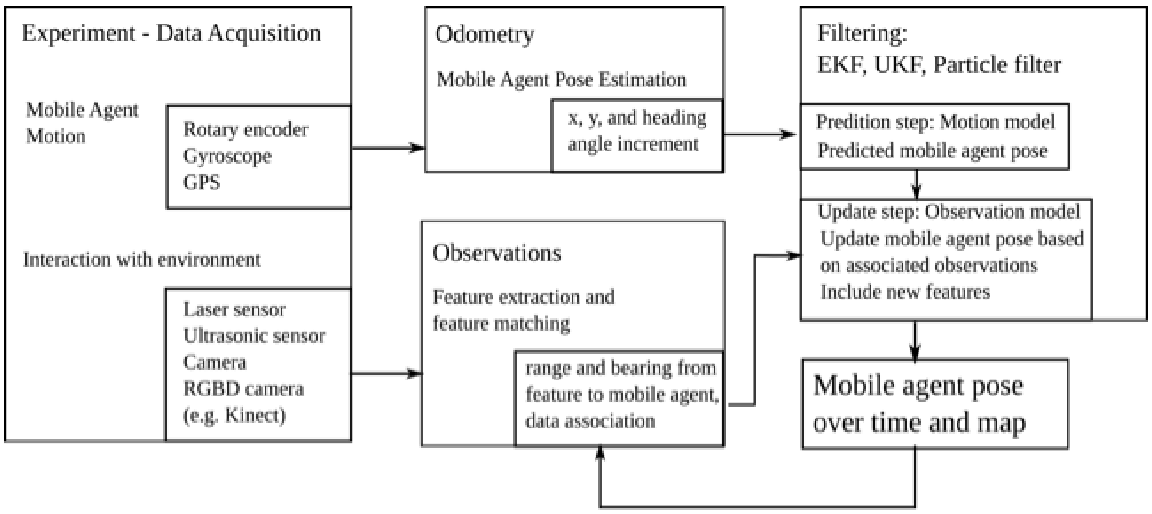

Block diagram describing the steps in SLAM.

Three-Year Schedule

Phase II:

April 1, 2009 to December 31, 2009: Carry out analytical and numerical investigations into SLAM algorithm based mobile platforms for representative geometrical profile measurements, and construction of experimental test platforms.

January 1, 2010 to December 31, 2010: Continuation of analytical, experimental, and numerical efforts, with one of the focus areas to be development of appropriate communication and motion planning protocols for co-operative multi-agent platforms. Construction of experimental setup for ground based mobile agents with attention to the environment.

January 1, 2011 to December 31, 2011: Continuation of experimental and numerical studies and formulation of recommendations for appropriate sensor and mobile platform configurations for use in oil tanks and pipes.

January 1, 2012 to March 31, 2012: Continuation of experimental and numerical studies for proof of concept for appropriate sensor and mobile platform configurations for use in oil tanks and pipes.

Appendix

Three-year schedule

Phase II:

April 1, 2009 to December 31, 2009: Carry out analytical and numerical investigations into SLAM algorithm based mobile platforms for representative geometrical profile measurements, construction of experimental test platforms, and preliminary experimental findings

January 1, 2010 to December 31, 2010: Continuation of analytical, experimental, and numerical efforts, with one of the focus areas to be development of appropriate communication and motion planning protocols for operations in harsh environments

January 1, 2011 to December 31, 2011: Continuation of experimental and numerical studies and formulation of recommendations for appropriate sensor and mobile platform configurations for use in oil tanks.

References

[1] Anderson, B., 1977 “Exponential stability of linear equations arising in adaptive identification," IEEE Transactions on Automatic Control, Vol. 22(1), pp. 83-88.

[2] Cao, M., Anderson, B. D., and Morse, A. S., 2006, “Sensor network localization with imprecise distances," Systems Control Letters, Vol. 55(11), pp. 887-893.

[3] Dandach, S., Fidan, B., Dasgupta, S., and Anderson, B. D., 2009, “A continuous time linear adaptive source localization algorithm, robust to persistent drift," Systems Control Letters Vol. 58 (1), pp. 7-16.

[4] Fox, D., Burgard, W., Kruppa, H., and Thrun, S., 2000, “A probabilistic approach to collaborative multi-robot localization," Autonomous Robots, Vol. 8 (3), pp. 325-344.

[5] Khalil, H., 2002, “Nonlinear Systems”, Prentice Hall, New Jersey.

[6] Pathirana, P., Bulusu, N., Savkin, A., and Jha, S., 2005 “Node localization using mobile robots in delay-tolerant sensor networks," IEEE Transactions on Mobile Computing, Vol. 4 (3), pp. 285-296.

[7] Patwari, N., Ash, J., Kyperountas, S., Hero, A.O., I., Moses, R., and Correal, N., 2005, “Locating the nodes: cooperative localization in wireless sensor networks," IEEE Signal Processing Magazine, Vol. 22 (4), pp. 54-69.

[8] Pourboghrat, F., Karlsson, M.P., 2002, “Adaptive control of dynamic mobile robot with nonholonomic constraints,” Computers & Electrical Engineering, Vol. 28 (4) pp. 241-253.

[9] Roumeliotis, S. and Bekey, G., 2002, “Distributed multirobot localization," IEEE Transactions on Robotics and Automation, Vol. 18 (5), pp. 781-795.

[10] Weiss, G., Wetzler, C., and von Puttkamer, E., 1994, “Keeping track of position and orientation of moving indoor systems by correlation of range-finder scans,” Proceedings of the IEEE International Conference on Intelligent Robots and Systems, pp.595-601 Vol.1, 12-16 September.

Development of a Probabilistic Model for Degradation Effects of Corrosion-Fatigue Cracking in Oil and Gas Pipelines

UMD Investigator: Mohammad Modarres
PI Investigators: Abdennour Seibi
GRA: Mohammad Nuhi
Start Date: Oct 2006

1. Objectives/Abstract

This research continues Phase-I mechanistic modeling of the corrosion-fatigue phenomenon for applications to pipeline health, risk and reliability management. The objective of this study is to perform additional mechanistic-based probabilistic models derived from physics of failure studies and validate them using the state-of-the-art experimental laboratory being developed at the PI as part of the Phase I of this study. Where possible, observed field data from ADNOC operating facilities will be used to supplement observations from the laboratory experiments based on the well-established Bayesian approach to mechanistic model updating and validation developed in Phase I. Uncertainties about the structure of the mechanistic models as well as their parameters will also be characterized and accounted for when such models are applied. The proposed models will allow the end users (e.g., maintenance analysts and Inspection crew) to integrate observed performance data from a wide range of pipelines and selected refinery equipment, such as pumps, compressors and motor-operated valves. Admitting the fact that modeling all degradation mechanisms would be a challenging undertaking, the proposed research will additionally address the following degradation phenomena related to the petroleum industry: creep, pitting corrosion, and stress cracking corrosion (SCC).

2. Summary of results

The following tasks have been completed in the last three months:

2.1. Theoretical effort in support of model development, rupture analysis with application to Al-7075 and X70 carbon steel

2.2. Experimental efforts in support of corrosion and creep model development.
- 2.2.1. Experiments on Al-7075-T6 materials
- 2.2.2. Experiments on X-70 carbon steels

2.1. Rupture analysis (justification for the proposed empirical model):

Strain rate estimation and time to rupture of the materials are used especially in mechanical engineering to estimate the lifetime of materials and to estimate the service and residual life of material in heat exchanger tubes and turbine blades in oil refineries and power plants. The rupture point of material represents the end point on the creep curve, and so it can be assumed to be an important part of a creep curve. It is usually taken to characterize the curve in relation to other parameters of the curve.

One of the most important relations is the Monkman and Grant [2] relation that gives a proportionality between the rupture time and the minimum creep rate which can be derived from the creep curve in Figure 1 [3], and is given by the relation below.

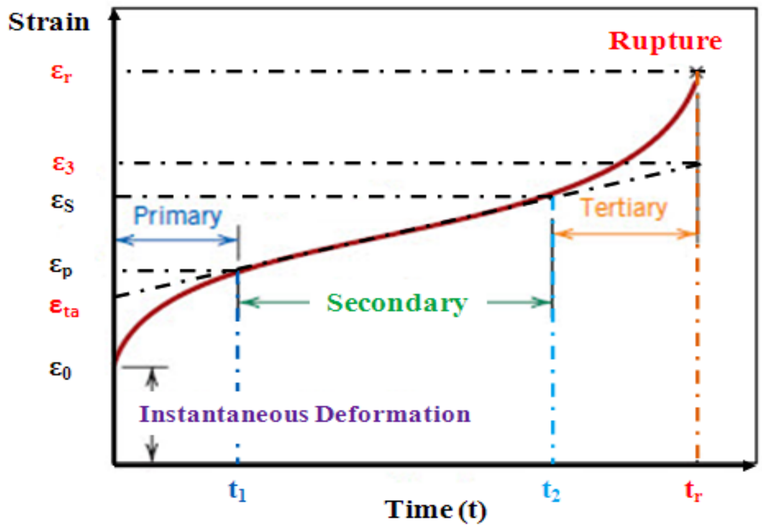

Figure 1. Creep curve.

$$\varepsilon_S = \varepsilon_3 - \varepsilon_{ta} t\ r = \varepsilon_S - \varepsilon_p t_2 - t_1, \quad or\ \varepsilon_S \cdot t_r = constant$$

This relation is applied to our experimental data given in Figure 2, for Al-7075-T6 samples at 400°C and applied stresses of 100Mpa (estimated after 44.3 hrs = 1.84 days).

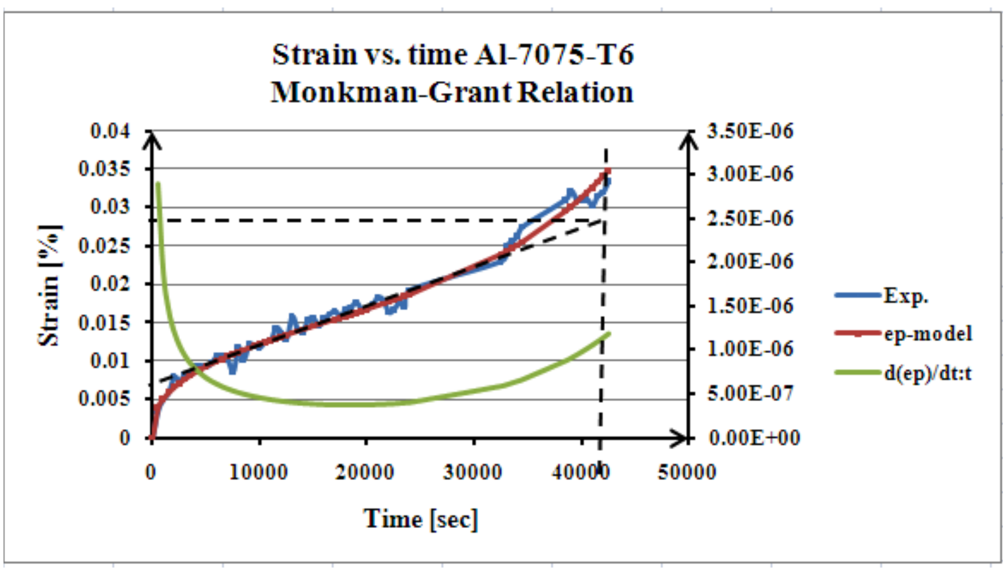

Figure 2. Creep curve of Al-7075-T6 samples at T= 400°C and σ = 100Mpa, after 44.3 hrs = 1.84 days.

$$\varepsilon_S = \varepsilon_3 - \varepsilon_{ta} t_r = 0.028 - 0.0065\, t_r[=11.7\ hrs] = 0.00184 \quad or\ \varepsilon_S \cdot t_r = 0.0215$$

The calculated value for the Monkman and Grant constant of 0.0215 is in good agreement with the given literature data of 0.02 for this material [4, 5].

In some other research about stainless steels, Garofalo et.al. [6], found the following relationships between the rupture time t_r and (t_2-t_1), duration of the secondary region of the creep curve, and t_2, the beginning time of the tertiary region:

$$t_r = A\cdot(t_2 - t_1)^{-n}, \quad and \; t_r = B\cdot(t_2)^m$$

where A and B are material parameters dependent on temperature, stress and other variables, and n and m are constants close to unity.

From these investigations it is obvious that the primary and the tertiary parts can be represented by the power low. These justify again the power law consideration for the primary and tertiary part used in our proposed empirical model.

The Larson-Miller parameter [7] is another important relation in the creep experiments that can be used to estimate the activation energy of creep of materials and is mostly used in praxis for estimation of the remaining life, in relation to the service life of materials.

This relation is derived and applied to our data to estimate the activation energy of Al-7075T6 and X-70 carbon steel. The calculated activation energies are in a good agreement with the creep literature data.

Based on the stress and temperature dependency of parameters mentioned above, it is easy to drive the following relation for the rupture time taken from the stress and temperature dependency of the strain rate given by Dorn [8] to:

$$t_r = constant\cdot\sigma^{-n}\cdot\exp\left(\frac{\Delta H}{RT}\right)$$

This relation builds the basis for the derivation of the important Larson-Miller parameter and other similar parameters discussed in mechanical engineering.

Derivation of Larson–Miller parameter:

If we consider the strain rate according to Dorn of

$$\dot{\varepsilon}_s = A\cdot\sigma^n\cdot\exp\left(-\frac{E_A}{RT}\right)$$

then

$$t_r = constant\cdot\sigma^{-n}\cdot\exp\left(\frac{\Delta H}{RT}\right)$$

Taking logarithms from both sides results in

$$\log t_r = \log constant - n\cdot\log\sigma + \frac{\Delta H}{2.3R}\cdot\frac{1}{T}$$

or

$$T\cdot\log t_r = T\cdot[\log constant - n\cdot\log\sigma] + \frac{\Delta H}{2.3R} = T\cdot\log C_* + \frac{\Delta H}{2.3R}$$

Then by a given stress σ (constant value):

$$T\cdot[\log t_r - \log C_*] = \frac{\Delta H}{2.3R}$$

Larson-Miller parameter: $PLM = \frac{\Delta H}{2.3R} = T\cdot[\log t_r + C], \; with \quad 10 < C < 20$

It is obvious from the above equation why the constant C takes a negative value on the logarithmic scale, and if we draw the $\log tr$ vs. $1/T$, then it is possible to estimate the activation energy of the creep process.

Parameter C for Al alloys in the 7xxxx series is C=10 for cyclic and C=14 for static creep in the literature [4, 5], and if we take a value of C=12 for our experiment with t_r = 11.7 hrs at T = 673K= (400°C), the activation energy can be calculated as:

$$\Delta H = QA = 169 \text{ kJmol}$$

This value is near the values of activation energies of (142 - 145 kJ/mol) given in the creep literature for these materials.

Monkman and Grant constant and activation energy (with C~20 for steels) were estimated for X70 carbon steel according to the following creep experiments data, given in Figure 3:

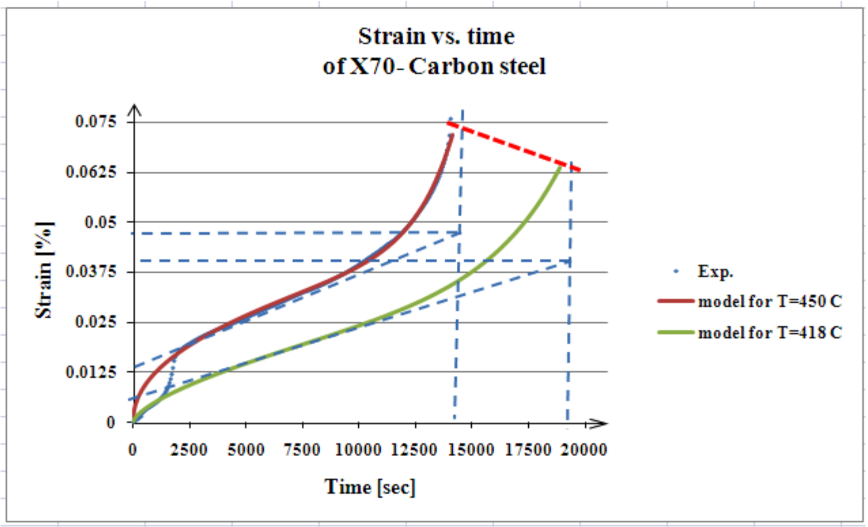

Figure 3: Creep curve of X70 carbon steel at T=450°C and predicted at T= 418°C and σ=348.8 MPa, fitted by our proposed model

$$\varepsilon S = \varepsilon 3 - \varepsilon a t r = 0.04 - 0.0125 \text{tr}[=3.82\ hrs] = 0.0072 \quad or \quad \varepsilon S \cdot tr = 0.0275$$

$$\Delta H = QA = 284.57 \text{ kJ-mol, for T=450°C and tr=3.82 hrs}$$

$$\Delta H = QA = 271.97 \text{ kJ-mol, for T=418°C and tr=3.82 hrs}$$

These values are in good agreement with the literature values given for steel materials (245-300 kJ/mol) [8].

2.2. Experimental efforts in support of corrosion and creep model development

2.2.1. Experiments on Al-7075-T6 materials

Creep experiments of Al-7075T6 samples were performed in an MTS tensile (810)-machine and in a homemade furnace extra prepared and equipped with tap water circulation (for cooling the grips connected to the samples). Grips were cooled additionally with two small fans to prevent the heat extending to the MTS grips and to provide a constant temperature for the samples during the creep experiments. The MTS-machine was equipped with furnace and computer connected for data acquisition and is shown in Figure 4.

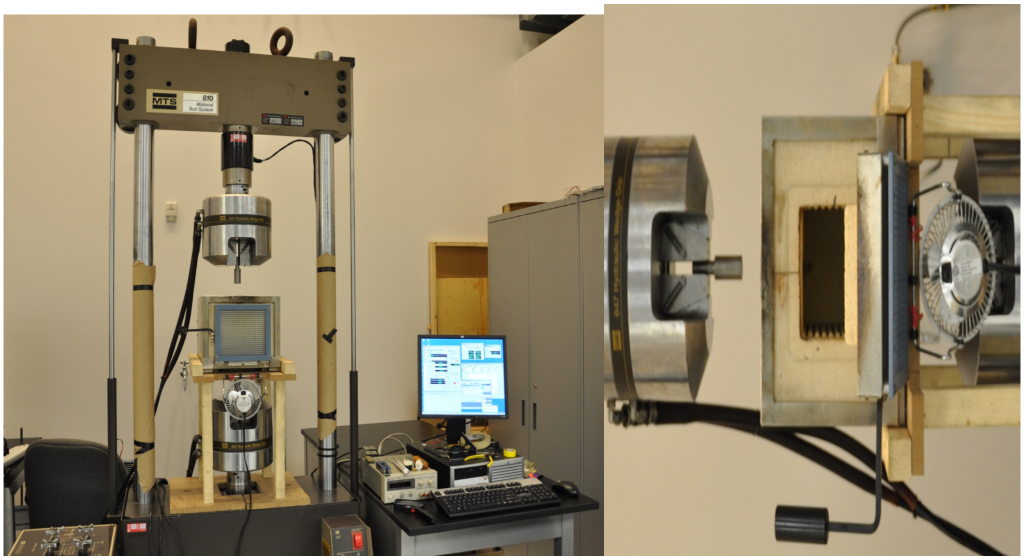

Figure 4. MTS-810 Material test system equipped with creep furnace and data acquisition.

It should be mentioned that cooling with ice-cooled water causes a negative creep rate in the samples during the creep experiment.

Al-samples used in the creep experiment are shown in Figure 5. The ductile cup and cone fracture cross section after the creep experiments are clearly visible in the figure.

Figure 5. Al-7075-T6 used in creep experiments with hardened grip holders.

The stress strain diagram is an important part of a creep experiment. The amount of stress applied during a creep experiment can be taken from the stress strain diagram. Applied stress is chosen usually 60 to 80 percent of the yield point (or of the ultimate strength) of materials. The estimated stress strain curve of Al-7075 material at different temperatures and its counterpart at room temperature [9] are given in Figure 6.

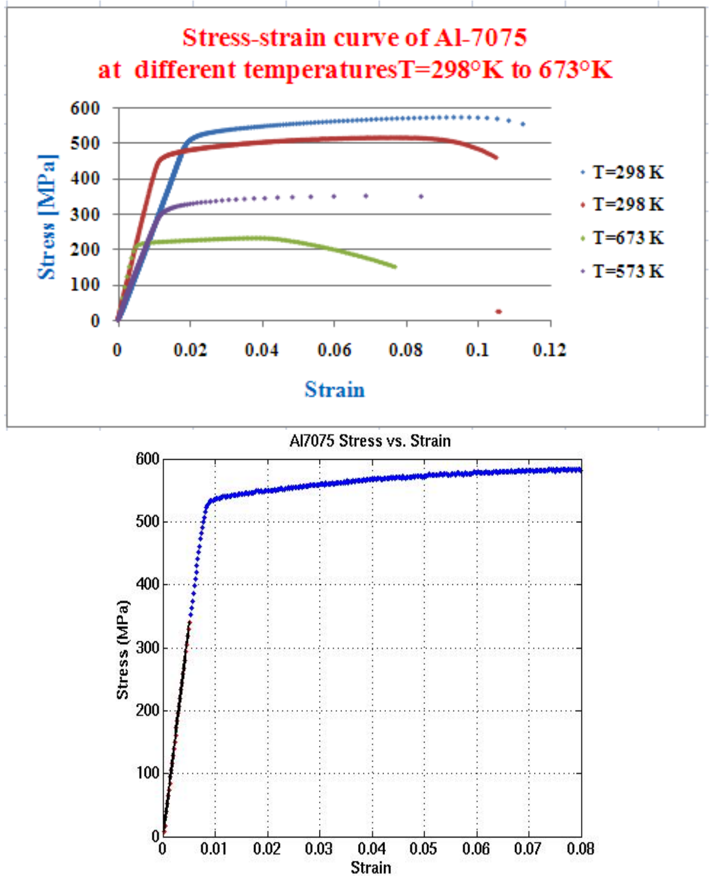

Figure 6: Stress strain curve of Al-7075 at different temperatures compared with the given stress strain curve at room temperature from the literature [9].

The creep experiment with MTS-810 has its own problems, as we mentioned in the last July report.

A complete creep experiment takes usually months or years, and because of the inability of the MTS machine to perform a long-term experiment we tried to accelerate our creep experiments. To get some acceptable data, we reduced the breaking times to hours or days. Figure 7 shows the creep curves experimentally taken and theoretically modeled and fitted with our proposed empirical model.

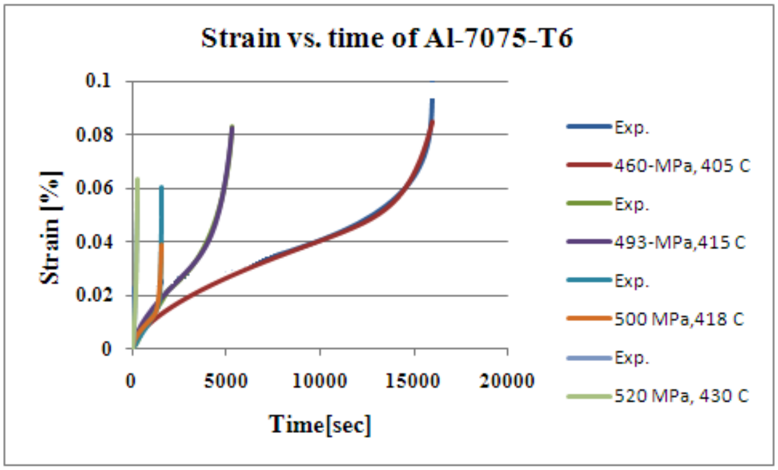

Figure 8. Creep curves of Al-7075 from experiment and fitted with the proposed empirical model.

The proposed empirical model had the following form, and the corresponding parameter values are given in Table 1.

$$\varepsilon = A \cdot t n + C \cdot t m \cdot \exp(p \cdot \cdot t)$$

where A, n, C, m, and p are material parameters and depend on temperature and applied stresses.

Table 1. Numerical values for corresponding parameters of the proposed empirical model

T [°C]					
	A	n	C	m	p
405	0.000157	0.602	1.90E-12	1.231	0.00073
415	0.00019	0.627	1.20E-10	1.51	0.00126
418	0.0002	0.58	2.60E-13	1.67	0.008
430	0.0003	0.75	1.97E-07	1.66	0.0108
σ [MPa]					
	A	n	C	m	p
460	0.000157	0.602	1.90E-12	1.231	0.00073
493	0.00019	0.627	1.20E-10	1.51	0.00126
500	0.0002	0.58	2.60E-13	1.67	0.008
520	0.0003	0.75	1.97E-07	1.66	0.0108

So it was possible to estimate the temperature and stress dependency of parameters. Parameters A, C, and p show exponential dependency on temperature and stresses, while parameters n, and m have a linear dependency on temperature and stress.

The exponential dependency on temperature for parameter A is known in the creep literature but important linear dependencies of n, and m parameters on temperature and stress are shown for the first time. Exponential dependency of parameters C and p on temperature and stresses are weak but possible and need more investigation.

The final equation for the empirical model thus changes to the following complex form:

$$\varepsilon = A' \cdot [\exp(\alpha \cdot \boldsymbol{\sigma}) \cdot \exp(QAR\boldsymbol{T})] \cdot \boldsymbol{t}\beta\boldsymbol{T} + \gamma\boldsymbol{\sigma} + \delta + C' \cdot \boldsymbol{t}\beta' \boldsymbol{T} + \gamma' \boldsymbol{\sigma} + \delta' \cdot \exp(p \cdot \boldsymbol{t})$$

where α, β, β’, γ, γ’, δ, and δ’ are now material parameters and their dependency on other material structural properties such as grain diameters or hardness is possible.

The final probabilistic model and estimation of final distributions for parameters A’, and C’ and estimation of their uncertainties with MATLAB and with Bayesian inference-based WINBUGs program are under investigation.

4.2.2. Experiments on X-70 carbon steels

Three dog-bone X-70 carbon steel samples with threaded parts at two ends were prepared. The threaded dog-bone samples have 4mm cross section diameter, and a gauge length of 45mm. Two threaded long grips for installation the samples in furnace were made.

Because of the softness of the grip materials (compared with the X70 carbon steel samples) two threaded long grips were tempered at 900°C for approximately 3 hours and quenched in oil (for surface hardening).
The threaded samples and the corresponding grips are shown in Figure 9.

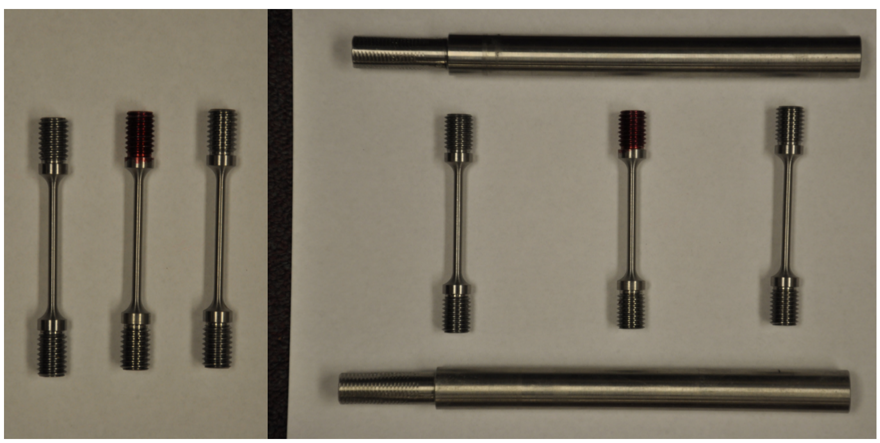

Figure 9. Dog-bone X70 carbon steel samples used for the creep experiment.

The broken sample for estimation of the stress strain curve at room temperature had a cup cone ductile form, while the broken samples after the creep experiments showed brittle fracture. These characteristics are shown in Figure 10.

Figure 10. Broken samples at room temperature with cup and cone ductile breakage (left) and two X70 carbon steel samples after creep experiment with brittle fracture types (right).

The creep curve estimated from one of the sample is shown in the Figure 11. The first part of the curve shows some fluctuation (because of the temperature variation from 418 °C to stabilized temperature of 450 °C). The creep curve with the completed secondary and tertiary parts is completely coverable with the proposed model.

The primary part up to 5000 seconds was then fitted with the proposed empirical equation after readjustment with a fracture lifetime estimated from the Monkman and Grant relation. Both experimentally found creep curve and two fitted parts with our proposed model are given in Figure 11.

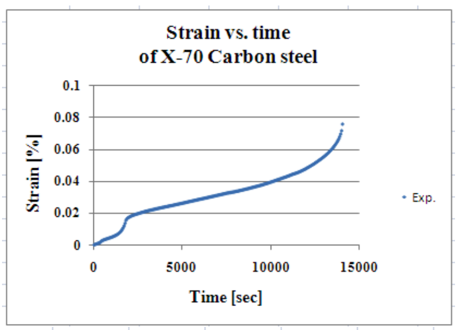

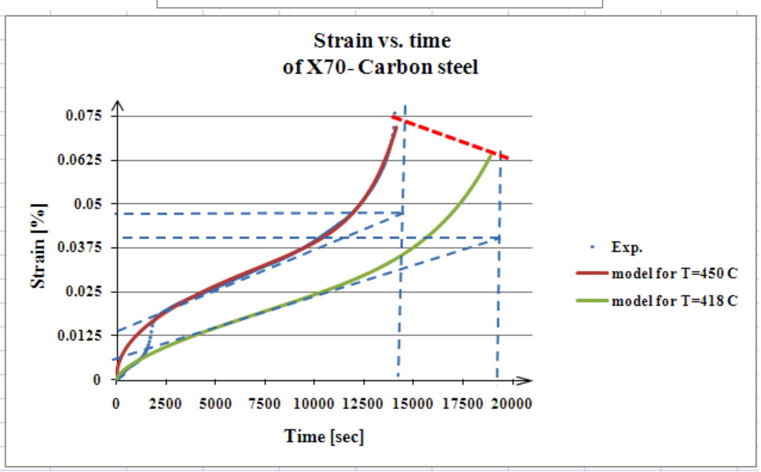

Figure 11. Creep curve of X70 carbon steel at T=450 °C and σ = 348MPa (left), and predicted creep curve at 418 °C both fitted with proposed empirical equation.

Empirical equations for both of the creep curves are given below:

$\varepsilon\text{-}450=0.000488\cdot t\text{-}0.4695+ (1.383\times10-10)\cdot t\text{-}1.2362\cdot\exp(0.0005198\cdot t)$

$\varepsilon\text{-}418=0.000056\cdot t\text{-}0.653+ (9.983\times10-10.)\cdot t\text{-}1.2362\cdot\exp(0.000265\cdot t)$

It should be mentioned here that exact estimation of temperature and stress dependencies of parameters need more time and samples (and therefore additional cost). In addition, creep experiments need their own creep equipment and specific high temperature extensometers (instead of a MTS machine that is more specified for estimation of stress-strain behaviors of metallic materials).

3. Future work

The model verification and justification by performing creep experiments of Al 7075 and X70 do-bone shaped specimens are 85% done and will be continued in the next phase of our study. The statistical evaluation of the experimental data and nonlinear regression analysis by the MATLAB program is about 60% done (i.e., the MATLAB program is formulated) and will be prepared for the next report. Finally, we will compare our model with other empirical models and BIC (Bayesian Information Criterion) [9, 10] with experimental data gathered for Al-7075-T6 and X70 carbon steel samples.

Near Future Plans:

1. Simulation and refinement of the stress and temperature dependency of creep parameters of mechanistic models (PoF models) for creep for Al-7075-T6 and X70 carbon steel samples.
2. The corresponding simulation and statistical tool to help both model development and field applications will be done.

4. References

[1] ASME-B31G, Manual for Determining the Remaining Strength of Corroded Pipelines. A Supplement of ASME B31G Code for Pressure Piping, ASME, New York, 1995.

[2] Monkman, F.C. and Grant, N.J.: An empirical relationship between rupture life and minimum creep rate in creep-rupture tests, Proc. ASTM,56,593, 1956

[3] Conway, J.B. ; Numerical methods for creep and rupture analysis, Gordon and Beach, Science Publisher, New York, 1967

[4] LEE, D.Y., PARK, J.G. and CHO, D.H.; High-temperature properties of dispersion-strengthened 7075-T6 aluminum alloy, JOURNAL OF MATERIALS SCIENCE LETTERS 16 (1997) 158–160

[5] BURT, H. and WILSHIRE, B. ; Theoretical and Practical Implications of Creep Curve Shape Analyses for 7010 and 7075, METALLURGICAL AND MATERIALS TRANSACTIONS A VOLUME 37A, MARCH 2006—1005

[6] Garofalo,F. Whitemore, R.W. et.al.; Creep and creep-rupture relationships in an austenitic stainless steel, Trans. AIME 221, 310, 1961.

[7] Larson,F.R. and Miller,J. ; A time-temperature relationship for rupture and creep stresses, Trans. ASME, 74, 765,1952
[8] Dorn, J. E. ; Some fundamental experiments on high temperature creep, J. Mech. Phys. Solids, 3, (1955)
[9] C. K. Syn, C.K. et al. ; Stress-Strain Rate Relations in Ultra High Carbon Steels Deformed in the Ferrite Range of Temperature, UCRL-JC-151884February 20,2003 THERMEC 2003 International Conference on Processing and Manufacturing of Advanced Materials; Leganes, Madrid, Spain, July 7-1 1, 2003
[10] ftp:// ftp.ccmr.cornell.edu/tmp/410/MS&E%20410/.../Schuren.ppt
[11] K.P.Burnham and D.R. Anderson," Model selection and multi-model inference, A practical Information-theoretic Approach, Spriger,2002
[12] Bayesian information criterion, en.wikipedia.org/wiki/Bayesian information criterion

Appendix

Background

A number of deterministic models have been proposed to assess reliability and life-remaining assessment of pipelines. Among these models is the ASME B31G [1] code, which is most widely used for the assessment of corroded pipelines. However, these models are highly conservative and lack the ability to estimate the true life of the pipelines and other equipment used in the oil industry. To address this shortcoming one needs to develop a best-estimate assessment of the life (to assess reliability and risk imposed) by these structures and equipment and assess the uncertainties surrounding such estimates. The proposed probabilistic mechanistic models, when fully developed, would integrate the physics of failure of some of the leading failure degradation mechanisms in the oil industry into the formal risk and reliability assessments. Such physical models will be validated using a state of the art reliability assessment laboratory (being developed at PI). Uncertainties about the model structures and parameters will also be quantified. Such models will incorporate inspection data (characterizing limited and uncertain evidences). The rate of degradation is influenced by many factors such as pipeline materials, process conditions, geometry and location. Based on these factors, a best estimate of the structure (pipeline) or equipment (primarily valves, pumps and compressors) service life (reliability and remaining life) is to be calculated and uncertainties associated with the service life quantified. This estimate would serve as a basis that guides decisions regarding maintenance and replacement practices.

Phase I of this research focused on developing a corrosion-fatigue model. It successfully proposed such a model and developed an advanced laboratory for testing this phenomenon at PI. The current research continues in the same line of research by investigating and developing additional degradation phenomena (SCC, pitting corrosion, and creep-fatigue) and integrates these phenomena with reliability and risk assessment through four different tasks. The long-term objective of this research is to develop a comprehensive library of probabilistic mechanistic models for all degradation phenomena pertinent to structures (piping, and pressure vessels) used in the oil industry.

Test Facilities

The test rig for this research exists at the University of Maryland. The rig is used to conduct experimental studies reflecting field conditions for model validation developed in EERC Phase I & II. The equipment include MTS fatigue machine, heating furnace, corrosion test cells, autoclaves, multiphase flow loops, and testing machines for slow strain rate and crack growth testing. This activity also requires a complete line of monitoring equipment for evaluation of corrosion, scaling, and chemical treatment for field and laboratory. This test rig will be a useful tool for performing fatigue, corrosion, corrosion-fatigue, creep, and creep-fatigue, as well as teaching and possibly training field engineers from operating companies.

Two-Year Schedule

This project involves three distinct tasks. The first task is the development of the mechanistic models, development of a corresponding simulation tool to help both model development and field applications. The second task focuses on experimental activities to generate relevant data to validate the proposed models of Task 1. Finally, the third task involves the actual validation of the models proposed in Task 1 with the experimental results obtained in Task 2, including Bayesian estimation of the model parameters.

Task 1: Develop the best estimate mechanistic (physics of failure) empirical models for pitting corrosion, SCC, and fatigue-creep. The model development involves the following activities.

Task1.1: Gather, review and select most promising physics of failure based methods and algorithms proposed in the literature.

- Literature surveys for creep and stress corrosion cracking (SCC) degradation mechanisms are almost completed and will be classified for finding the relevant models (100% done).

Task1.2: Select, develop or adopt a detailed mechanistic model (one deterministic model for each phenomenon) that properly describes the degradation process.

- Development of the mechanistic models and of a corresponding simulation tool to help both model development and field applications after classifying the models and choosing the appropriate one should be done in the next future (95% complete).

Task 1.3: Develop a Monte-Carlo based mathematical simulation routine on MATLAB depicting the detailed mechanistic model of each degradation phenomenon (far faster than real-time).

- This part was completed for the empirical model developed based on the works of the PI interns for pitting corrosion. After proposing the similar models for SCC and creep-fatigue, it will be repeated (85% completed).

Task 1.4: Based on the results of the simulation a simplified empirical model that best describes the results of simulation will be proposed. Such a model relates the degradation (e.g., depth of the pit or the crack growth rate) to applied loads such as pipeline internal pressure and chemical composition of the product inside the pipeline, as a function of time or cycle of load application.

- This part is completed for the pitting corrosion and corrosion-fatigue (100% complete).

Task 2: A PoF reliability analysis laboratory has been designed and being developed at PI. The advanced corrosion-fatigue purchased by the PI that was installed at the University of Maryland (the Cortest Rig) has been sent to Cortest to ship to PI. (100% done).

Task 2.1: Completing the remaining corrosion-fatigue tests being conducted by Mr. Nuhi and Chookah. (100% Completed)

Task 2.2: Pitting Corrosion Experiments (develop test plan, prepare samples and the facility, perform the test, and evaluate the test results) (100% Completed).

Task 2.3 SCC Experiments (develop test plan, prepare samples and the facility, perform the test, and evaluate the test results). (Not started yet)

- This task will be done in the near future, but SCC specimen holders have already designed and made according to the recent patents and ASTM-Standard.

Task 2.4 Creep-Fatigue Experiments: The equipments and samples are completely ready (100% completed); the tests will be performed in future and the results will be evaluated.

- A small-scaled corrosion-fatigue (or creep) chamber has been designed (not as part of this project), made and tested for dog-bone and CT specimens and checked its workability on the UMD MTS machines using Aluminum alloy samples. Moreover, another chamber has been made for long dog boned specimens.
- A heating chamber has been designed and tested for creep experiments.
- New dial gauges with stand are prepared and tested for four and three points bending of SCC and pitting corrosion experiments.

Task 3: This task involves modification, advancement and use of the WinBUGs' Bayesian formalism for model validation using experimental data and integration of the field data and information including sensor-based data (acoustics and/or optical) to update the empirical models and estimate the remaining life of oil pipelines and structures. (85% Complete)

- The WinBUGs' Bayesian formalism for model estimation and validation was developed as part of M. Chookah's work. This formalism is being updated and new applications of the formalism have been performed using past experimental data and new data of corrosion and fatigue obtained since departure of Dr. Chookah. Further work with this software for integration the experimental data has already be done.

Schedule/Milestones/Deliverables

Tasks 1.1-1.3 (5/1/09-12/15/09); Task 1.4 (12/15/09-3/1/10); Task 2.1 (completed 7/1/09); Task2.2 (7/1/09-12/15/09); Task 2.3 (12/15/09 – 6/1/10); Task 2.4 (6/1/10-2/1/11); Task 3 (12/15/09-3/15/11).

The project is on schedule and there are no issues or delays at this point.

Visits

- Dr. A.Seibi visited UMD in July 2009
- Dr. A.Seibi visited UMD in July 2010
- Two PI students Abdullah Al Tamimi, and Mohammad Abu Daghah took parts at summer internship (2009).
- A PI student Taher Abu Seer took parts at summer internship (2010).
- Prof. Modarres attended the 1st Annual PI Partner Schools Research Workshop. The Petroleum Institute, Abu Dhabi, U.A.E. January 6-7, 2010.

Papers Published and prepared for publishing by the Team

1- M. Chookah, M. Nuhi, and M. Modarres, "Assessment of Integrity of Oil Pipelines Subject to Corrosion-Fatigue and Pitting Corrosion", presented by Prof. Modarres at the International Conference of Integrity- Reliability-Failure (IRF) in Porto, Portugal, July 20-24 2009. (The cost of the conference and associated travels was not covered by EERC)

2- M. Chookah, M. Nuhi, and M. Modarres, A. Seibi "A Probabilistic Physics of Failure Model for Prognostic Health Monitoring of Piping Subject to Pitting and Corrosion –Fatigue" is sent for publication to the "Journal of Reliability Engineering and System Safety".

3- A paper on "Development of a Database of Mechanistic Models of Failure for Application to Pipeline and Equipment Risk, Reliability and Health Management (Pitting Corrosion- Pit Depth and Density), prepared for publication at a conference. We are studying the possibility that the PI interns present the paper.

4- A paper on “Reliability Analysis for Degradation Effects of Pitting Corrosion in Carbon Steel Pipes” is prepared and sent it to a conference in Italy. This paper was presented by PI members on ICM conference. This paper is published in Procedia Engineering 10 (2011) 1930–1935.
5- A Paper on “A probabilistic Physics-of-Failure model for prognostic health management of structures subject to pitting and corrosion fatigue” is published in the journal of Reliability Engineering and System Safety 96 (2011) 1601–1610